ESPOO 2004 VTT RESEARCH NOTES 2274

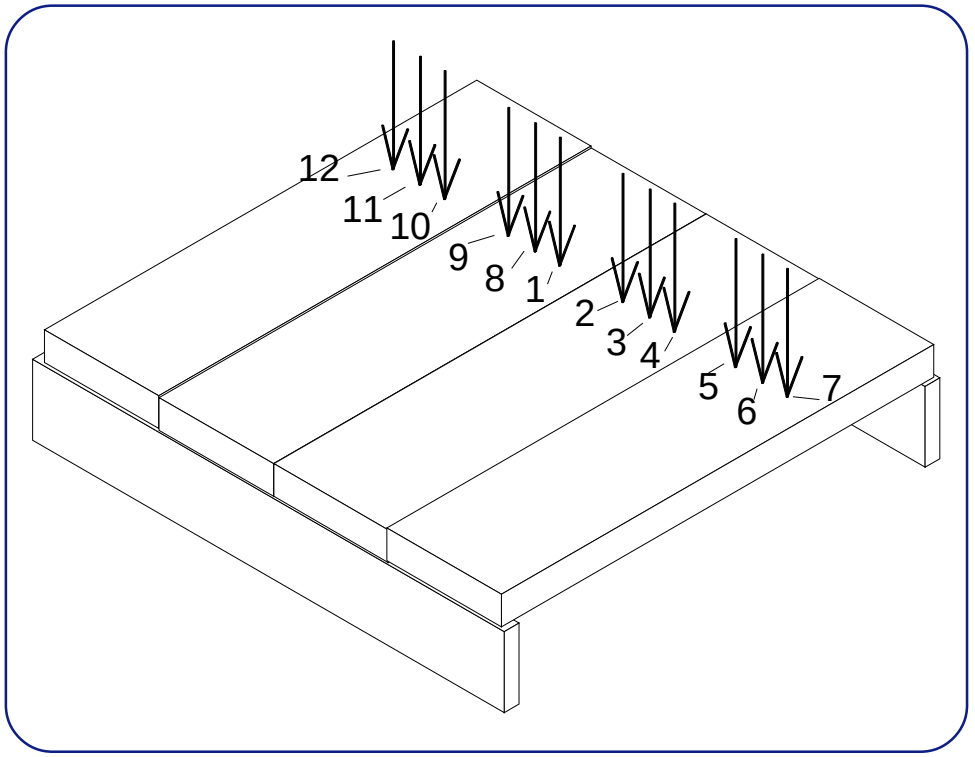

Matti Pajari

Shear–torsion tests on 400 mm hollow core floor

VTT TIEDOTTEITA – RESEARCH NOTES 2274

Shear-torsion tests on 400 mm hollow core floor

Matti Pajari
VTT Building and Transport

ISBN 951–38–6518–5 (URL: http://www.vtt.fi/inf/pdf/)
ISSN 1455–0865 (URL: http://www.vtt.fi/inf/pdf/)

Copyright © VTT 2004

JULKAISIJA – UTGIVARE – PUBLISHER

VTT, Vuorimiehentie 5, PL 2000, 02044 VTT
puh. vaihde (09) 4561, faksi (09) 456 4374

VTT, Bergsmansvägen 5, PB 2000, 02044 VTT
tel. växel (09) 4561, fax (09) 456 4374

VTT Technical Research Centre of Finland, Vuorimiehentie 5, P.O.Box 2000, FIN–02044 VTT, Finland
phone internat. + 358 9 4561, fax + 358 9 456 4374

VTT Rakennus- ja yhdyskuntatekniikka, Kemistintie 3, PL 1805, 02044 VTT
puh. vaihde 020 722 111, faksi 020 722 7007

VTT Bygg och transport, Kemistvägen 3, PB 1805, 02044 VTT
tel. växel 020 722 111, fax 020 722 7007

VTT Building and Transport, Kemistintie 3, P.O.Box 1805, FIN–02044 VTT, Finland
phone internat. +358 20 722 111, fax +358 20 722 7007

Technical editing Leena Ukskoski

Pajari, Matti. Shear-torsion tests on 400 mm hollow core floor. Espoo 2004. VTT Tiedotteita – Research Notes 2274. 30 p. + app. 82 p.

Keywords shear tests, torsion tests, hollow core slabs, floors, testing, test specimens, load testing, failure loads, load distribution, concrete, precast, prestressed, structure

Abstract

Fifteen load tests on a floor comprising four prestressed hollow core slabs were carried out to clarify the interaction of shear and torsion. The slabs were 400 mm in depth, 1.2 m in width and 7 m in length. The ends of the slabs were simply supported on concrete beams. The loads in each test comprised one or two concentrated loads close to the support.

In twelve tests the loads were limited to a typical service load or to a somewhat higher load. In these tests the behaviour of the floor was relatively linear and no sign of failure could be observed. In three tests the floor was loaded to a local failure. The observed failure loads were 25–97% higher than in a reference test on a single slab unit with identical support conditions. In the first failure test with one point load the failure mode was punching. In other two tests with two point loads, as well as in the reference test with one point load, the failure was a typical shear-torsion failure.

As a subtask of HOLCOTORS project, the test results have been used by Chalmers University of Technology for calibration of computerized calculation methods they have developed. This work is published elsewhere. Therefore, the present design practice has not been evaluated here in view of the obtained results.

Preface

In 2002–2004, a European research project named HOLCOTORS was carried out. It aimed at providing numerical methods for analysis and simplified methods for design of prestressed hollow core floors subjected to shear and torsion. The calculation models were developed by Chalmers University of Technology, Sweden. The tests used for verification of the models were carried out and documented by VTT, Finland. The researchers in the involved research institutes were

Helen Broo	Chalmers
Björn Engström	Chalmers
Karin Lundgren	Chalmers
Matti Pajari	VTT
Mario Plos	Chalmers.

In addition to the researchers, the following representatives of the industrial partners participated in the work as members of the steering group and by participating in the workshops organised on the day before the steering group meetings:

Olli Korander	Consolis Technology, Finland, Chairman
Arnold van Acker	Belgium
Willem Bekker	Echo, Belgium
David Fernandez-Ordonez	Castelo, Spain
Ronald Klein-Holte	BVSH (VBI) The Netherlands
Gösta Lindström	Strängbetong, Sweden
Aad van Paassen	BVSH (VBI), The Netherlands
Nordy Robbens	Echo, Belgium
Bart Thijs	Echo, Belgium
Jan de Wit	IPHA (Dycore), The Netherlands
Javier Zubia	Castelo, Spain.

Gösta Lindström also worked in close co-operation with the researchers, participated in extra workshops between the steering group meetings and made proposals for the future design practice.

The experimental part of the research project, a part of which is documented in this report, was financed by the Fifth Framework Programme of European Commission (Competitive and Sustainable Growth, Contract Nº G6RD-CT-2001-00641); International Prestressed Hollow Core Association, Bundesverband Spannbeton-Hohlplatten, Castelo, Consolis, Echo, Strängbetong, and VTT. The test specimens were provided by Parma Betonila, Finland.

Contents

Abstract....3

Preface....4

1. Introduction....6

2. Test arrangements....7

3. Results of load tests....14
   3.1 Tests with service load....14
   3.2 Failure tests....18

4. Strength of concrete....24

5. Analysis of results....26

6. Discussion....29

References....30

Appendices

A Photographs

B Measured slab cross-sections

C Measured forces, strains and displacements

D Initial part of load-deflection curves

1. Introduction

The tests documented in this report were planned to clarify the effect of shear and torsion on the deflection and resistance of a floor made of prestressed hollow core slab units. By placing the load close to the support, bending failure modes were eliminated.

In all figures of this report, the measures are given in millimetres unless otherwise specified.

2. Test arrangements

12 tests with service load were carried out. In these tests the floor was subjected to one point load which was increased monotonously until a certain predefined limit load was achieved. After that the load was moved to another position and the same procedure was repeated. All positions of the service point load are shown in Fig. 1.a.

After the service load tests the floor was loaded to failure in three tests. In the first test there was one point load, in the second and third test two point loads. Their location is illustrated in Fig. 1.b. Some characteristics of the test specimens are given in Table 1. Different tests are identified by symbol PF400:x where x is the number of the test shown in Fig. 1.

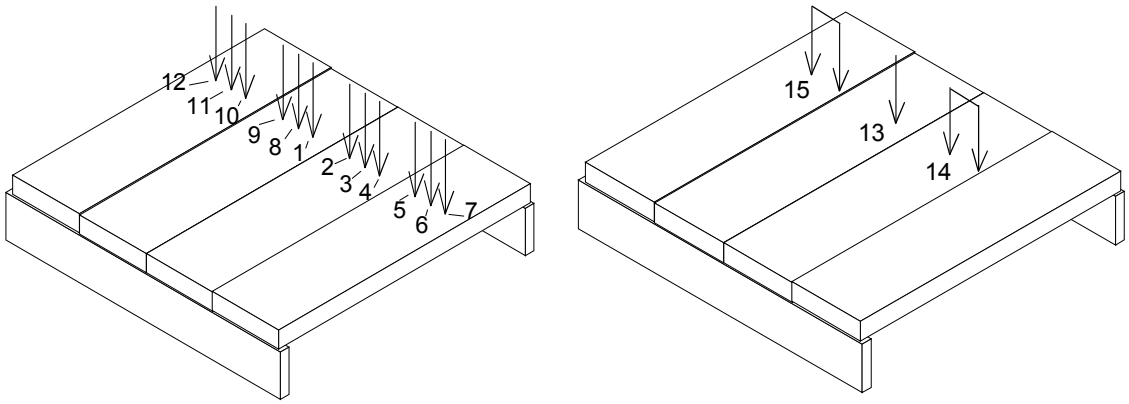

a) *b)*

Fig. 1. General view on loading arrangements. a) Location of point load in tests PF400:1–12. b) Location of point loads in tests PF400:13–15.

Table 1. Characteristics of slab units in test PF400.

Thickness mm	Strands	Initial prestress MPa	Length m	Cast
400	11 *d* 12.5	1000	7080	26.6.2002

For comparison, a load test called ST400E1M with similar support conditions as in the present floor but with only one slab unit was carried out, see Fig. 2. This test has been reported elsewhere [3].

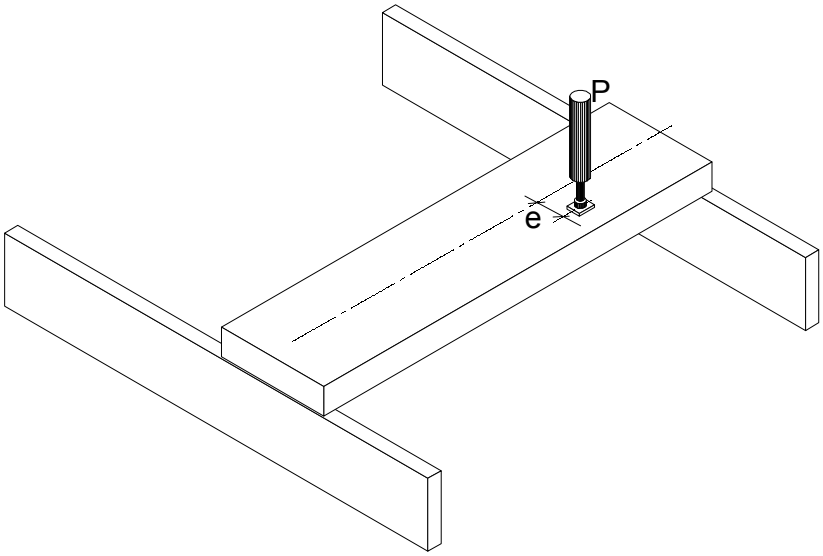

Fig. 2. Loading arrangements in test ST400E1M [3].

The material data provided by the manufacturer of the slab units are collected in Table 2.

Table 2. Data provided by the slab manufacturer.

Concrete	K60
Cement	CEM I 52,5 R
Cement kg/m^3	270
Water l/m^3	145
Maximum aggregate size # [mm]	16
Number of aggregates	4
Strands - strength/0.2% yield strength [MPa] - initial prestress [MPa]	 1860 / 1640 1000

The nominal cross-section of the slab units is given in Fig. 3 and the measured geometry in Appendix B. For the shape of the hollow cores see also Fig. 34. The geometry of the supporting beams is specified in Fig. 6.a and the arrangements at the support in Figs 6.b and 7.

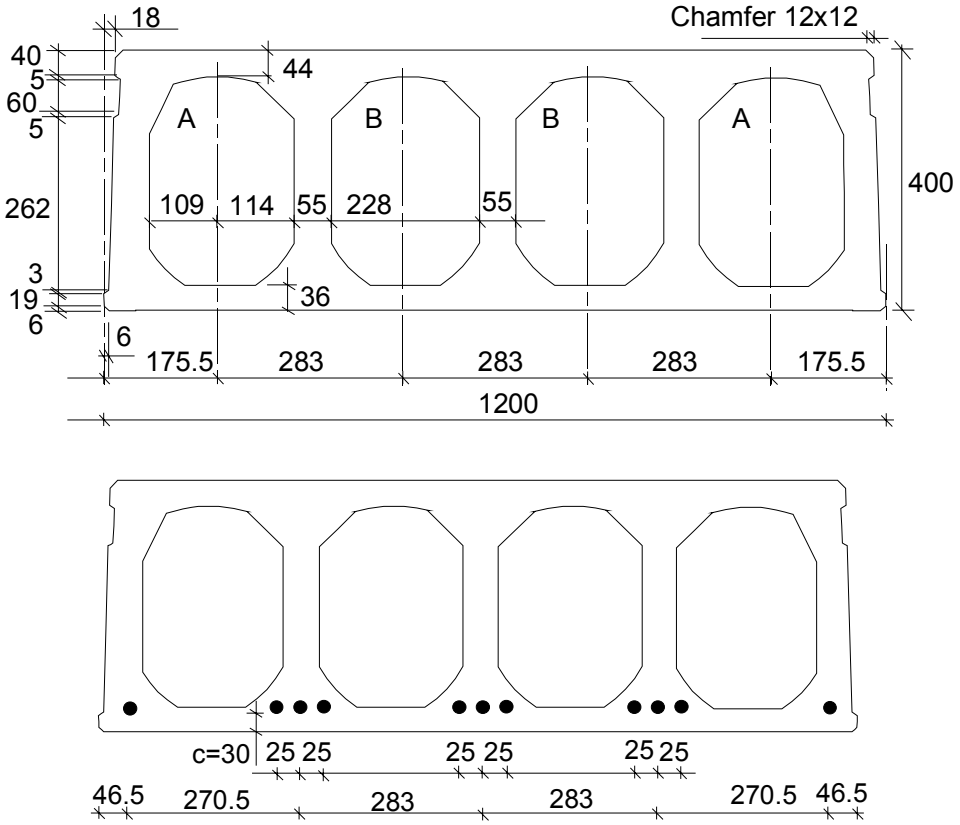

Fig. 3. Nominal cross-section and location of strands in slab units. c refers to concrete cover below the strand.

The supporting beams were placed on the floor of the laboratory without any smoothing material. The slab units were placed on the beams. The longitudinal joints were grouted on the 16th of September 2002. On the next day the joints were precracked by wedges, see Figs 1–4 in App. A. The crack widths measured after the precracking and before casting the tie beams are shown in Fig. 4.

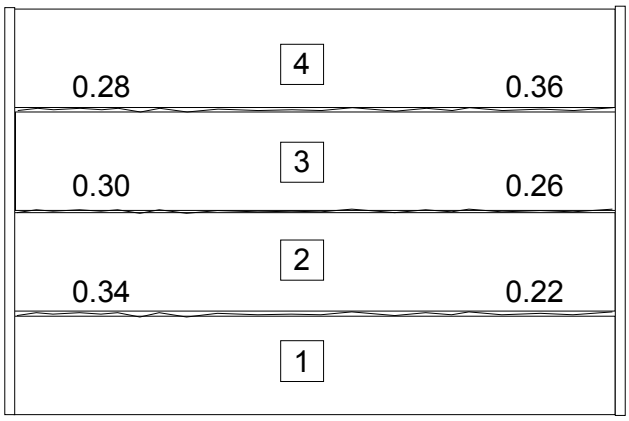

Fig. 4. Crack width after precracking.

The tie beams were cast on the 18th of September 2002.

The support conditions and test arrangements are roughly presented in Fig. 5 and in more detail in Figs 6–11.

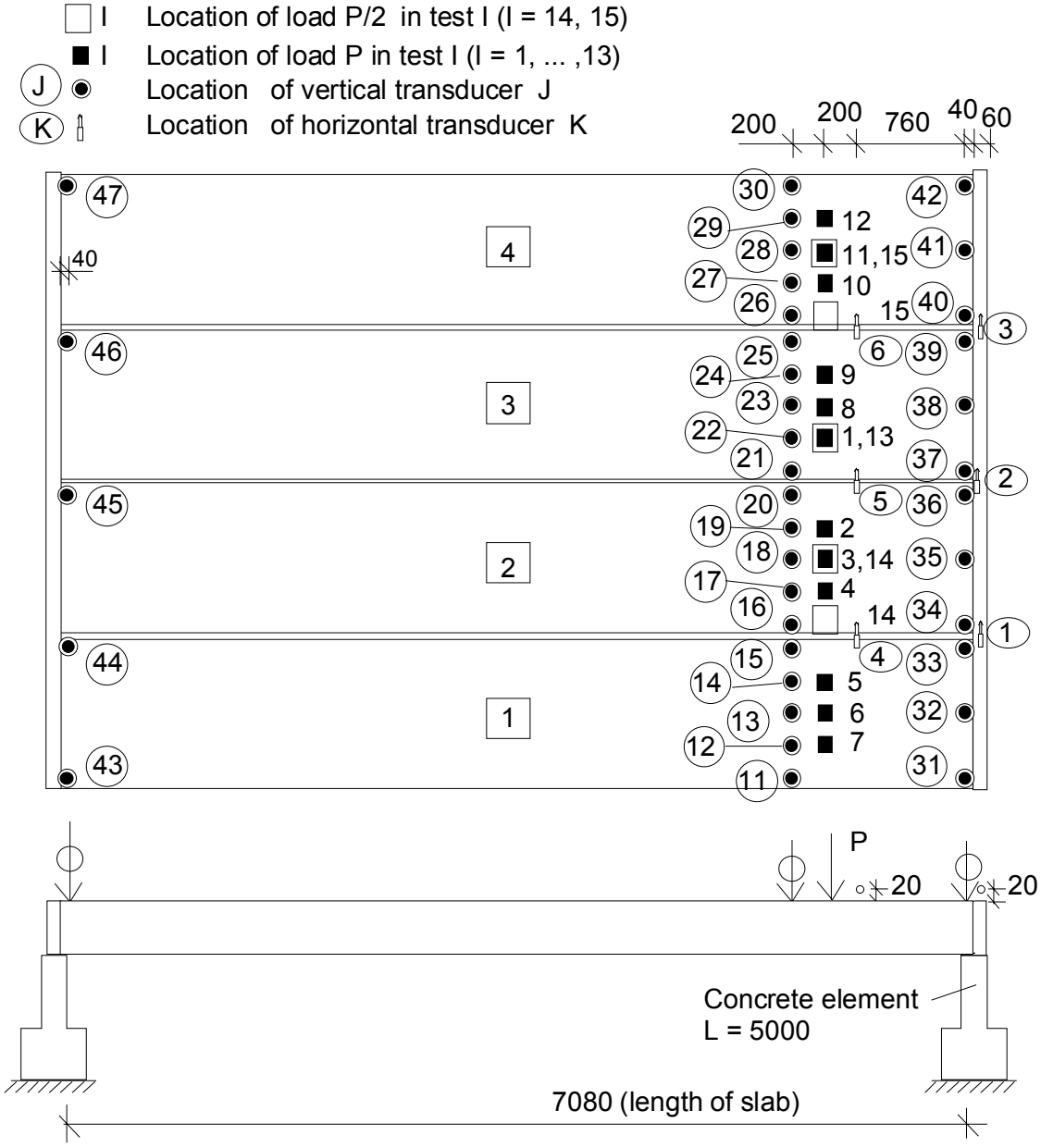

Fig. 5. Numbering and location of horizontal transducers 1–6 and vertical transducers 11–47 as well as location of loads in tests PF400:1–PF400:15.

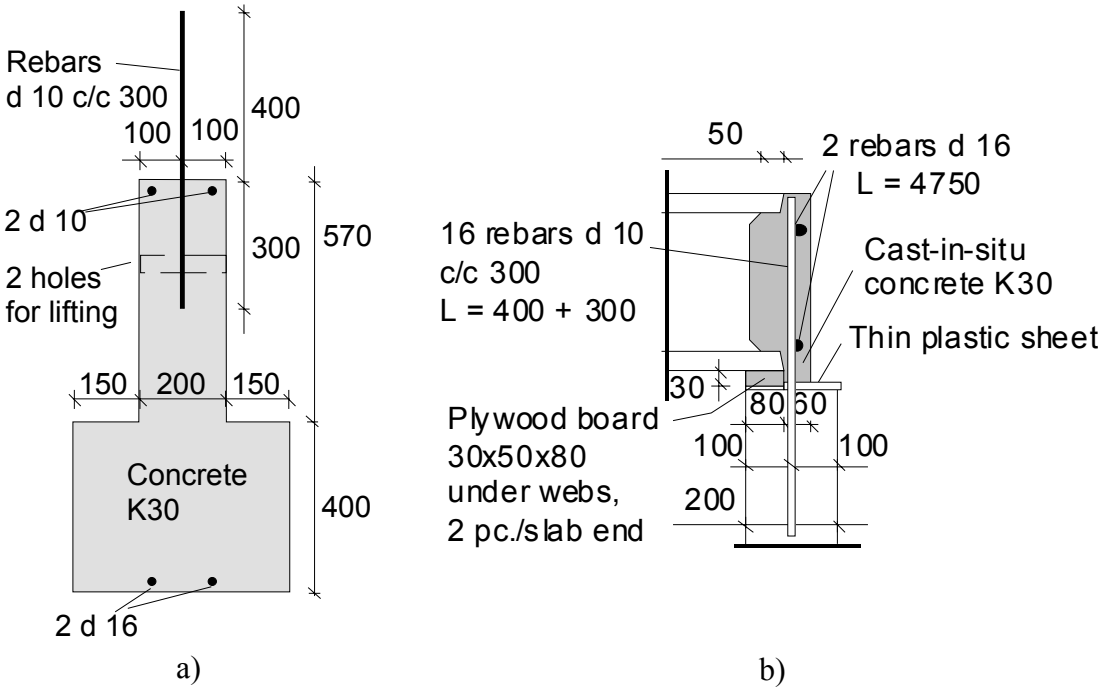

Fig. 6. a) Supporting beam, length = 5.0 m. b) Arrangements at support. See also Fig. 7. d x refers to a reinforcing bar with diameter x.

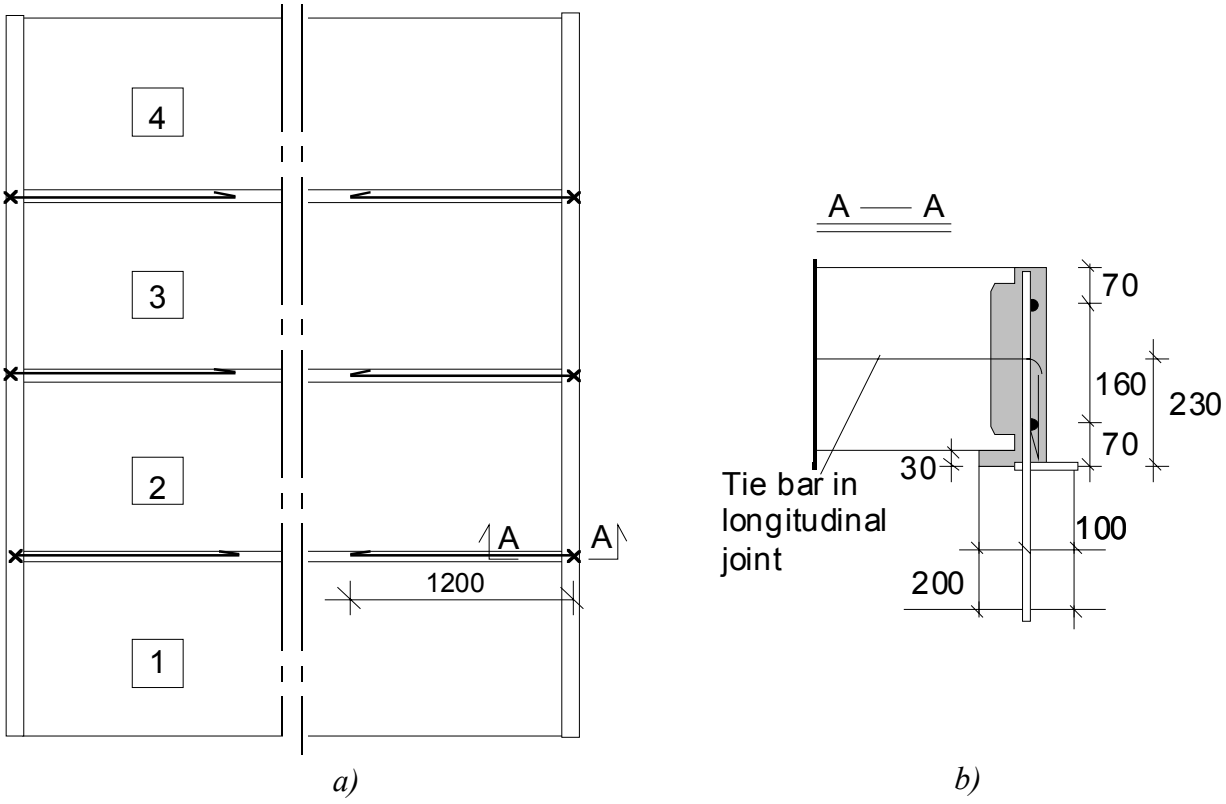

Fig. 7. Tie reinforcement in longitudinal joints. a) Plan. b) Elevation.

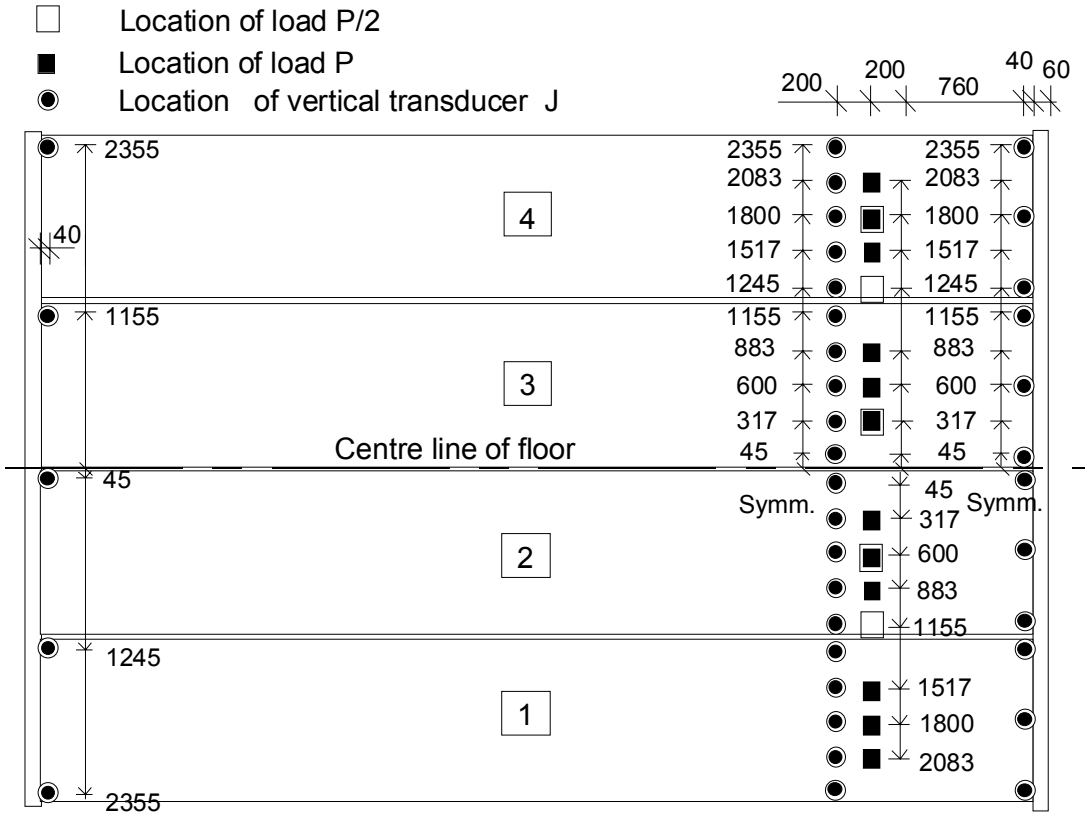

Fig. 8. Location of loads P and vertical transducers. See Fig. 5 for numbering of transducers.

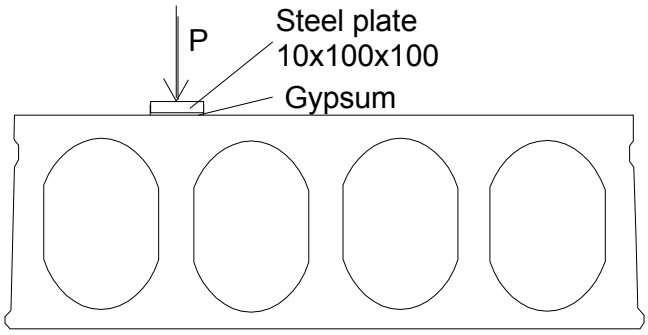

Fig. 9. Arrangements below one point load.

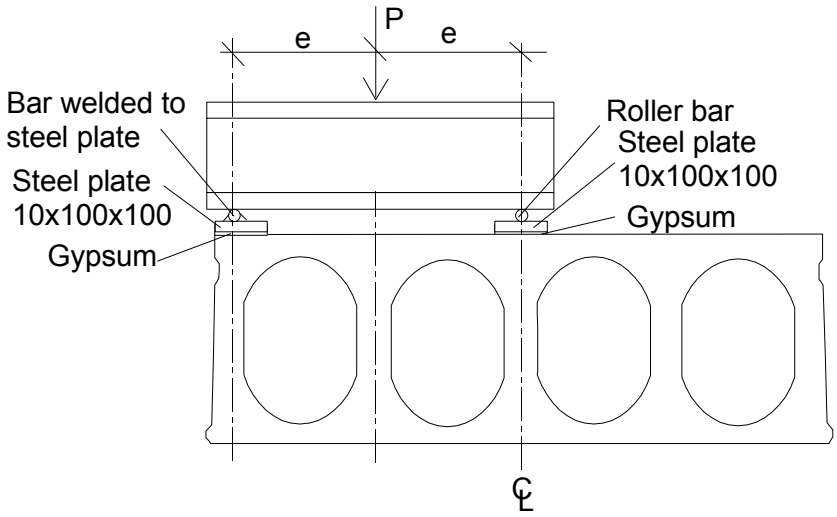

Fig. 10. Arrangements when two point loads are applied.

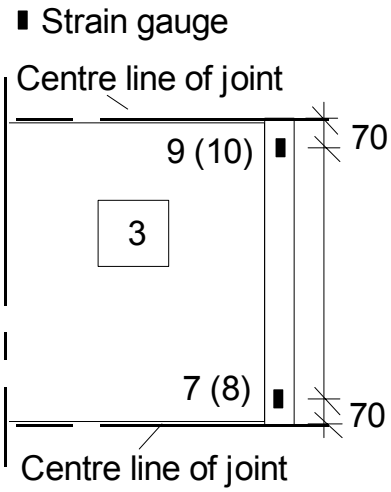

Fig. 11. Location of strain gauges 7–10 fixed to horizontal steel bars in tie beam at the loaded end. See also Fig. 3 in App. A. The numbers in parentheses refer to gauges glued to the lower bar.

The tests were carried out by keeping the rate of elongation of the actuator at a predefined level. When necessary, this level was shifted. The rate of loading was measured. It is given in App. C for each test.

3. Results of load tests

3.1 Tests with service load

In tests PF400:1–PF400:12 the floor was loaded with one point load. Before each test the measuring devices were zero-balanced. The load was increased monotonously up to a value which was estimated to be 50% or less of the failure load. The load-time relationship as well as the measured strains, crack widths and displacements are given graphically in App. C and some details in App. D. In test PF400:1 there was a sudden, uncontrolled increase in the load to 250 kN. In other tests the loading was under control all the time.

The displacements measured along the transverse line close to the loads were small, in all tests less than 1.1 mm. The settling of the supports was negligible, the highest value being of the order of 0.1 mm. The measured strains in the reinforcement of the tie beam were also small. Their highest value corresponded to the stress 22 MPa in the steel.

The ascending part of the load-deflection curves for the span (transducers 11–30) showed certain bilinearity in many cases, see Appendices C and D. This might have been due to cracking of the concrete, but then it would not have occurred during reloading (load on the next web).

The maximum change of crack width was of the order of 0.02 mm. This is much less than 0.3 mm which was the order of the crack width after precracking.

Figures 12–23 illustrate the deflection of the slab along a transverse line close to the load. In many cases there is a considerable discontinuity over the joints.

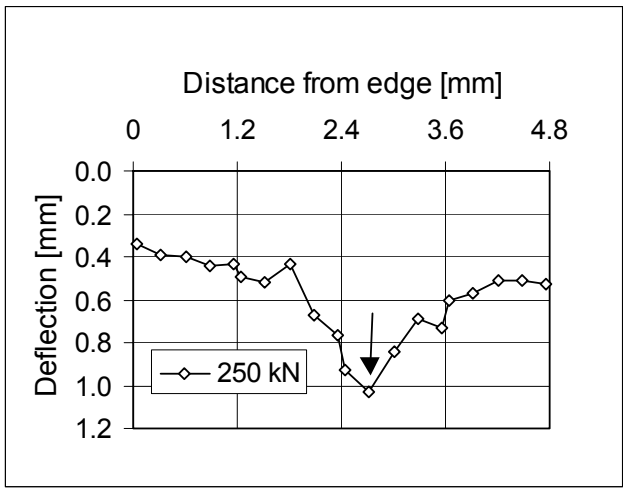

Fig. 12. PF400:1. Deflection measured by transducers 11–30 at maximum load.

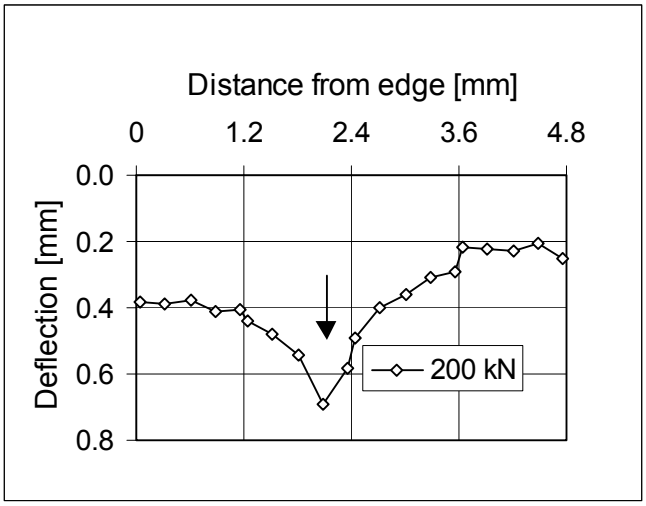

Fig. 13. PF400:2. Deflection measured by transducers 11–30 at maximum load.

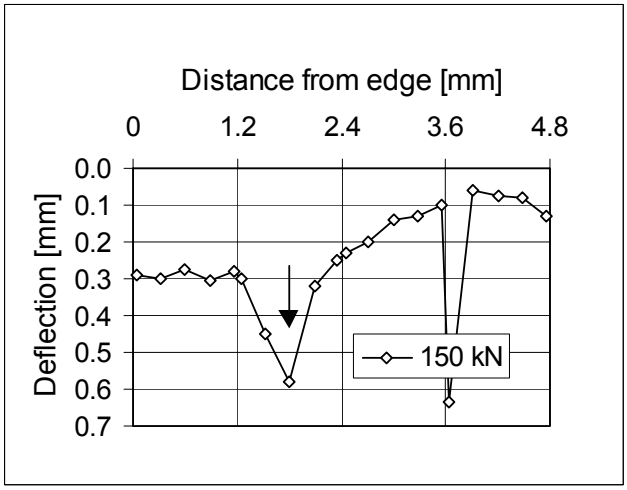

Fig. 14. PF400:3. Deflection measured by transducers 11–30 at maximum load. Transducer 26 (fifth from the right) out of action, see also App. C, Fig. 27.

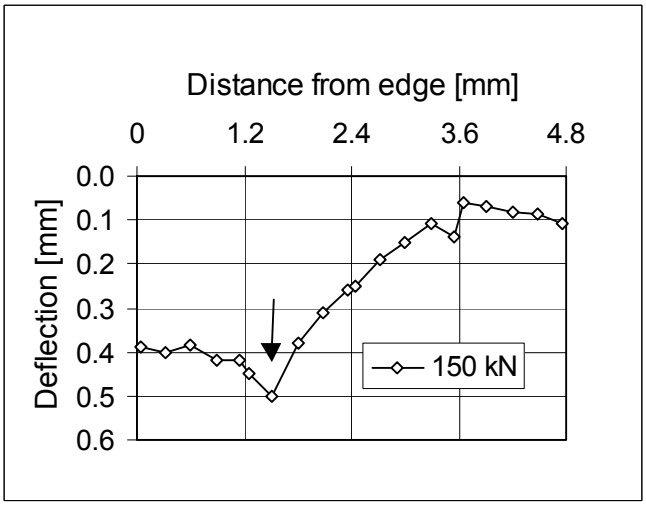

Fig. 15. PF400:4. Deflection measured by transducers 11–30 at maximum load.

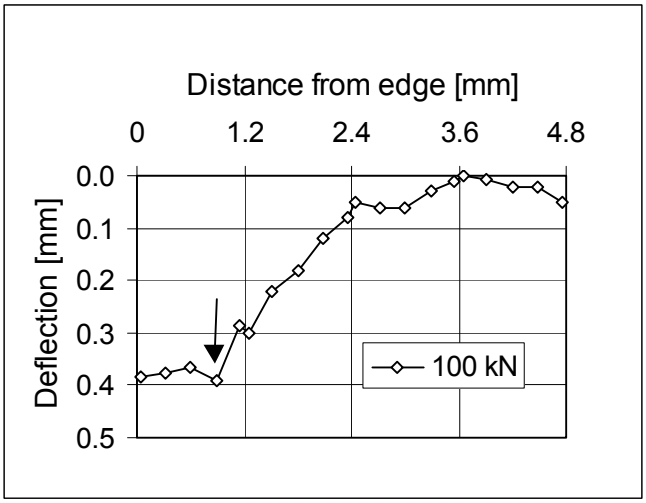

Fig. 16. PF400:5. Deflection measured by transducers 11–30 at maximum load.

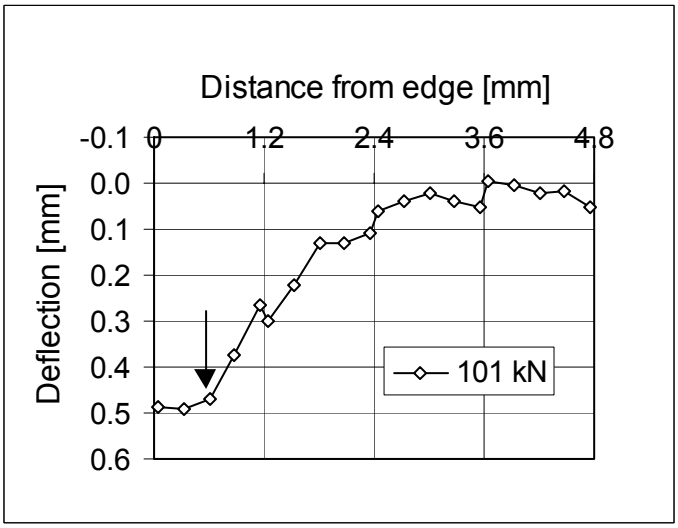

Fig. 17. PF400:6. Deflection measured by transducers 11–30 at maximum load.

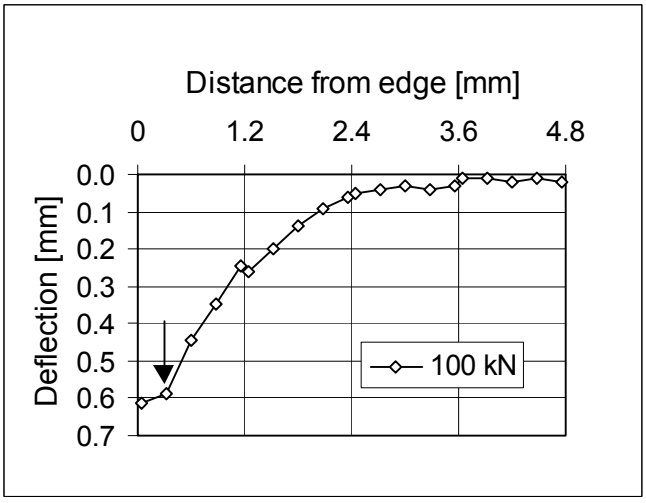

Fig. 18. PF400:7. Deflection measured by transducers 11–30 at maximum load.

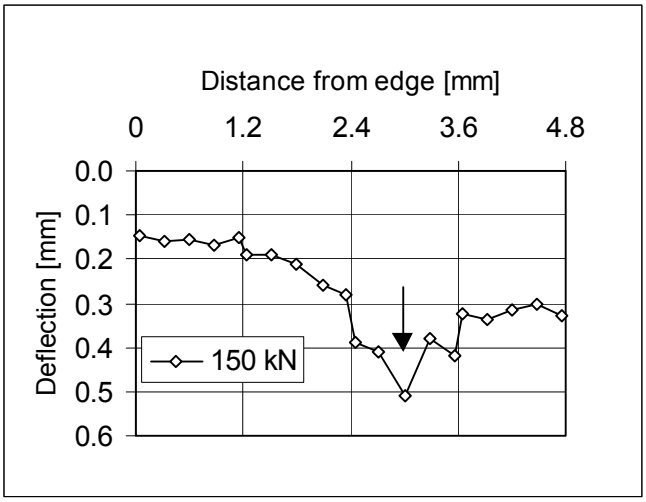

Fig. 19. PF400:8. Deflection measured by transducers 11–30 at maximum load.

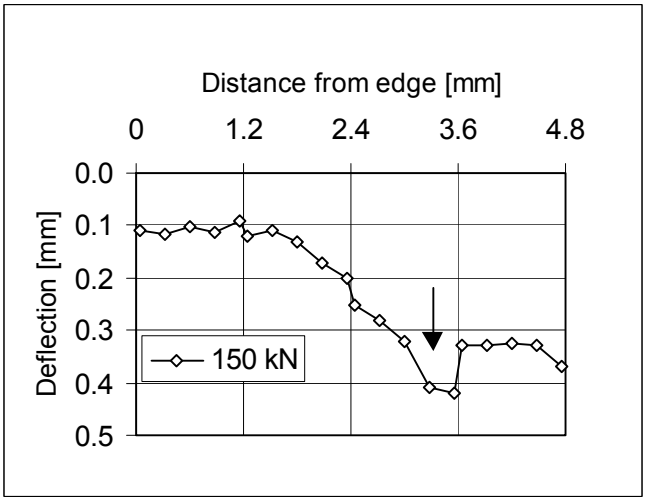

Fig. 20. PF400:9. Deflection measured by transducers 11–30 at maximum load.

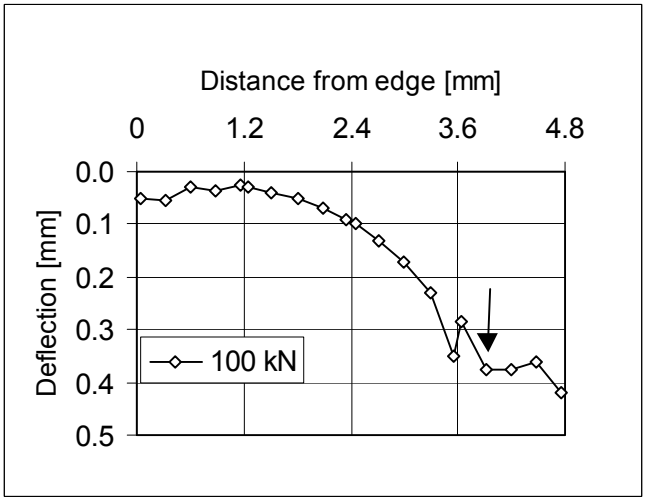

Fig. 21. PF400:10. Deflection measured by transducers 11–30 at maximum load.

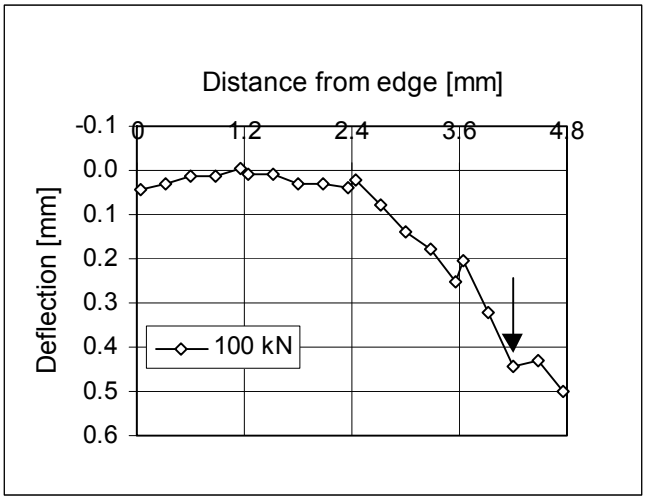

Fig. 22. PF400:11. Deflection measured by transducers 11–30 at maximum load.

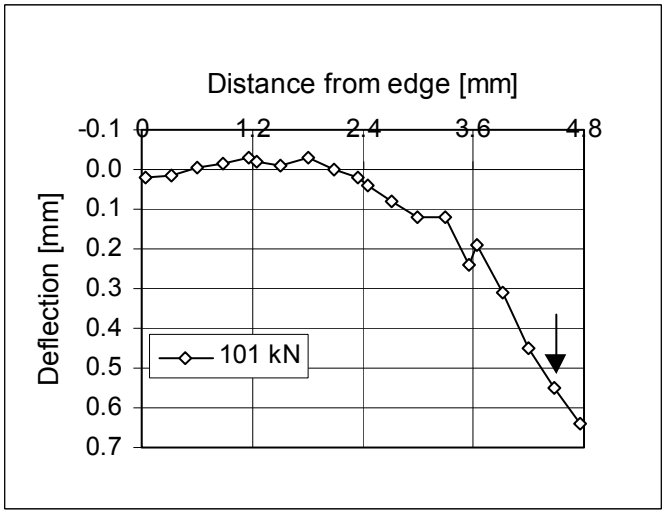

Fig. 23. PF400:12. Deflection measured by transducers 11–30 at maximum load.

3.2 Failure tests

In test PF400:13 the floor was loaded with one point load. The failure mode was punching failure. To avoid this unintended failure mode in the remaining failure tests, the floor was loaded with two point loads in tests PF400:14 and PF400:15. In all three tests the load was increased monotonously until failure load. All measuring devices were zero-balanced before each test.

The load vs. time relationship as well as the measured strains, crack widths and displacements are given graphically in App. C. The failure loads are summarized in Fig. 24. The cracking patterns are illustrated in Figs 25–27 and in App. A, Figs 9–15, 17–26 and 31–36. See also Table 8 in which the observations made during the tests are

documented. The joint between the slab ends and cast in situ concrete remained uncracked, if some very thin shrinkage cracks are ignored, but there was a crack along the plastic sheet shown in Fig. 6 along the whole length of both supporting beams.

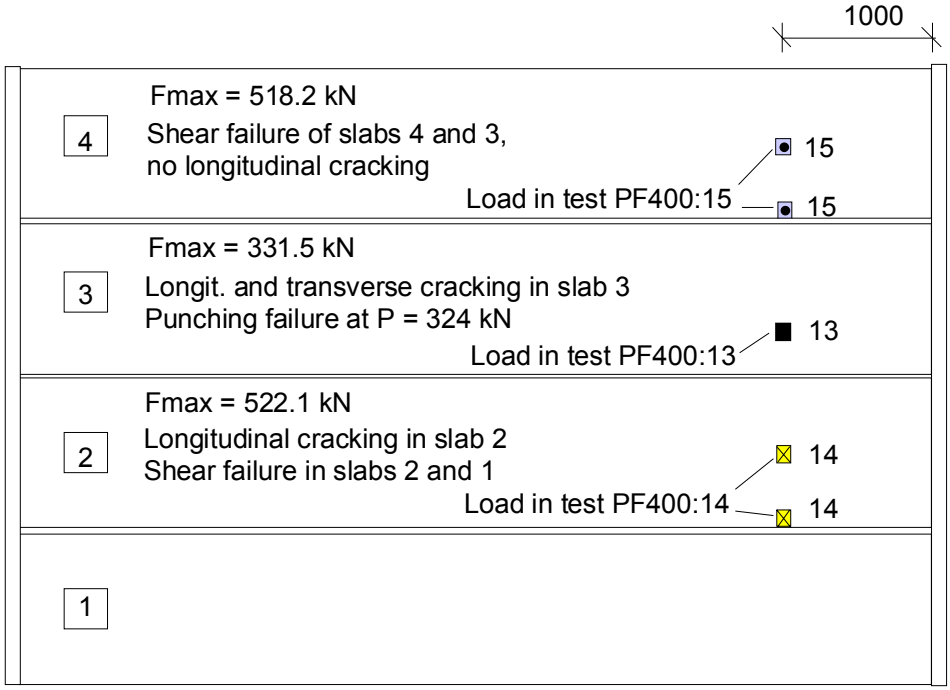

Fig. 24. Maximum imposed load F_{max} and failure mode in failure tests.

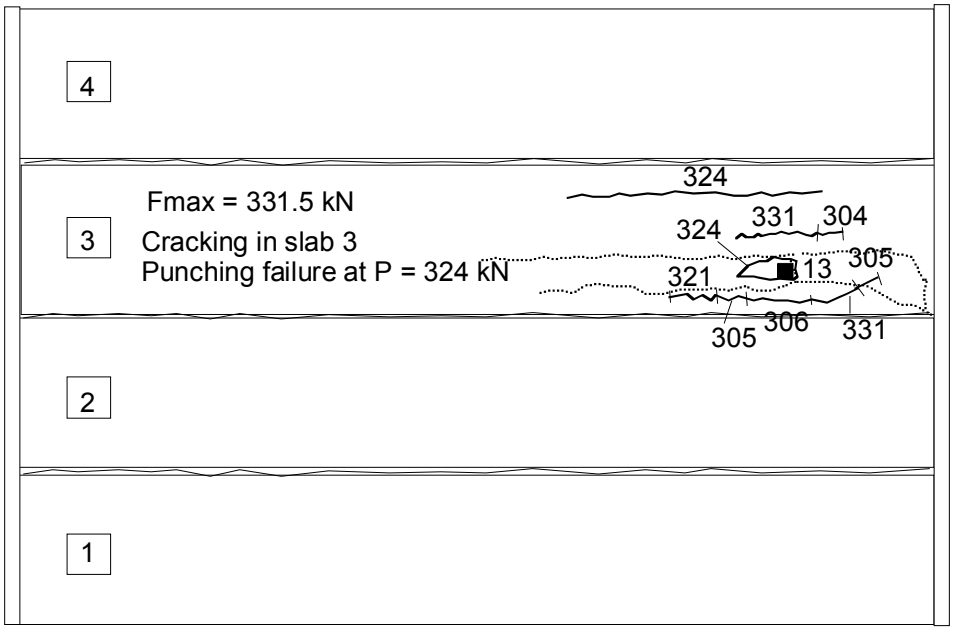

Fig. 25. Cracks observed during test PF400:13. The numbers refer to actuator force P when the crack became visible. The continuous and dashed lines represent cracks on the top and bottom surface, respectively.

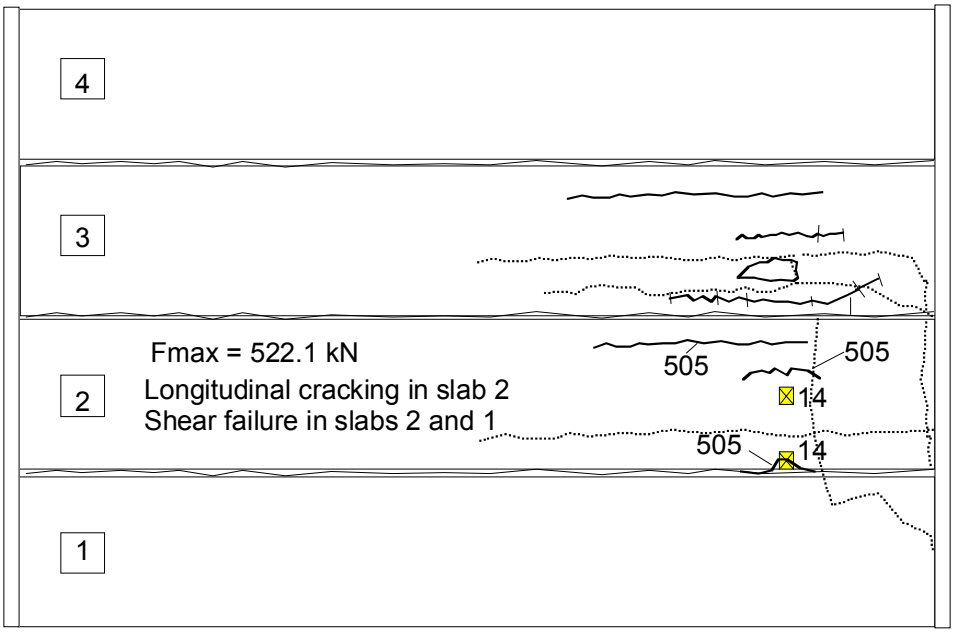

Fig. 26. Cracks observed during test PF400:14. The numbers refer to actuator force P when the crack became visible. The continuous and dashed lines represent cracks on the top and bottom surface, respectively.

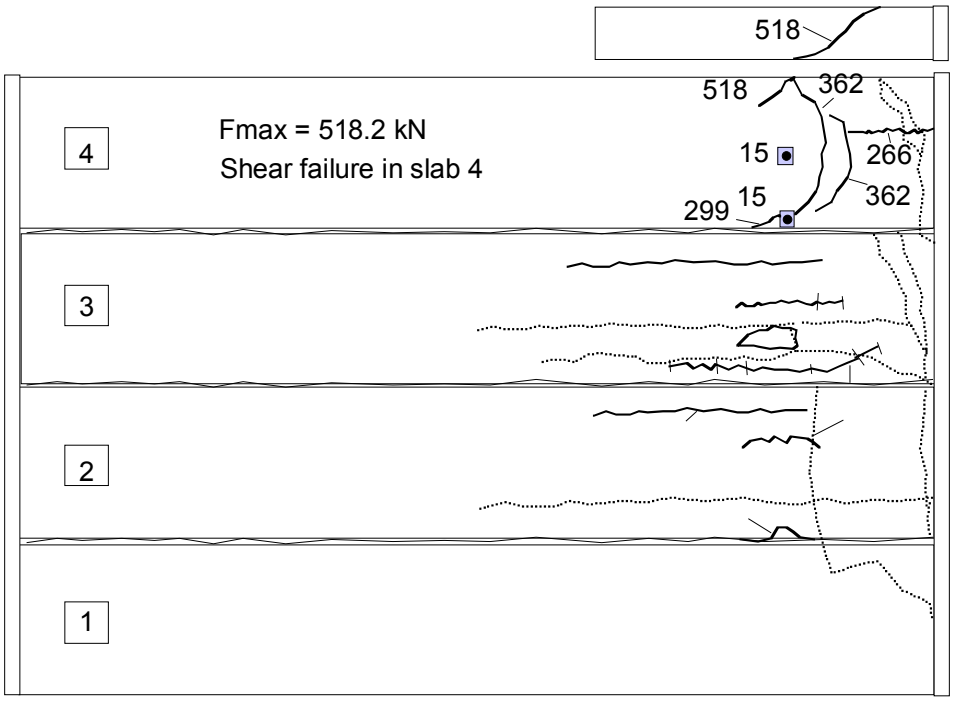

Fig. 27. Cracks observed during test PF400:15. The numbers refer to actuator force P when the crack became visible. The continuous and dashed lines represent cracks on the top and bottom surface, respectively.

As in tests with service load, the ascending part of the load-deflection curves for the span (transducers 11–30) was bilinear in many cases, see Appendices C and D. Furthermore, the

initial parts of the curves in tests PF400:13 and PF400:14 are close to those in tests PF400:1 and PF400:4. This is difficult to explain by cracking of the concrete but it may be attributable to the possible tilting of the supporting beams, which was not measured.

At maximum load, the displacements measured along the transverse line close to the loads were small, in all tests less than 3.5 mm. The settling of the supports was also negligible, the highest value being of the order of 0.3 mm. The measured strains in the reinforcement of the tie beam were also small. Their highest value corresponded to the stress 90 MPa in the steel in test PF400:15, but in other tests the stresses were below 12 MPa.

The maximum change of crack width was of the order of 0.08 mm. This is much less than 0.3 mm which was the order of the crack width before the test series was started.

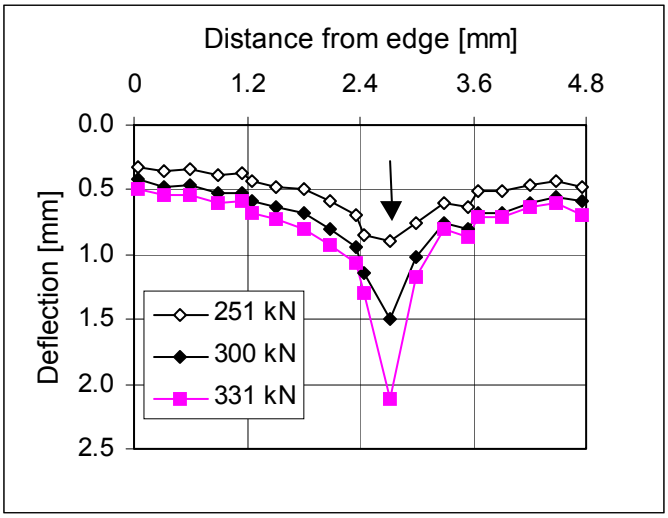

Fig. 28. PF400:13. Deflection measured by transducers 11–30 at different loads.

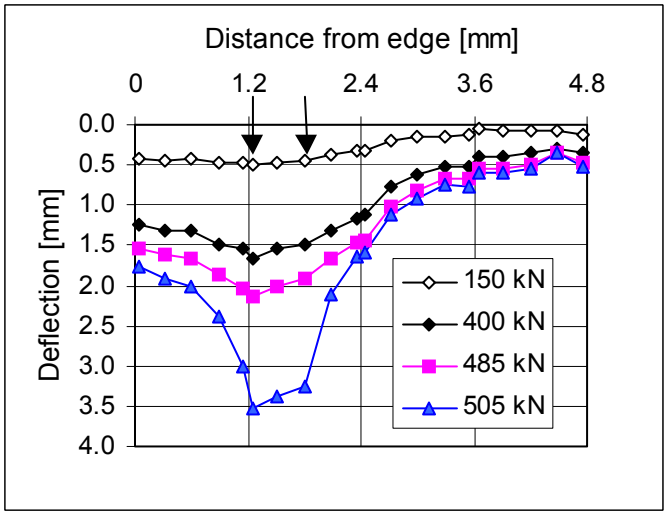

Fig. 29. PF400:14. Deflection measured by transducers 11–30 at different loads.

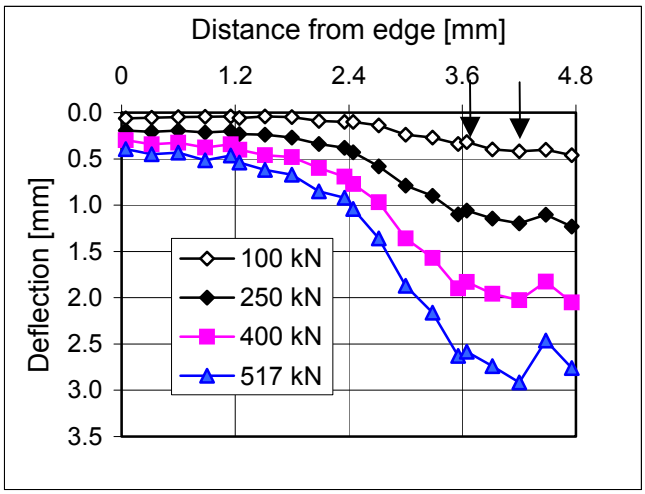

Fig. 30. PF400:15. Deflection measured by transducers 11–30 at different loads.

In Figs 31–33 the deflection measured in failure test is compared with the deflection measured in service load test. The deflections coincide rather well despite the permanent deformations and cracking which had taken place before the last two tests were started.

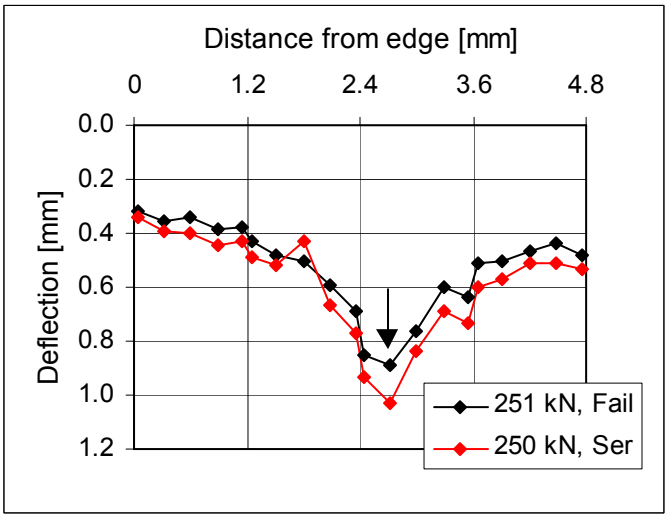

Fig. 31. Tests PF400:1 (Ser) and PF400:13 (Fail). Deflection measured by transducers 11–30 at load $P \approx 250$ kN.

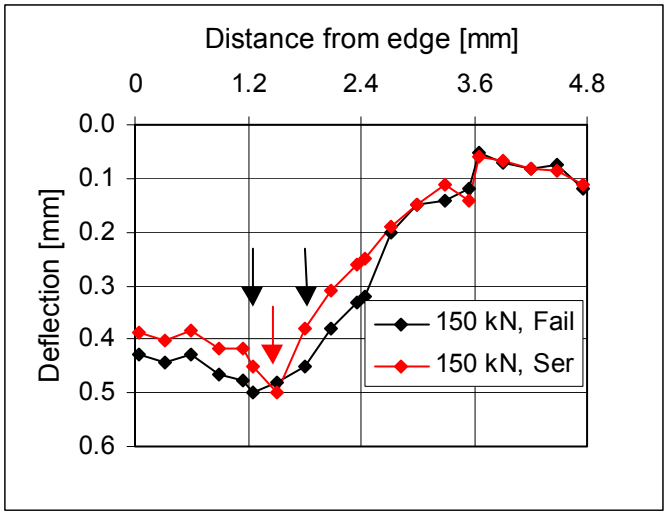

Fig. 32. Tests PF400:4 (Ser) and PF400:14 (Fail). Deflection measured by transducers 11–30 at load P = 150 kN.

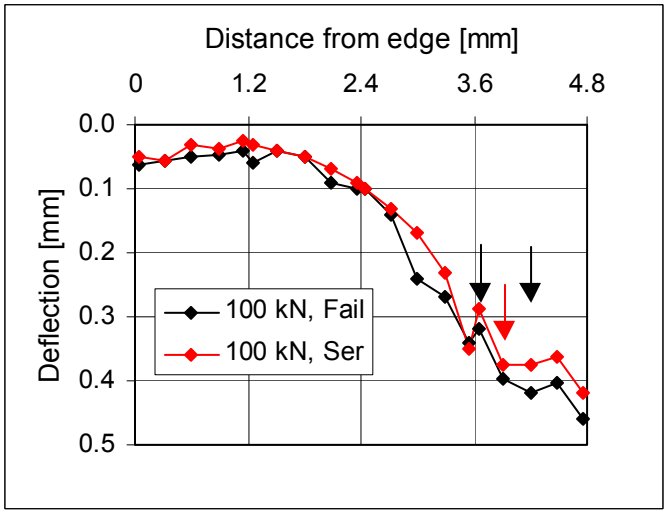

Fig. 33. Tests PF400:10 (Ser) and PF400:15 (Fail). Deflection measured by transducers 11–30 at load P = 100 kN.

4. Strength of concrete

The strength of the concrete was measured from 50 x 50 mmcores for the slab units and from 150 mm test cubes for the cast-in-situ concrete. The results are given in Tables 3–5. The cores were covered with plastic after drilling in such a way that they were still wet when tested. The test cubes were kept in the same temperature and relative humidity as the floor test specimen until testing.

Table 3. Strength and density of 50x50 mm cores drilled from slab units 2 and 3 and tested on 9th of October 2002.

Specimen	Strength MPa	Density kg/m3
21 (slab 2)	75.5	2440
22 (slab 2)	67.0	2430
23 (slab 2)	71.5	2430
31 (slab 3)	79.0	2450
32 (slab 3)	79.0	2440
33 (slab 3)	77.0	2440
Mean x	74.8	2438
Standard deviation s	4.8	8
Characteristic strength $f_{ck,C50} = x - 1.65s$	66.8	

Table 4. Strength and density of 150 mm test cubes cast from grouting in the longitudinal joints and tested on 3rd of October 2002.

Specimen	Strength MPa	Density kg/m3
S1	37.5	2250
S2	38.5	2240
S3	38.0	2250
S4	39.5	2270
S5	39.0	2260
S6	38.0	2250
Mean x	38.4	2253
Standard deviation s	0.7	10
Characteristic strength $f_{ck,K150} = x - 1.65s$	37.2	

Table 5. Strength and density of 150 mm test cubes cast from grouting in the tie beams and tested on 3rd of October 2002.

Specimen	Strength MPa	Density kg/m3
P1	37.5	2260
P2	36.5	2260
P3	36.5	2240
P4	37.0	2270
P5	37.0	2230
P6	37.5	2260
Mean x	37.4	2253
Standard deviation s	1.1	15
Characteristic strength $f_{ck,K150} = x - 1.65s$	35.6	

5. Analysis of results

It is assumed that the strength measured from 50 mm drilled cores gives directly the cubic strength measured from 150 mm cubes and that the cylinder strength is equal to 85% of the cubic strength. In this way, the lower characteristic cylinder strength $f_{ck,C150}$ (150 x 300 mm cylinders) given in Table 6 is obtained. From this, the mean tensile strength

$$f_{ctm} = 2{,}12 \ln\left(1 + \frac{f_{ck} + 8MPa}{10MPa}\right) \tag{1}$$

is obtained according to Eurocode 2 [2].

Table 6. Strength $f_{c,C50}$ measured from 50 mm cores, corresponding cylinder strength $f_{c,C150}$ and mean tensile strength f_{ctm}.

	$f_{c,C50}$ MPa	$f_{c,C150}$ MPa	f_{ctm} MPa
PF400	66.8	56.8	4.27

To give an impression about the shear resistance observed in tests PF400:13–PF400:15, a virtual load test PFR400 is analysed according to the product standard EN 1168 [1]. In this test a single slab element, identical to those in floor test and with similar support conditions, is loaded with a line load P at a distance of 1.0 m from slab end. It is assumed that the critical point is at the mid-depth of the cross-section and at a distance of 280 from the slab end (200 mm from the inner edge of the support). Since Eurocode 2 does not state clearly, which value can be regarded as the mean transfer length, two different values, 395 and 700 mm, are used for the transfer length. It is not clear, either, what would be the exact value for the loss of prestress. Therefore, calculations are made with two values: 5% and 10% of the initial prestressing force.

The cross-sectional characteristics of the slab are calculated from the nominal cross-section shown in Fig. 34 with the exception that the measured value 276 mm, see App. B, is used for b_w, the sum of the web widths. In this way, the values given in Table 7 are obtained. In addition to the support reaction due to the imposed load $P_{u,pre}$, $V_{u,pre}$ also includes the support reaction due to the dead weight of the slab.

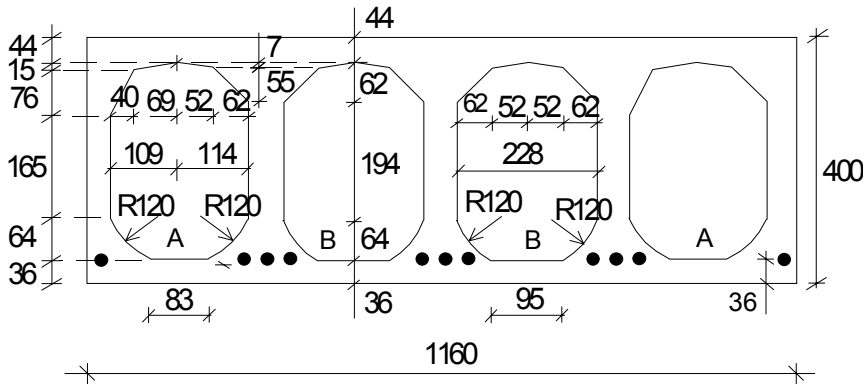

Figure 34. Geometry used for calculating A, S and I.

Table 7. Virtual shear test PF400R. Distance from centroid of strands to the bottom fibre e_p, distance from centroidal axis to bottom fibre e, sum of web widths b_w, cross-sectional area A, second moment of area I and first moment of area above centroidal axis S, assumed transfer length l_b, Assumed loss of prestress and predicted shear resistance $V_{u,pre}$ (shear force at support).

	e_p	e	b_w	A	I	S	l_b	*Loss*	$P_{u,pre}$	$V_{u,pre}$
	mm	mm	mm	mm^2	mm^4	mm^3	mm	%	kN	kN
PF400R	35	200	276	210800	$4.43 \cdot 10^9$	$1.41 \cdot 10^7$	395	5	551	493
	"	"	"	"	"	"	395	10	495	488
	"	"	"	"	"	"	700	5	545	445
	"	"	"	"	"	"	700	10	491	441

Comparison of the calculated resistances $V_{u,pre}$ indicates that the exact value of the loss is of little importance but the transfer length plays a major role. In Table 7 also the imposed load $P_{u,pre}$ corresponding to the shear resistance is given. It is of the same order as the eccentric failure loads in tests PF400:14 and PF400:15.

In Table 8 the obtained resistances for different failure tests, virtual test PFR400 included, are compared.

Table 8. Failure load $F_{max} = P_{max} + P_{eq}$ (P_{max} is the actuator force, P_{eq} is the weight of loading equipment), its eccentricity e and description of response. $P_{eq} = 0.8$ kN for tests PF400:14 and PF400:15. For other tests $P_{eq} = 0.3$ kN.

	F_{max} kN	e mm	Observations
PF400:13 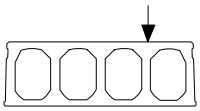	331.5	283	First cracks on the top of the floor at P = 305 kN. Load decreased with increasing displacements until P = 289 kN and started to increase again. At P = 331 kN there was a drop to 303 kN. The load could still be increased until at 324 kN a punching failure took place.
PF400:14 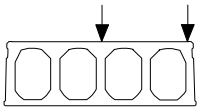	522.1	283	Shear or shear torsion failure in slabs 2 and 1 at P = 521 kN. With decreasing load at P = 505 kN cracks could be seen on the top surface.
PF400:15 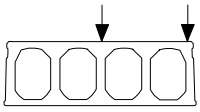	518.2	283	At P = 266 kN a short longitudinal crack on the top of slab 4, see Fig. 27. At P = 517 kN shear failure in slab 4, but the load could still be kept at P = 340–360 kN for a longer period.
ST400E1M[1)] 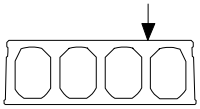	264.8	283	Shear-torsion failure, test on a single slab unit supported on mortar bearing.
PFR400 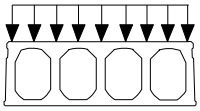	491–551	0	*Virtual test on a single slab unit*. Shear tension failure. F_{max} depends on assumed transfer length and loss of prestresss..

[1)] *See report [3]*

6. Discussion

The test specimens seemed to be typical of normal production. The strength of the concrete was high enough and the slippage of the strands was small in all elements. The loading and measuring equipment worked as intended with some insignificant exceptions.

The observed failure loads were higher than expected on the basis of the design practice presented in EN 1168 [1]. In the first failure test with one point load, a punching failure took place instead of the desired shear-torsion failure. In the remaining two failure tests with two point loads each, the failure mode was shear-torsion failure. In these two tests the local failure in the previous test(s) may have slightly reduced the observed resistance, but it is on the safe side to use the observed resistances as the real ones.

In view of the obtained high failure loads, the loads in most service load tests might have been higher. On the other hand, the response of the floor was so linear in the failure tests that increasing the maximum loads in the service load tests would not have affected the observed stiffness too much.

In most tests the load-deflection relationship looked bilinear in such a way that at the beginning the response was considerably stiffer than thereafter. It is not easy to explain this behaviour by clamping of the slab ends at the beginning and subsequent cracking because the bilinearity did not disappear after the first test. In fact, it was there still in the failure tests PF400:13–PF400:15 as shown in App. D in which the initial parts of the load-deflection curves are presented not only for the failure tests but also for the corresponding service load tests. Other possible explanations are hysteresis and tilting or horizontal sliding of the supporting beams along the supporting floor. The tilting or sliding cannot be confirmed by measurements because the horizontal displacements of the beams were not measured.

References

1. EN 1168. Precast concrete products – Hollow core slabs. 2005.

2. EN 1992-1-1. Eurocode 2: Design of concrete structures – Part 1: General rules and rules for buildings. 2004.

3. Pajari, M. Shear-torsion interaction tests on single hollow core slabs. Espoo 2004. VTT Research Notes 2275. 76 p. + app. 122 p. http://www.vtt.fi/inf/pdf/tiedotteet/2004/T2274.pdf

Appendix A: Photographs

The numbers on the surface of the slabs refer to the actuator load. They tell the load at which the crack grew until the indicated position.

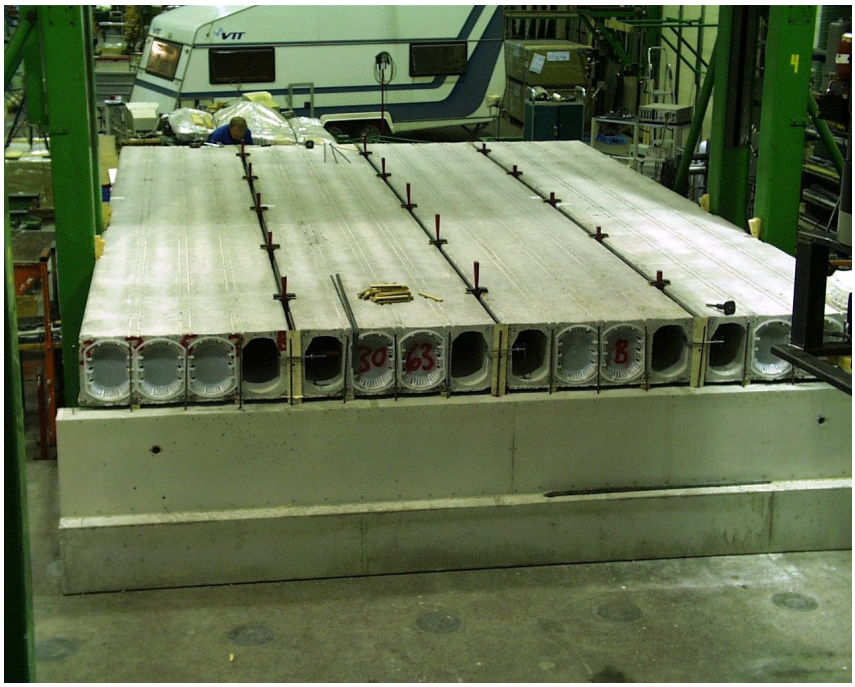

Fig. 1. Arrangements before jointing.

Fig. 2. Design of wedging equipment to create longitudinal cracks in the joints.

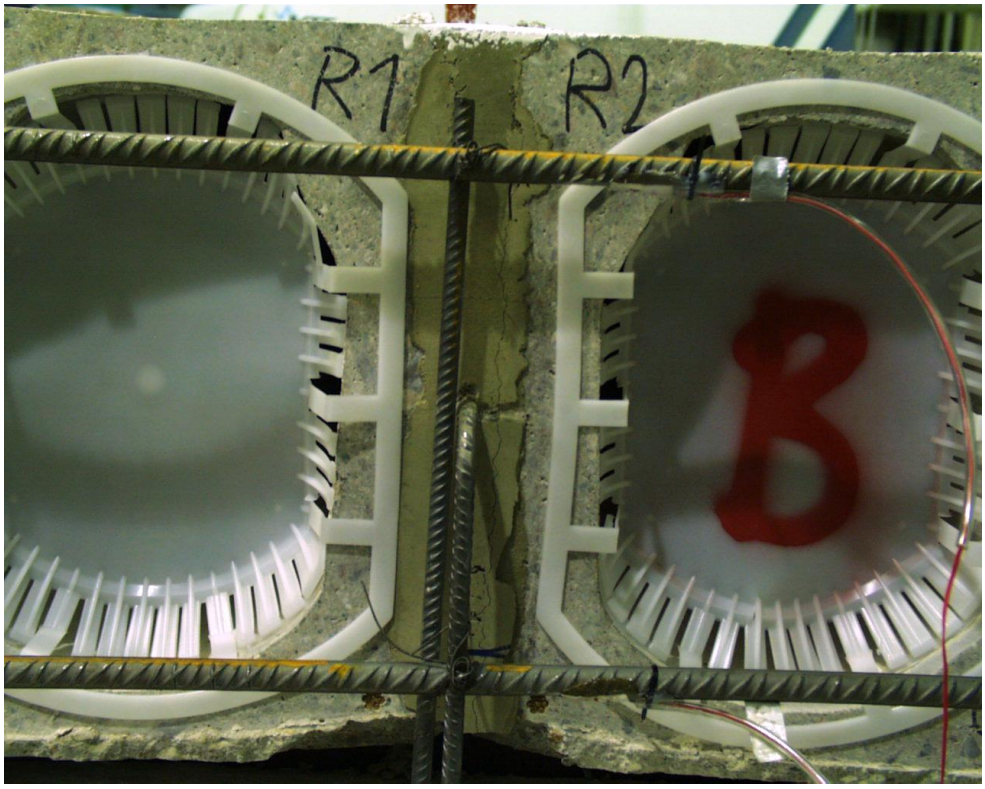

Fig. 3. Crack in joint due to wedging.

Fig. 4. Crack in joint due to wedging.

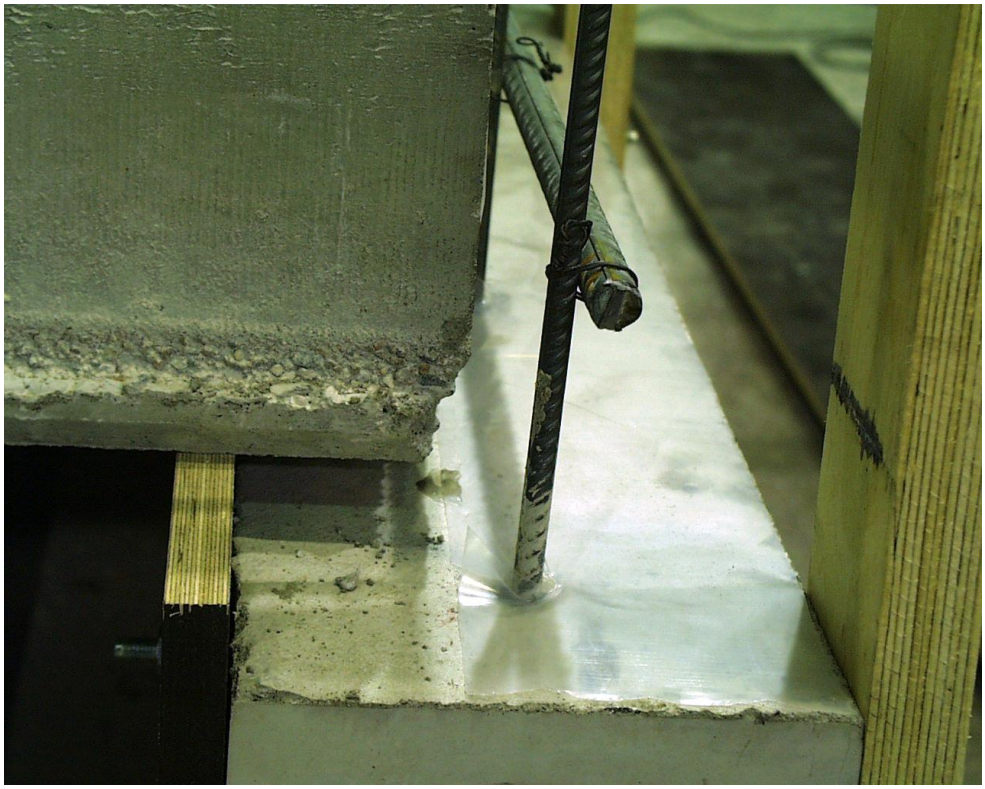

Fig. 5. Top surface of beam before grouting. Note the plastic sheet.

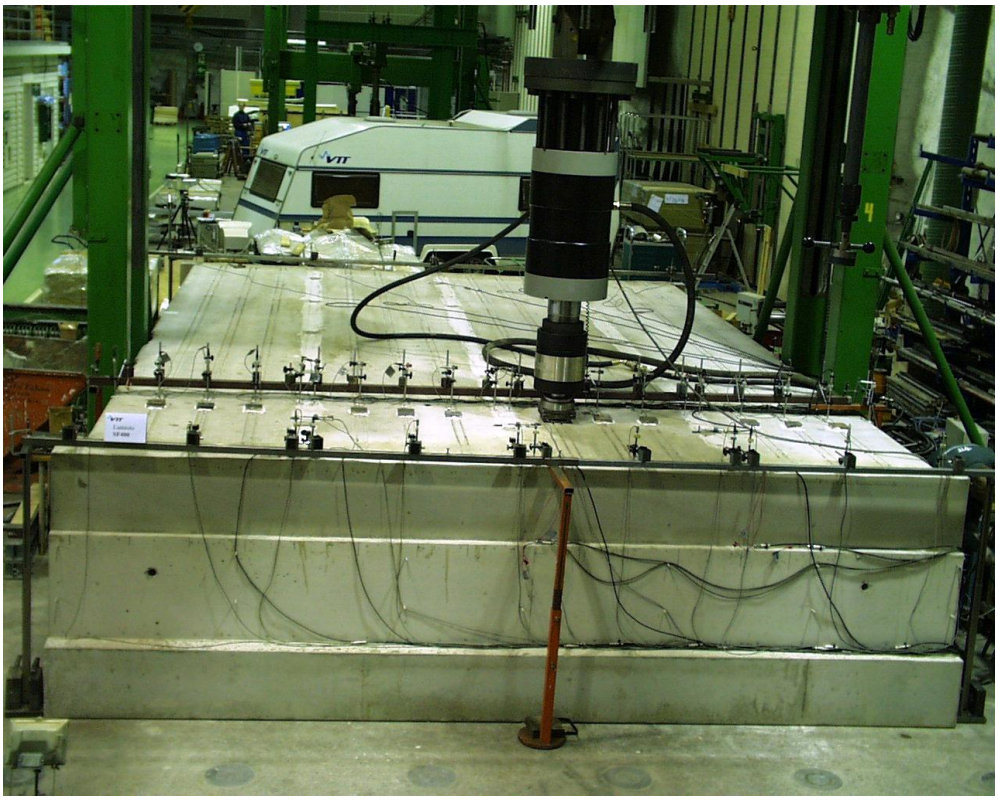

Fig. 6. Overview on test arrangements.

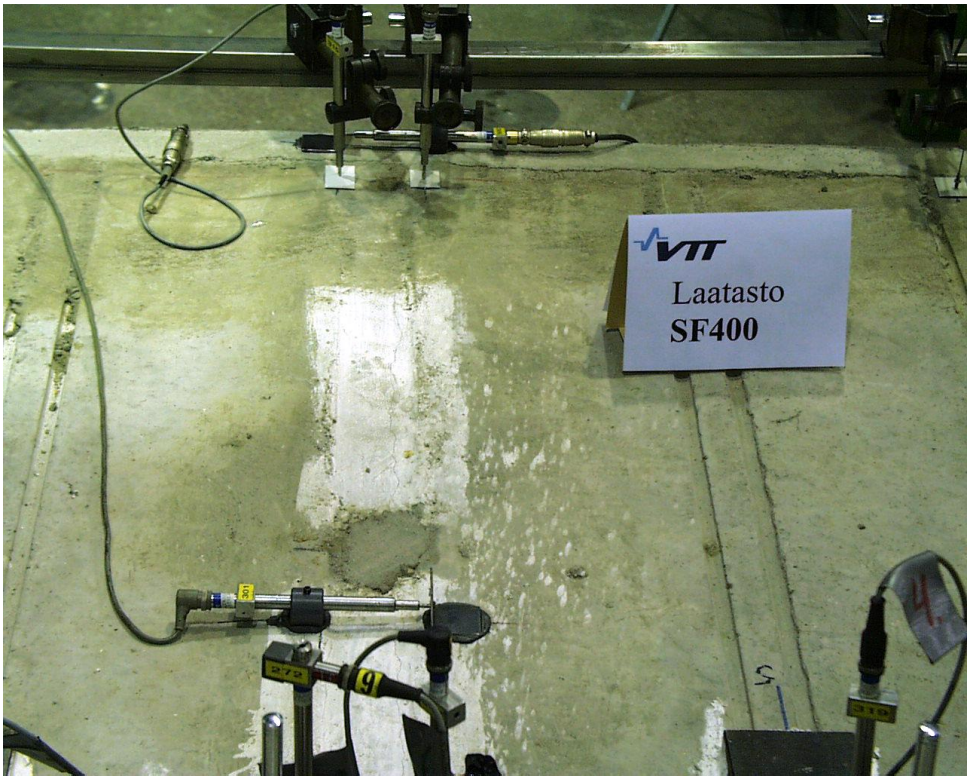

Fig. 7. Horizontal transducers for measuring crack opening.

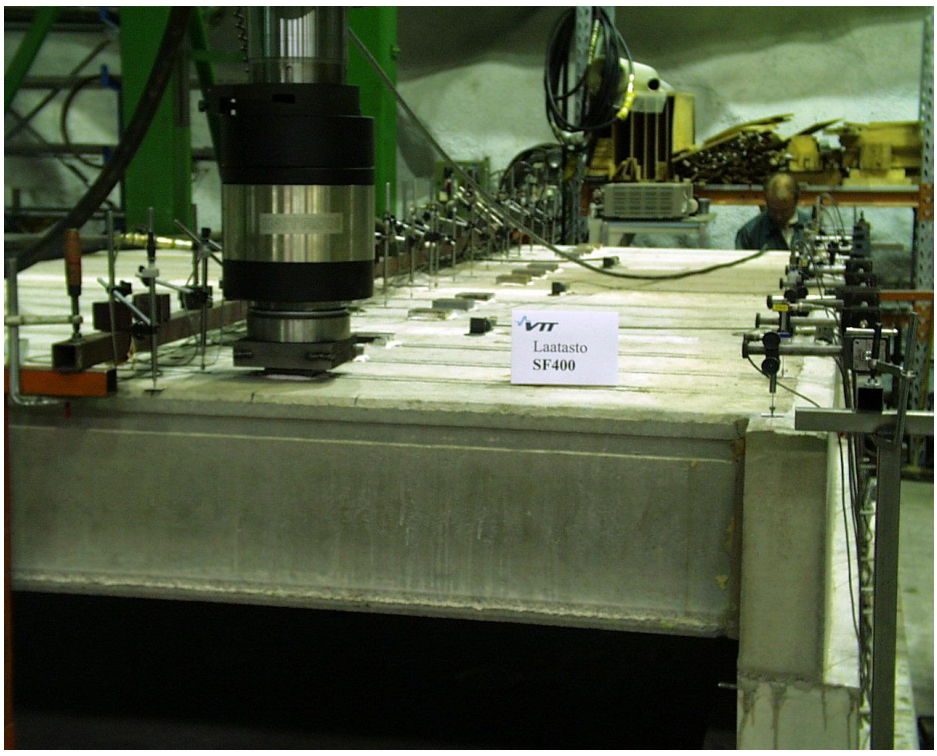

Fig. 8. Load at the edge of the floor.

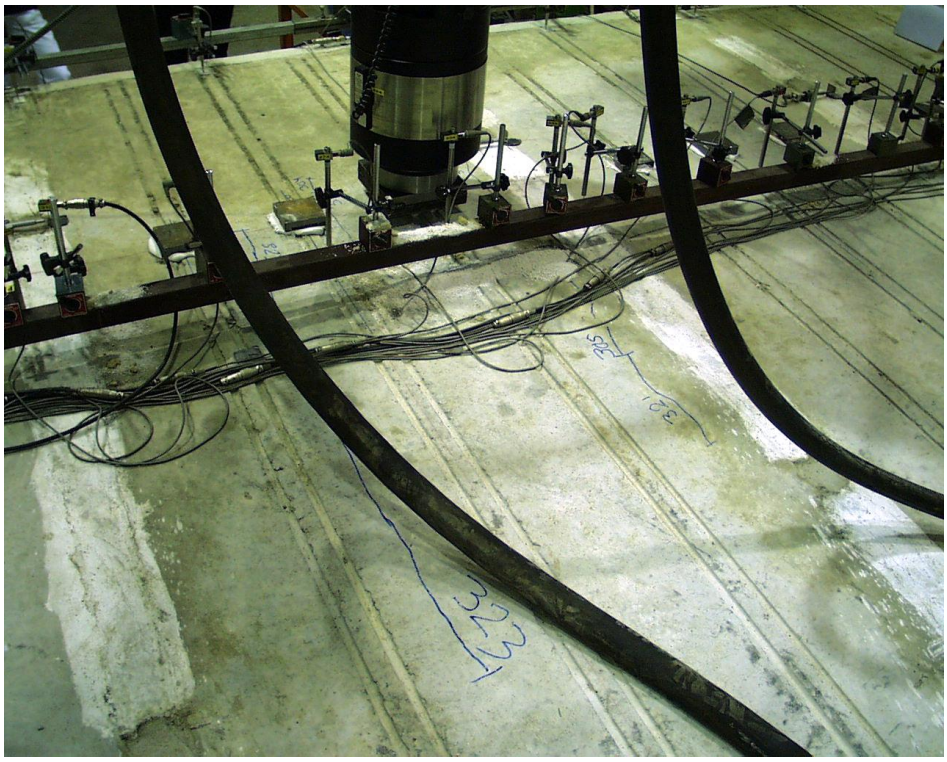

Fig. 9. PF400:13. Cracks after failure.

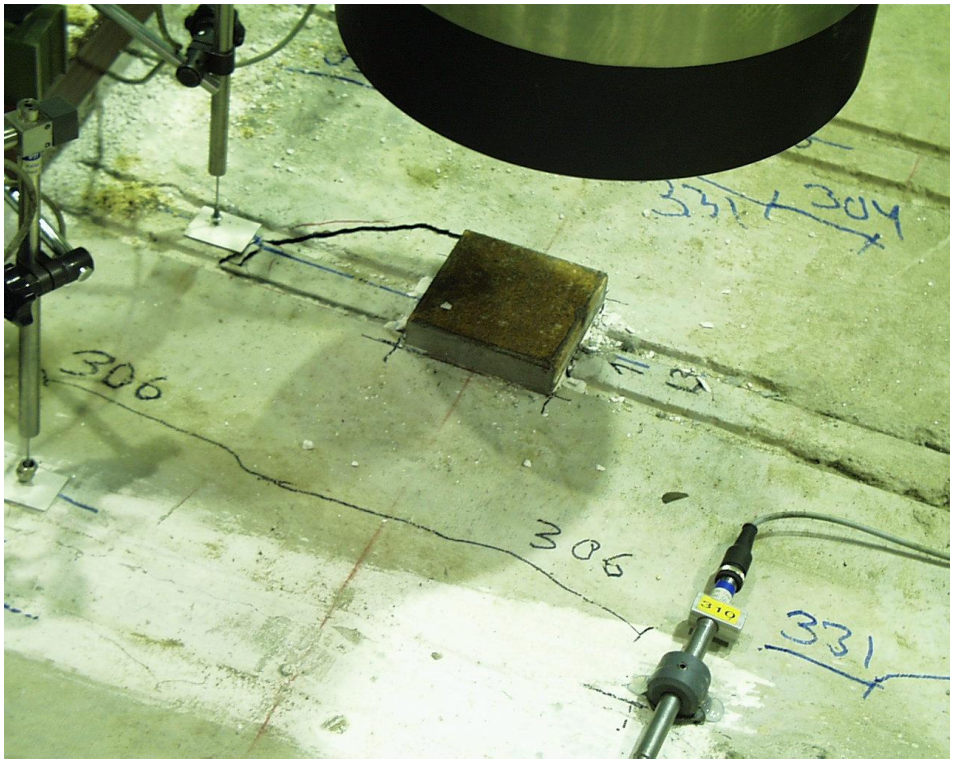

Fig. 10. PF400:13. Cracks after failure.

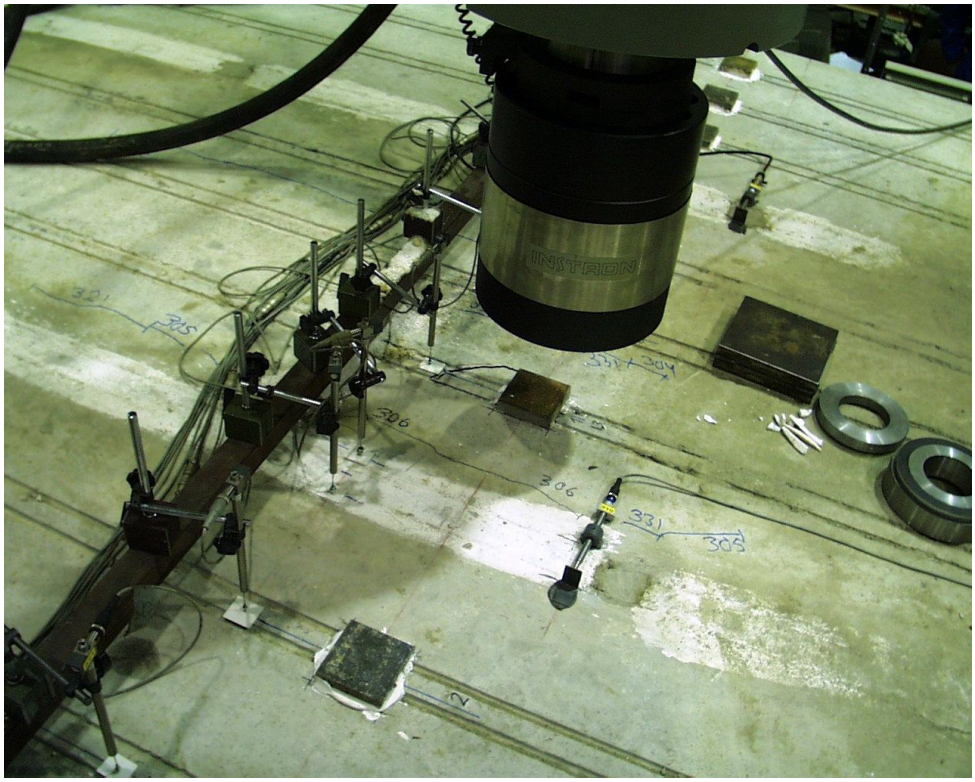

Fig. 11. PF400:13. Cracks after failure on the top.

Fig. 12. PF400:13. Cracks in soffit of slab 3 after failure.

Fig. 13. PF400:13. Cracks in soffit of slab 3 after failure.

Fig. 14. PF400:13. Longitudinal cracks in soffit of slab 3 after failure.

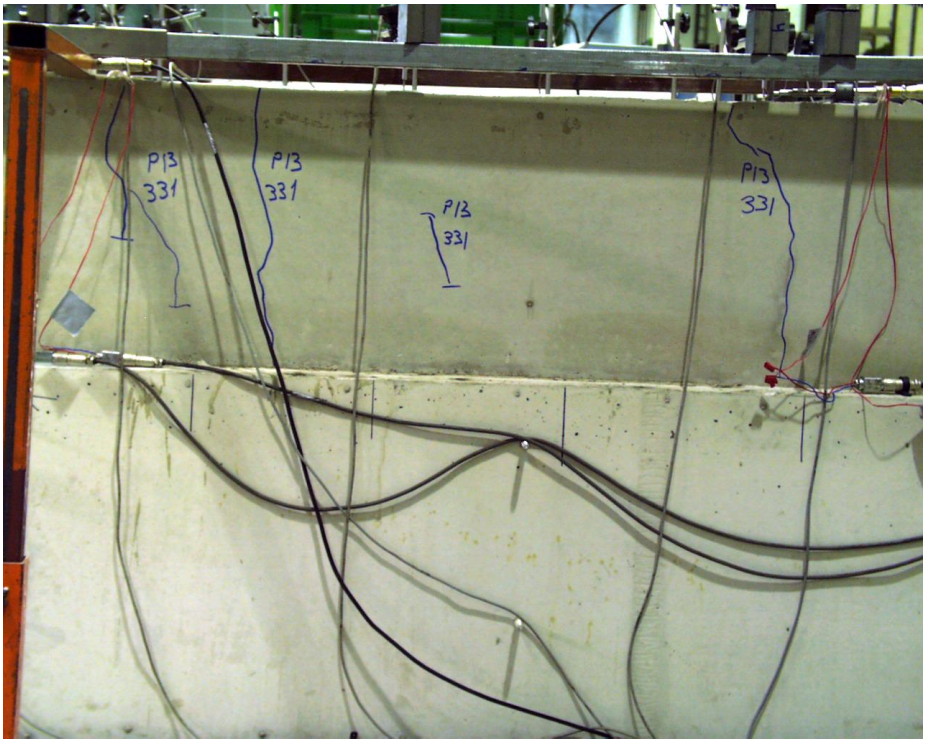

Fig. 15. PF400:13. Cracks in tie beam at the loaded end after failure.

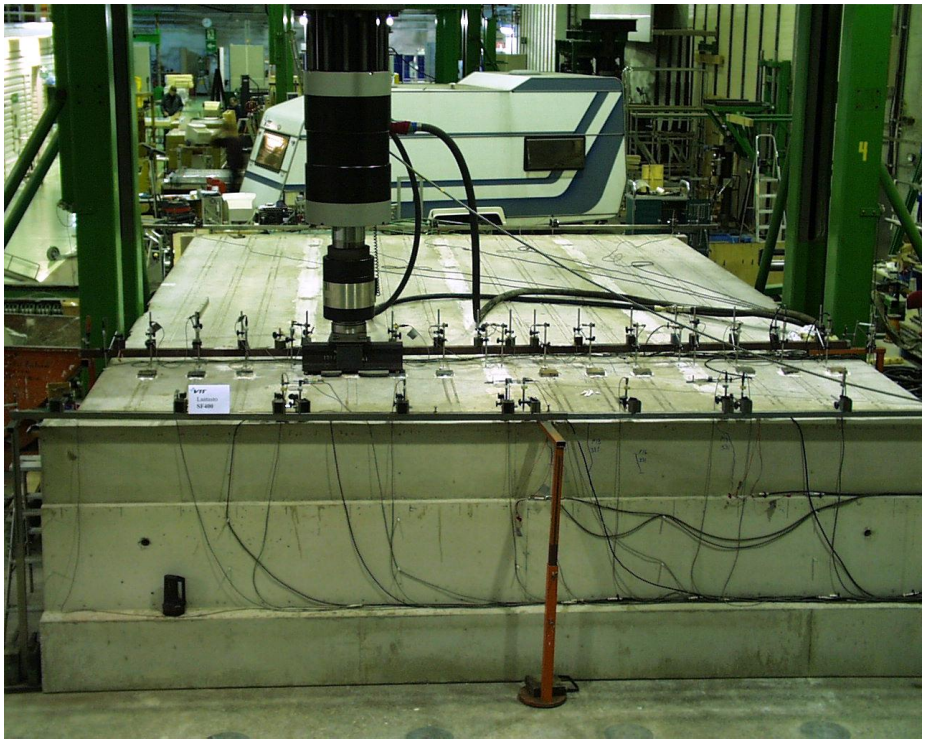

Fig. 16. PF400:14. Overview on arrangements.

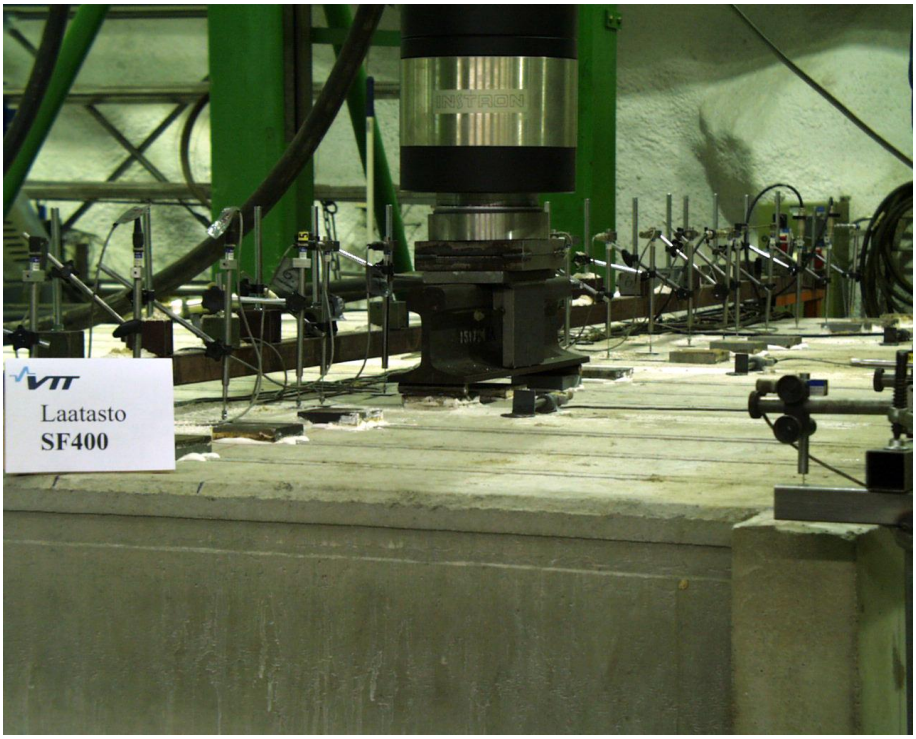

Fig. 17. PF400:14. View on loading details.

Fig. 18. PF400:14. Cracks in tie beam at the loaded end shown in red colour.

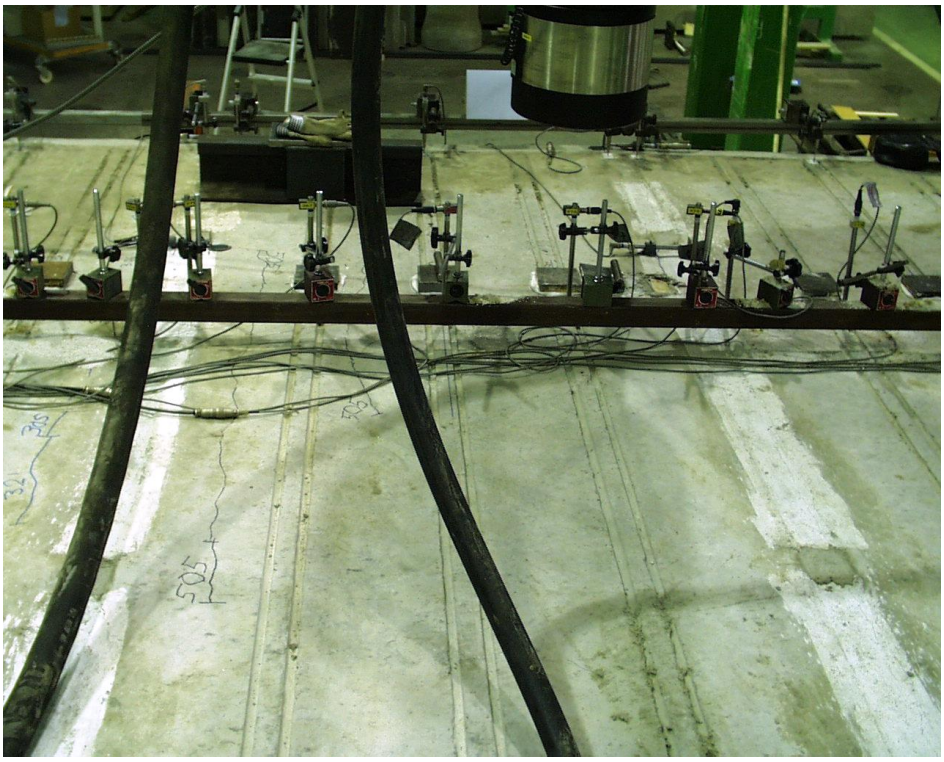

Fig. 19. PF400:14. Cracks after failure.

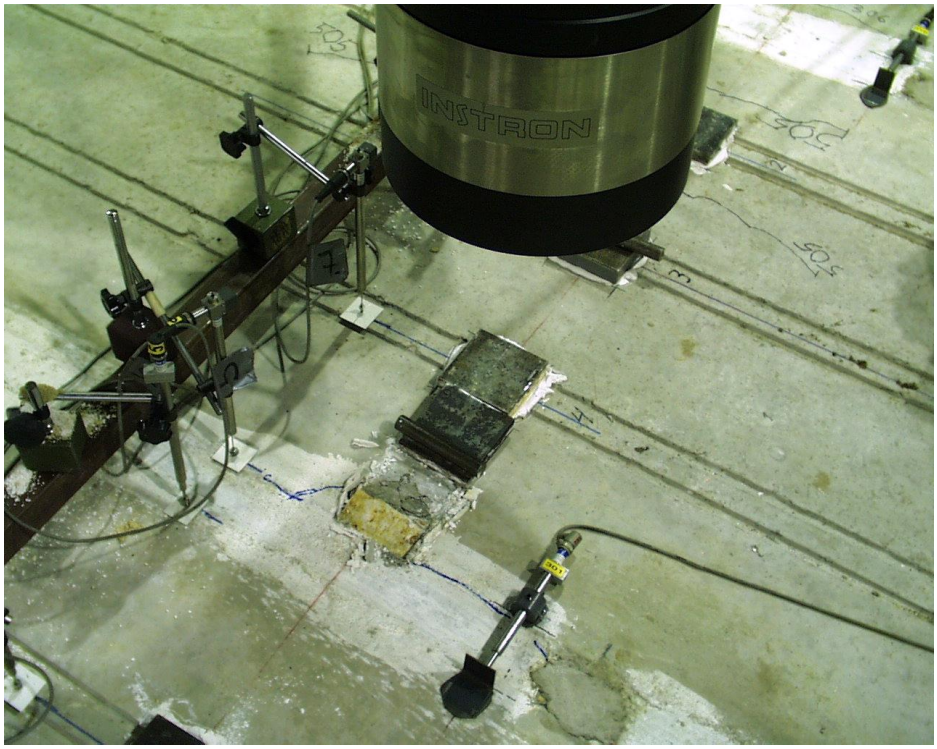

Fig. 20. PF400:14. Cracks after failure.

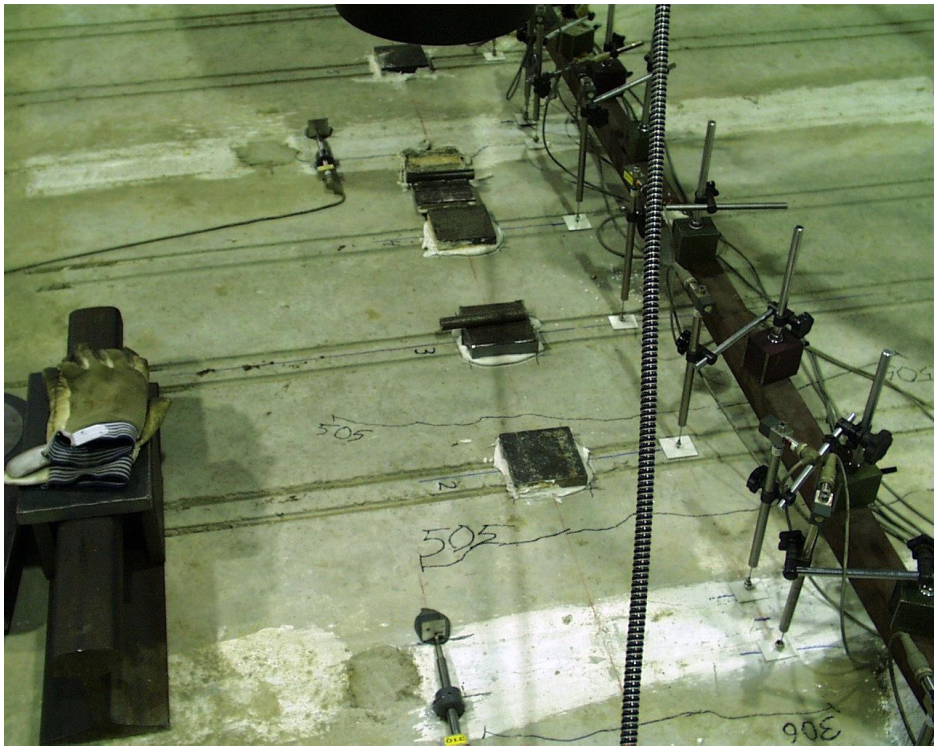

Fig. 21. PF400:14. Cracks after failure.

Fig. 22. PF400:14. Soffit after failure. Slab 1 in the front.

Fig. 23. PF400:14. Soffit after failure. Slab 2 on the left, slab 1 on the right.

Fig. 24. PF400:14. Soffit after failure. Slab 2 on the left, slab 1 on the right.

Fig. 25. PF400:14. Soffit after failure. Slab 1 in the front.

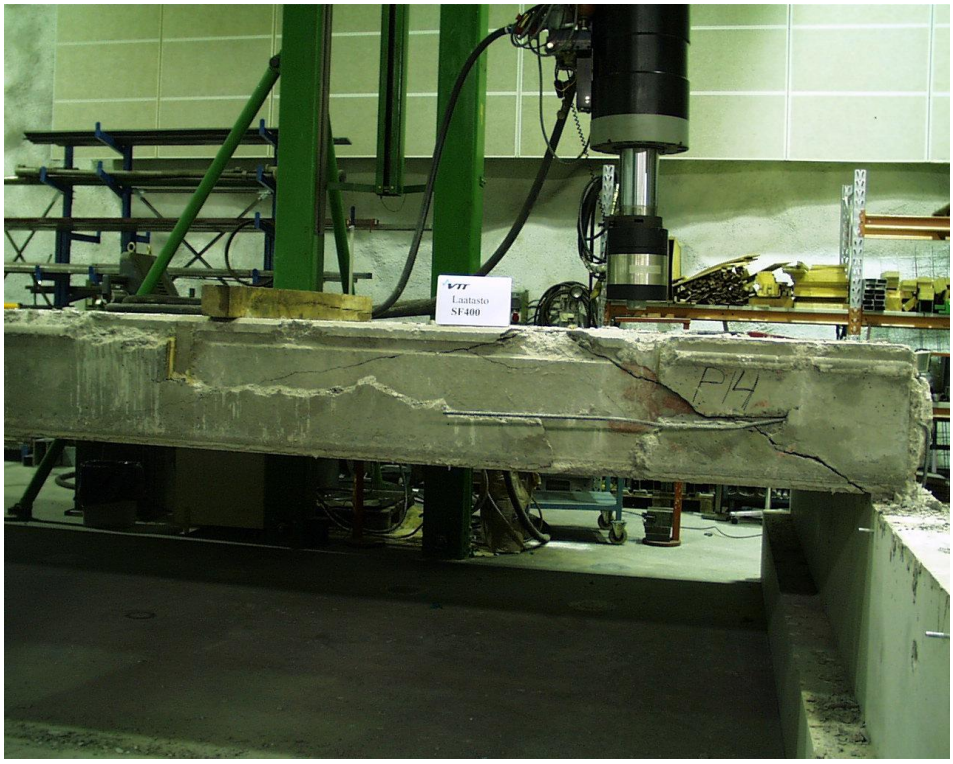

Fig. 26. PF400:14. PF400:14. Diagonal shear crack in slab 2 photographed after removal of slab 1.

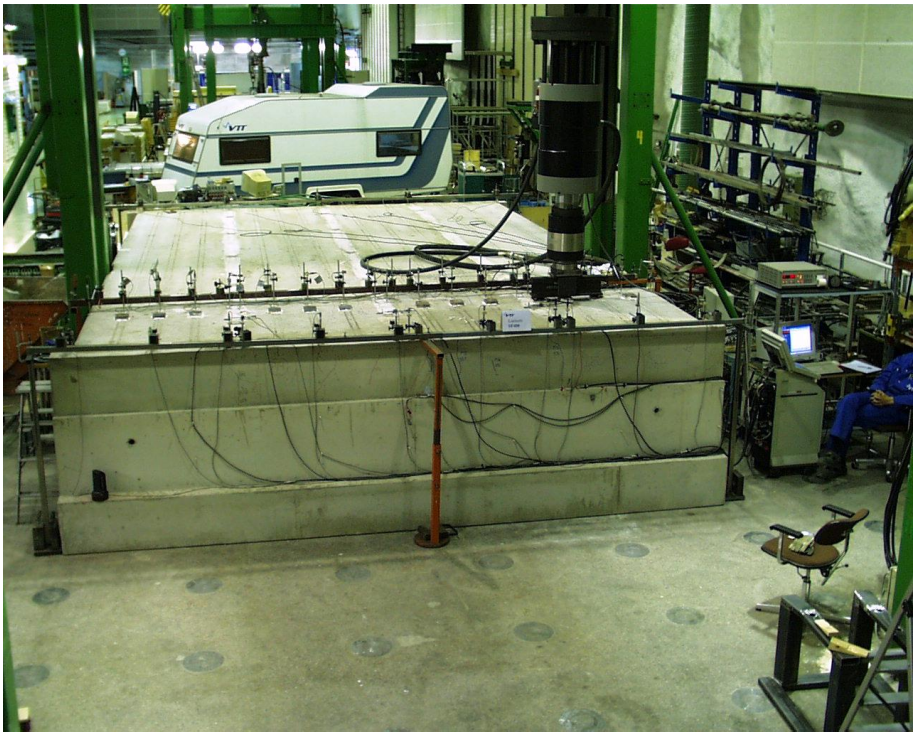

Fig. 27. PF400:15. Overview on arrangements.

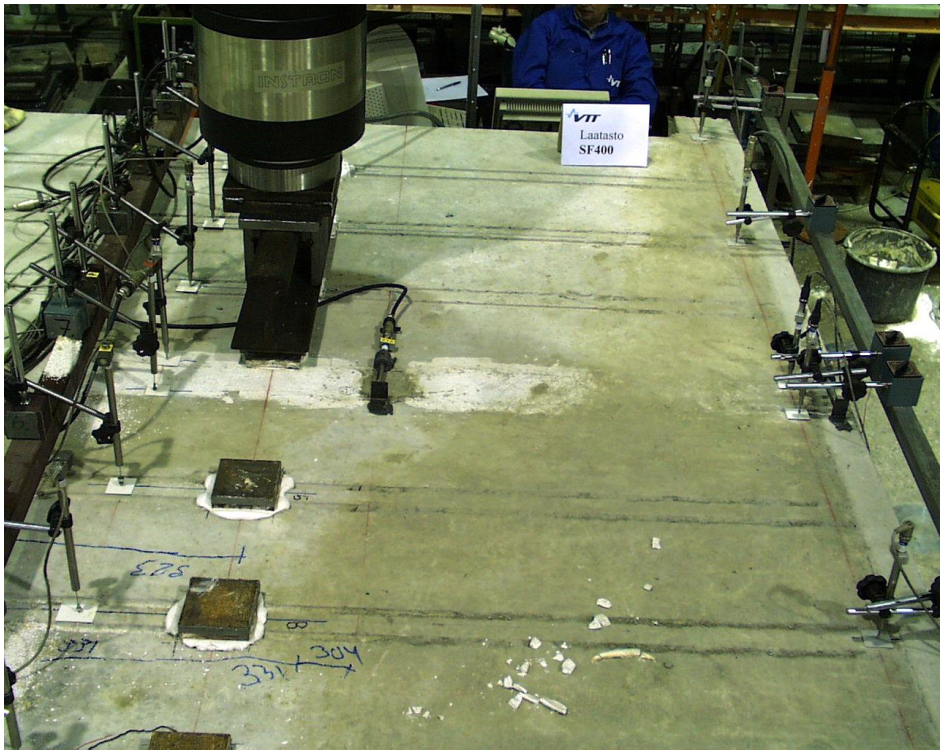

Fig. 28. PF400:15. Loading arrangements.

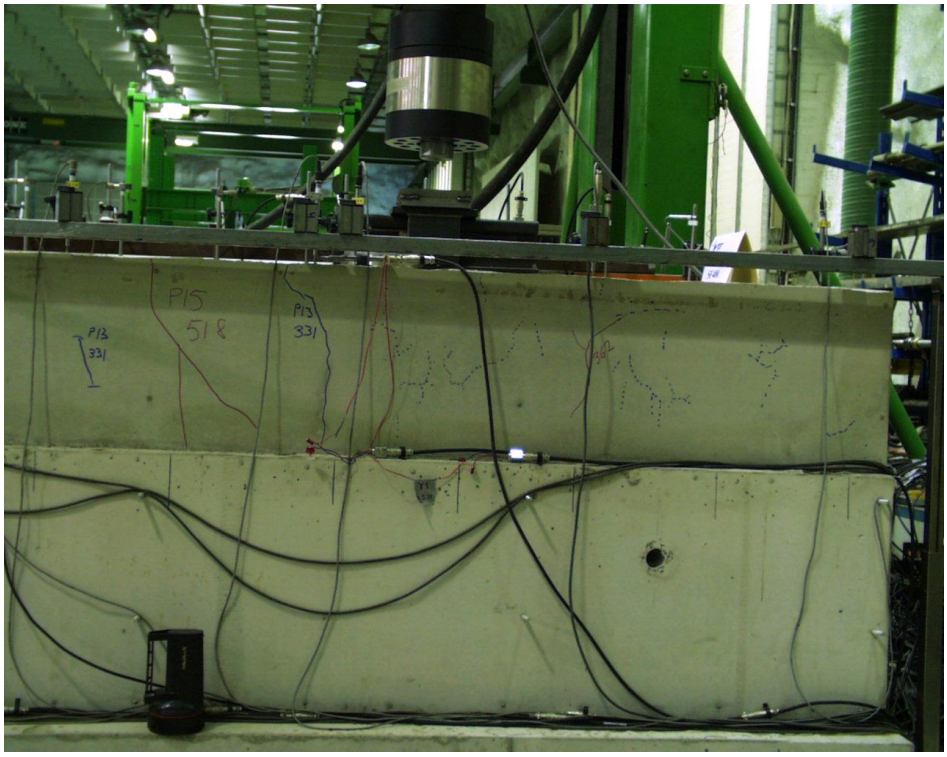

Fig. 29. PF400:15. Cracking pattern in Western tie beam after failure.

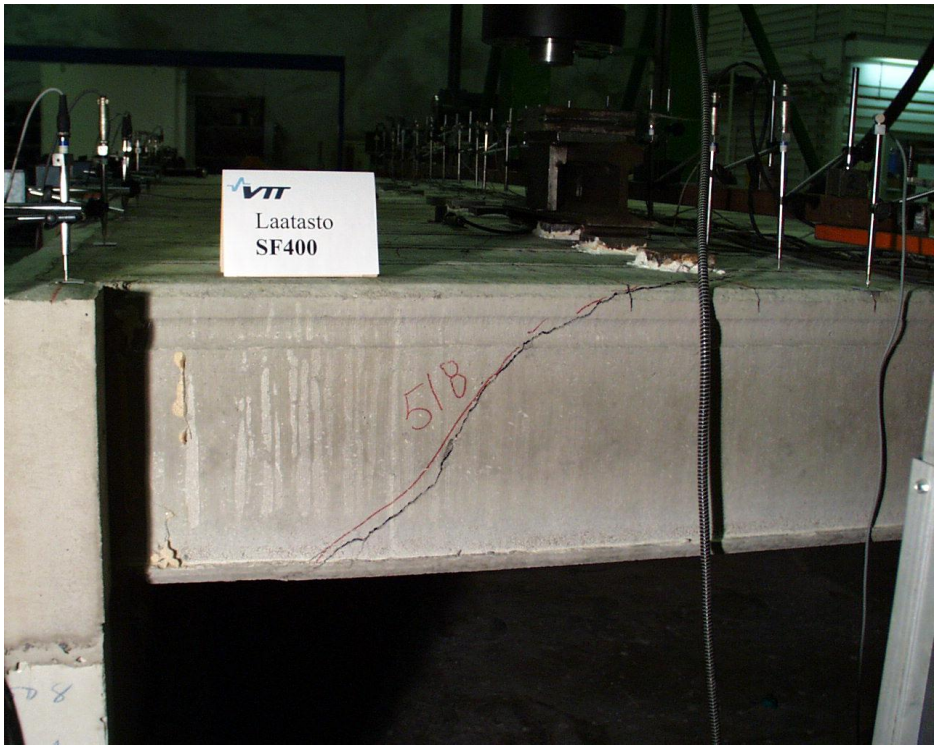

Fig. 30. PF400:15. Cracking after failure.

Fig. 31. PF400:15. Soffit of slab 4 after failure.

Fig. 32. PF400:15. Soffit of slabs 4 and 3 (in the rear) after failure.

Fig. 33. PF400:15. Soffit of slabs 4 (on the left) and 3 after failure.

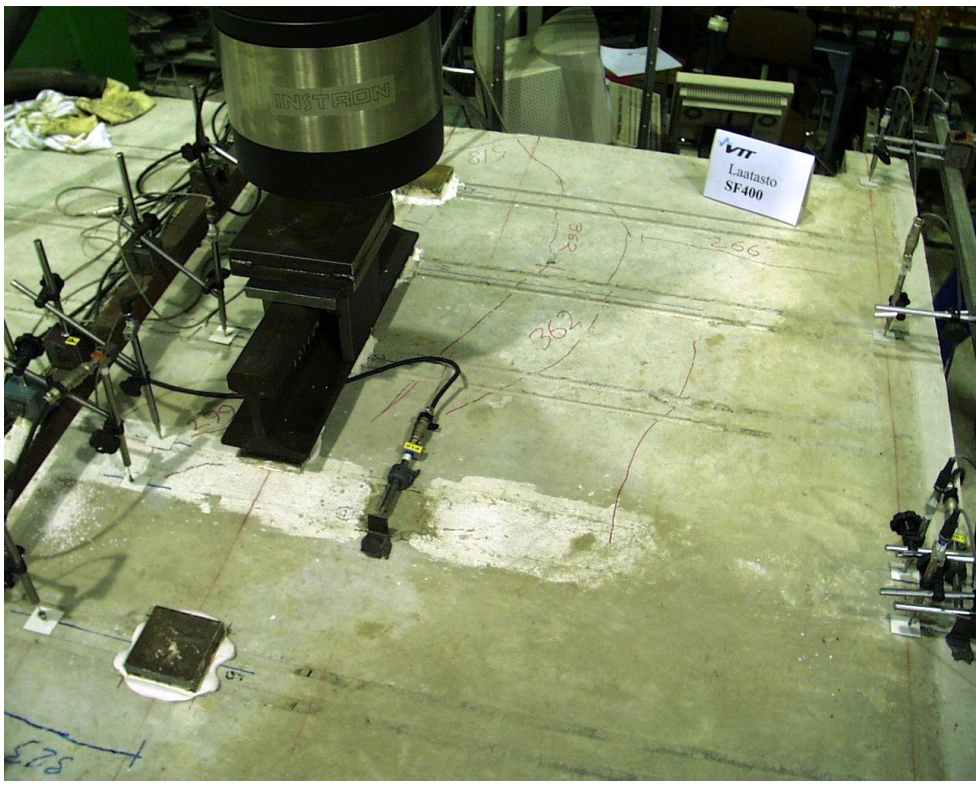

Fig. 34. PF400:15. Top surface after failure.

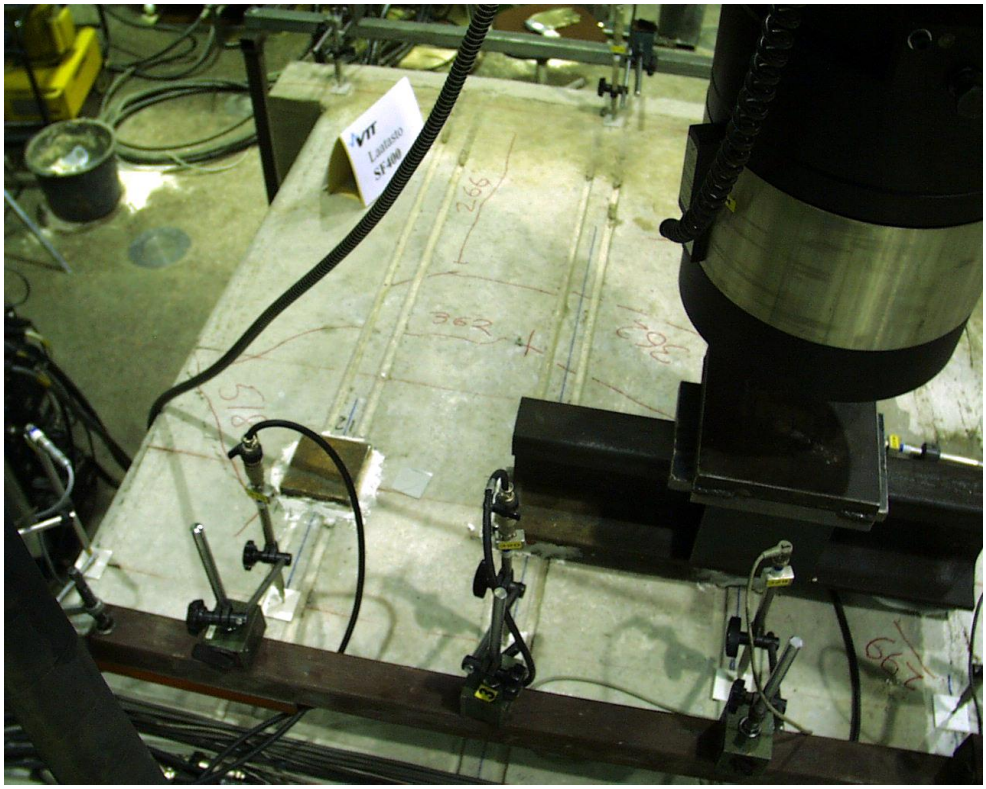

Fig. 35. PF400:15. Top surface after failure.

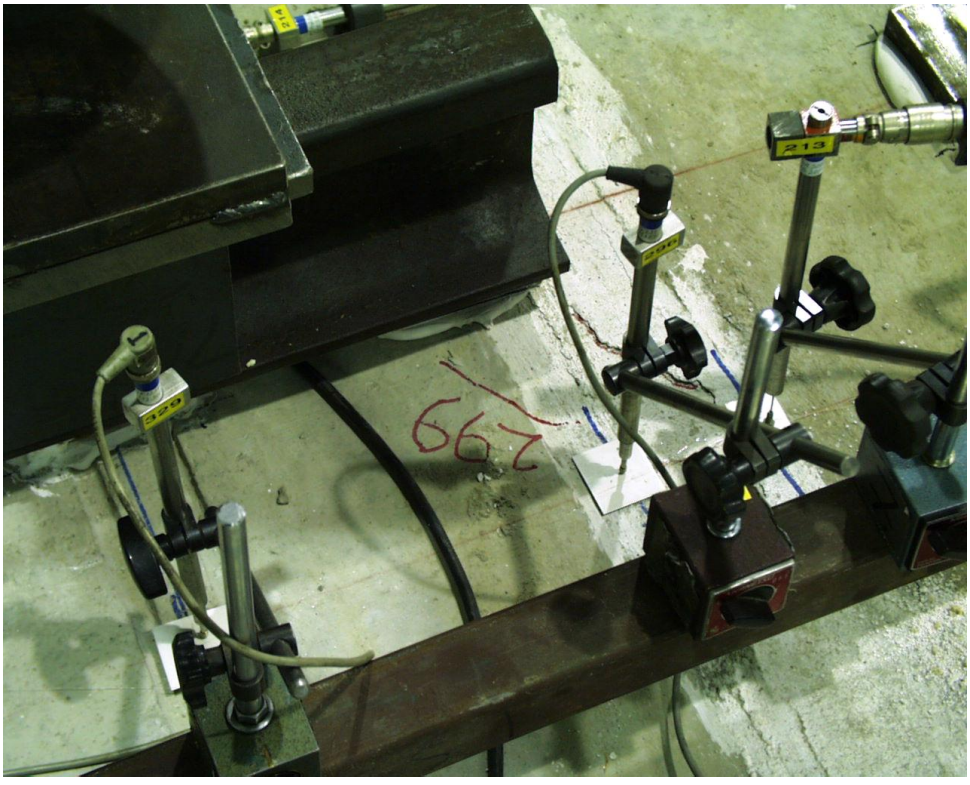

Fig. 36. PF400:15. Detail of top surface after failure.

Appendix B: Measured slab cross-sections

End 1 of slabs 1–4, see Figs 1–4, was the loaded end in floor test. The underlined figures give the measured spillage of the strands.

Slab 1

Lower strands : 11 d 12.5, prestress = 1000 MPa

Length : 7081 mm
Mass : 3600 kg

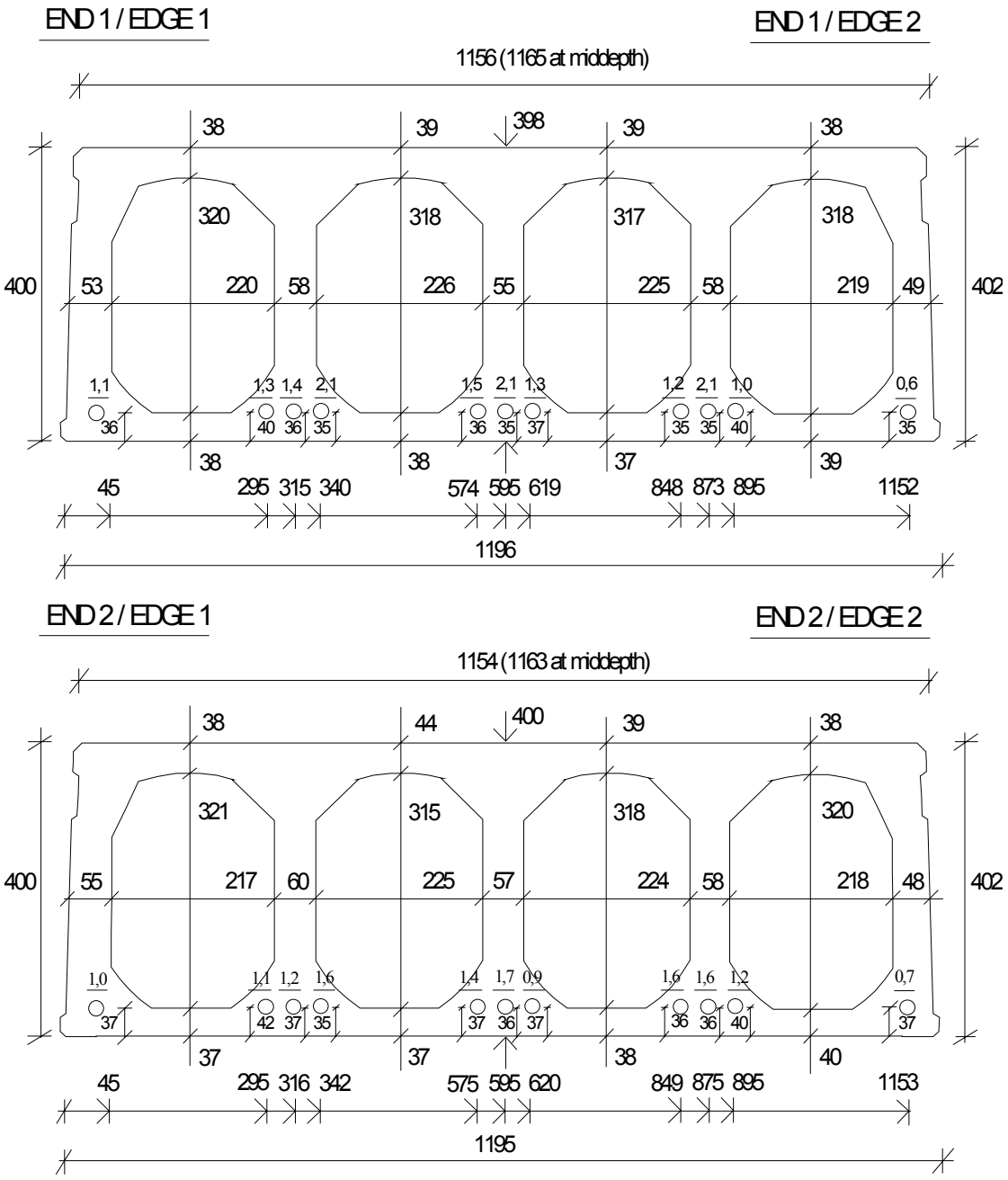

Fig. 1. Slab 1.

Slab 2

Lower strands : 11 d 12.5, prestress = 1000 MPa

Length : 7068 mm
Mass : 3580 kg

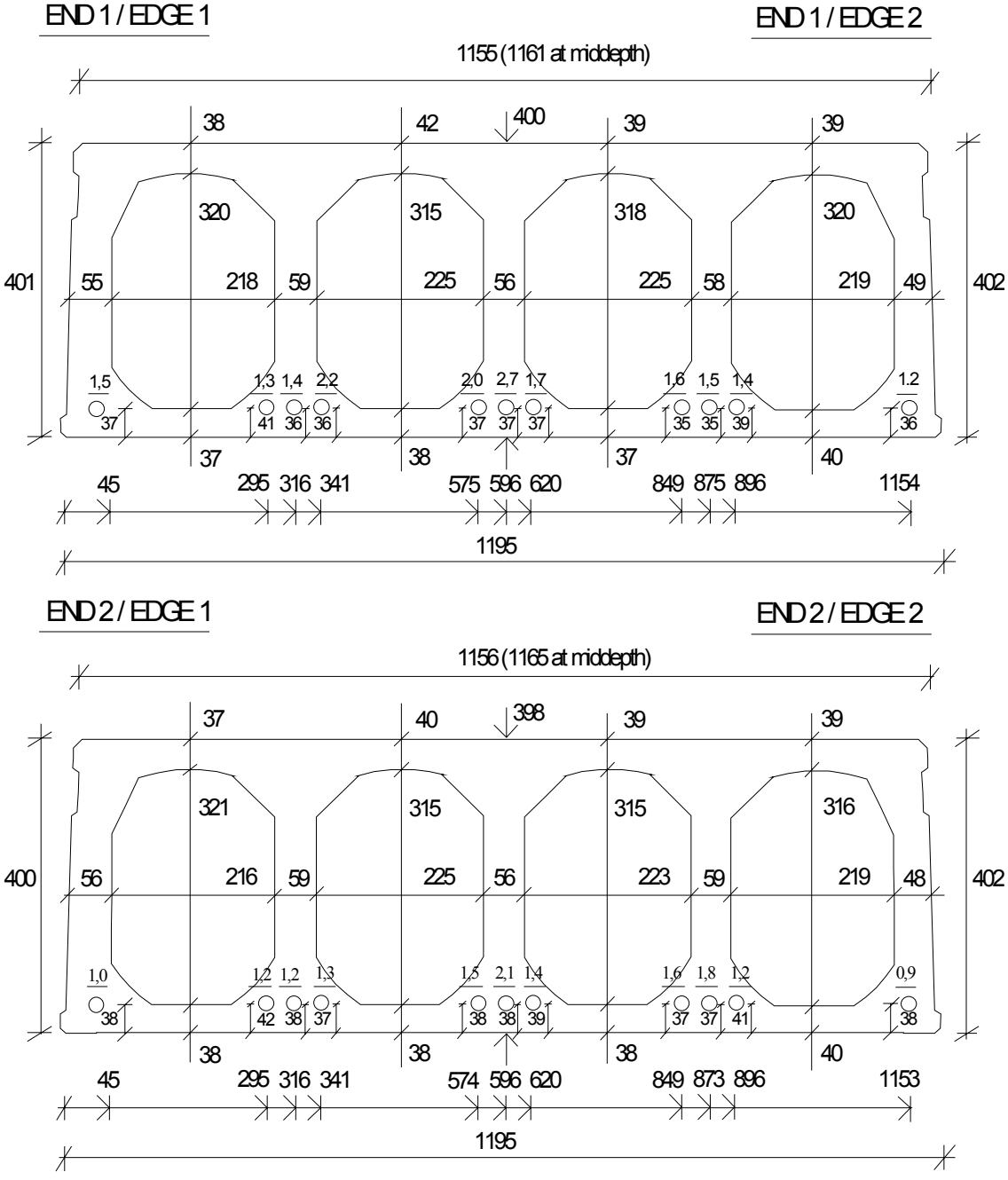

Fig. 2. Slab 2.

Slab 3

Lower strands : 11 d 12.5, prestress = 1000 MPa

Length : 7078 mm
Mass : 3590 kg

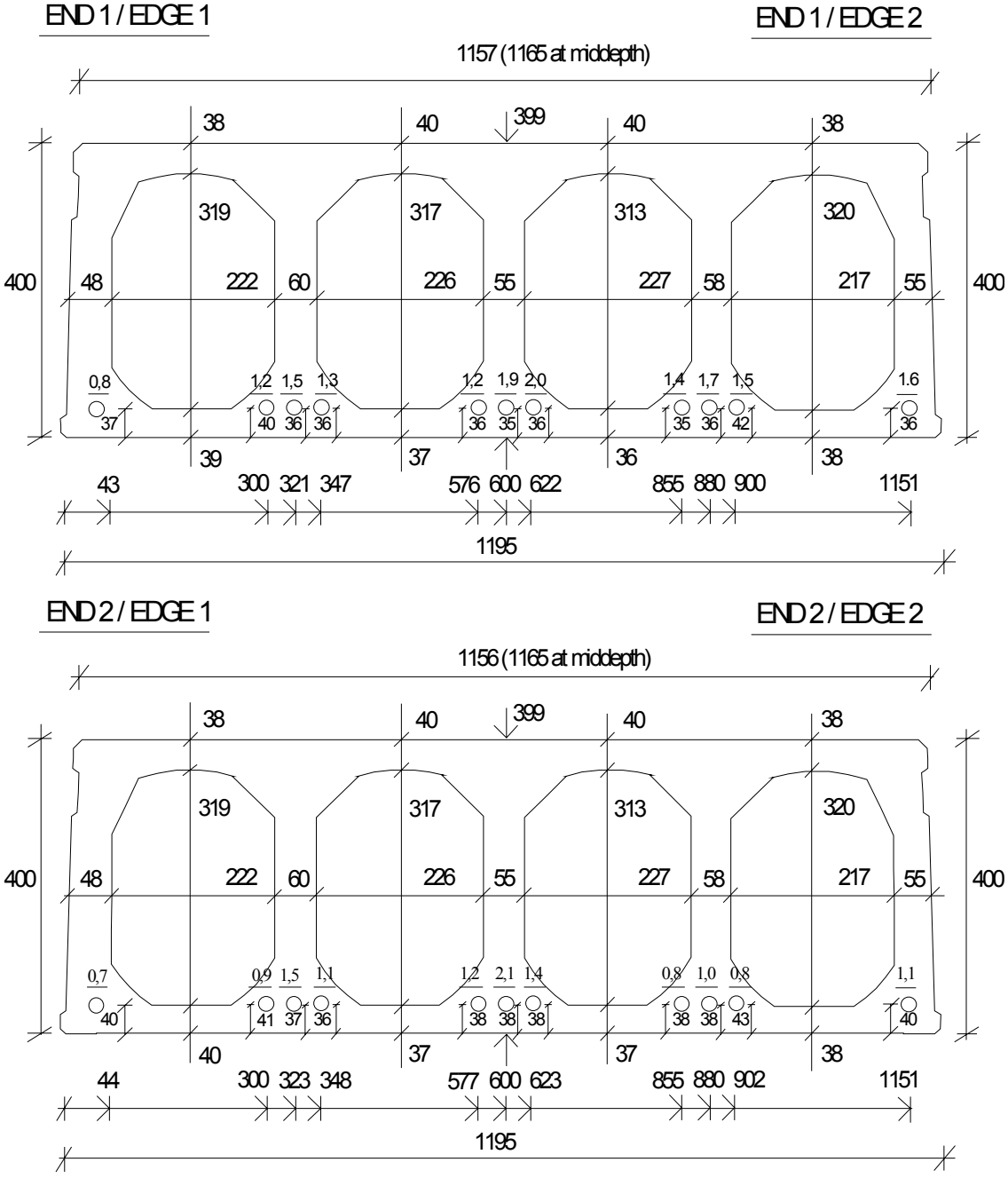

Fig. 3. Slab 3.

Slab 4

Lower strands : 11 d 12.5, prestress = 1000 MPa

Length : 7084 mm
Mass : 3600 kg

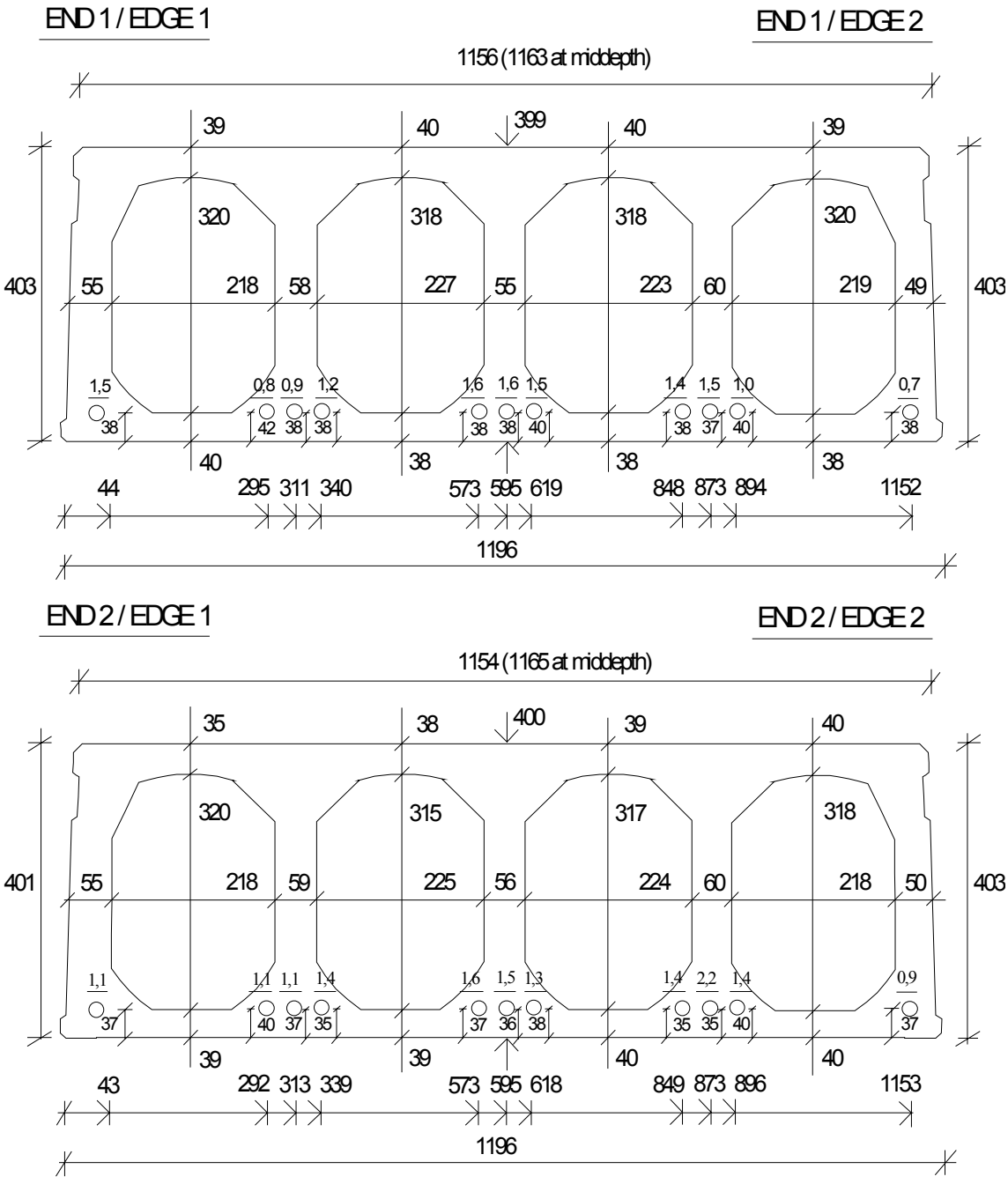

Fig. 4. Slab 4.

Appendix C: Measured forces, strains and displacements

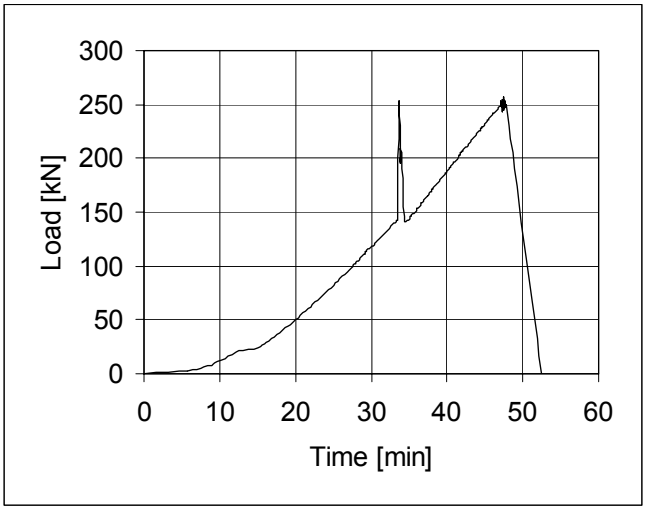

Fig. 1. PF400:1. Load-time relationship.

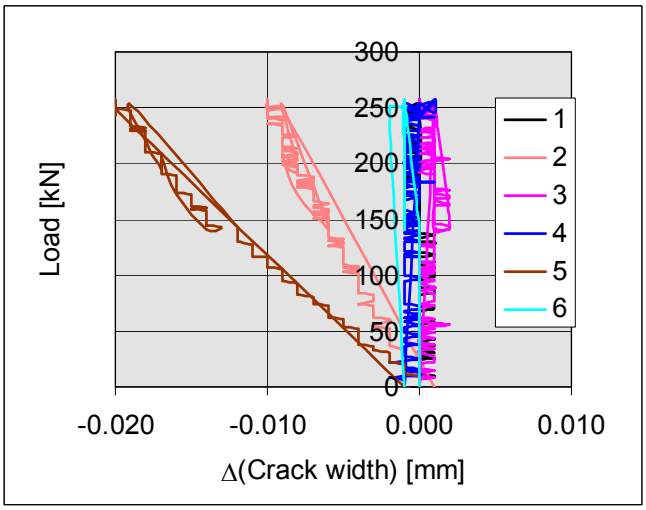

Fig. 2. PF400:1. Change of crack width measured by transducers 1–6.

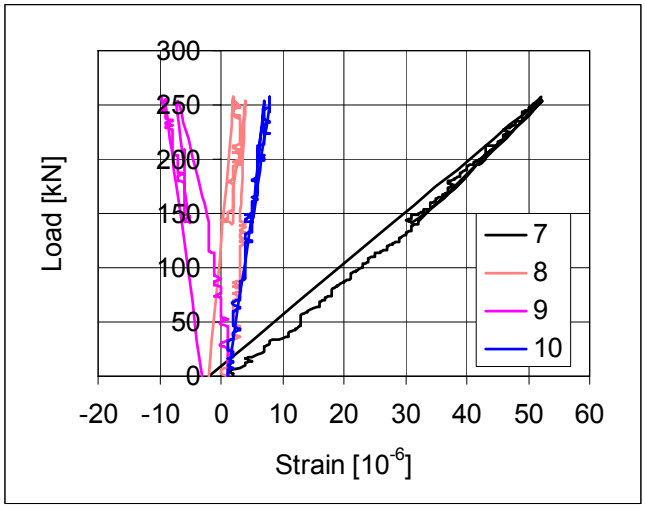

Fig. 3. PF400:1. Strain in tie reinforcement measured by transducers 7–9.

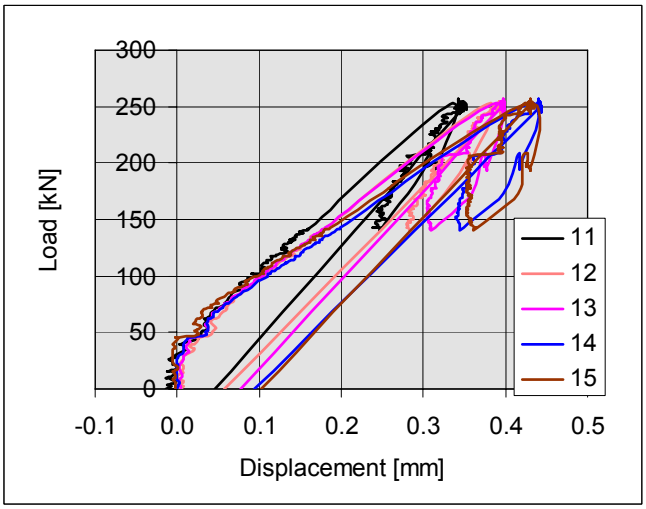

Fig. 4. PF400:1. Vertical displacement measured by transducers 11–15.

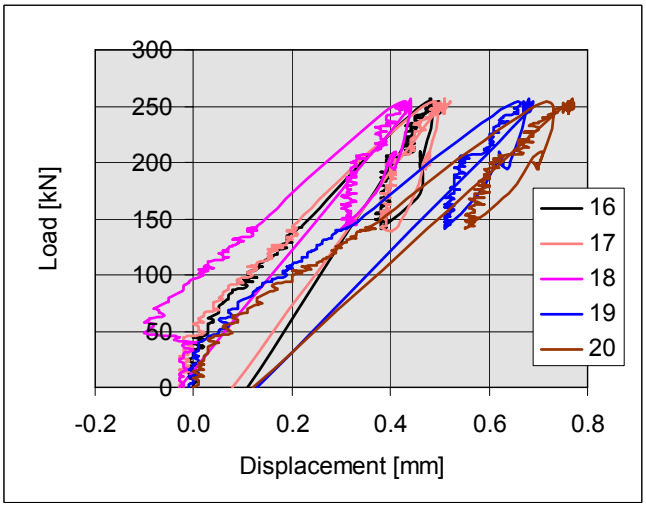

Fig. 5. PF400:1. Vertical displacement measured by transducers 16–20.

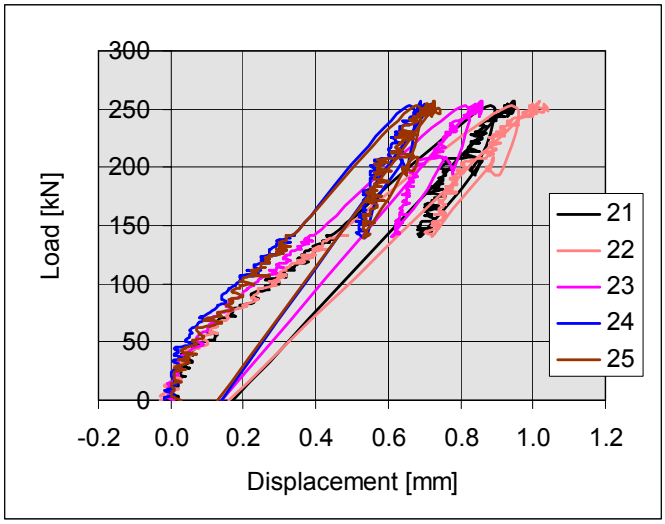

Fig. 6. PF400:1. Vertical displacement measured by transducers 21–25.

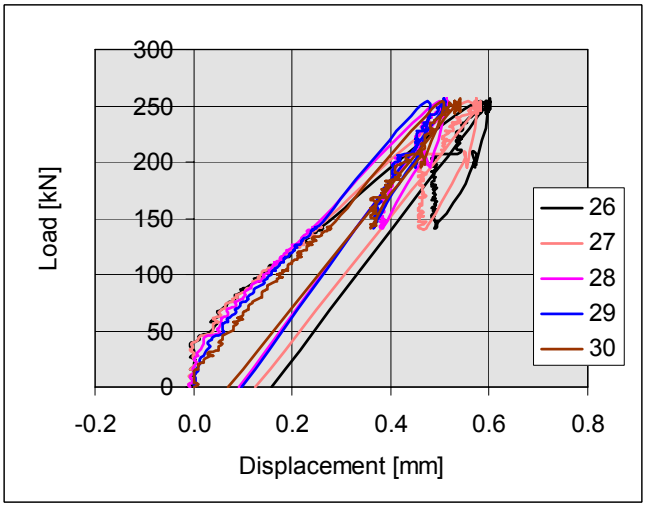

Fig. 7. PF400:1. Vertical displacement measured by transducers 26–30.

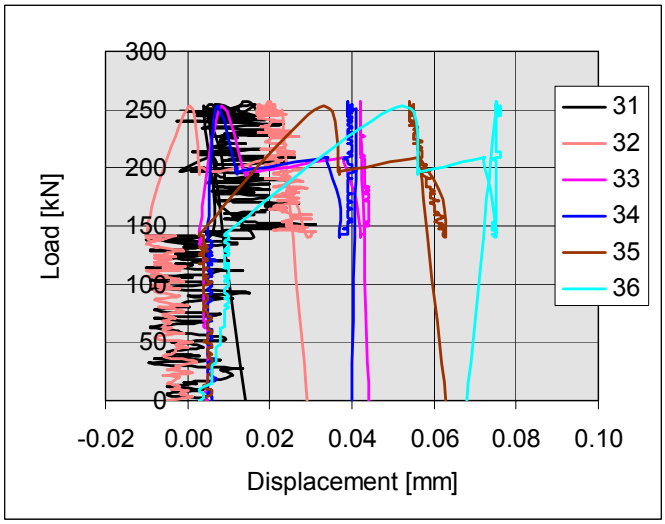

Fig. 8. PF400:1. Vertical displacement measured by transducers 31–36.

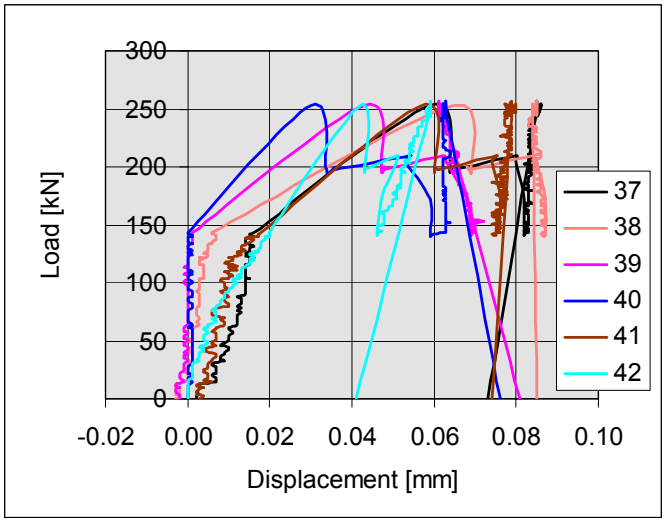

Fig. 9. PF400:1. Vertical displacement measured by transducers 37–42.

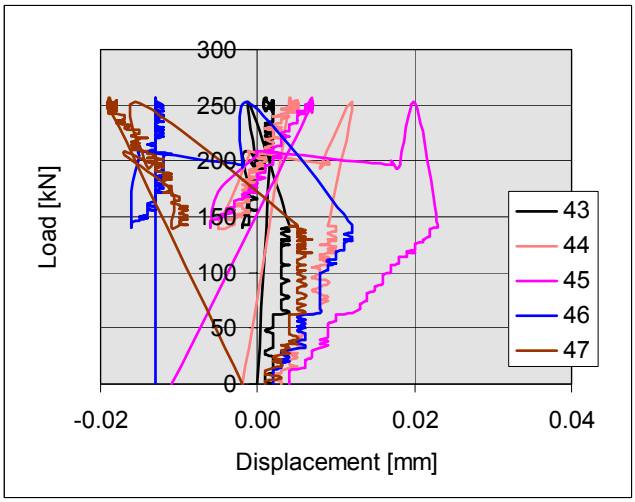

Fig. 10. PF400:1. Vertical displacement measured by transducers 43–47.

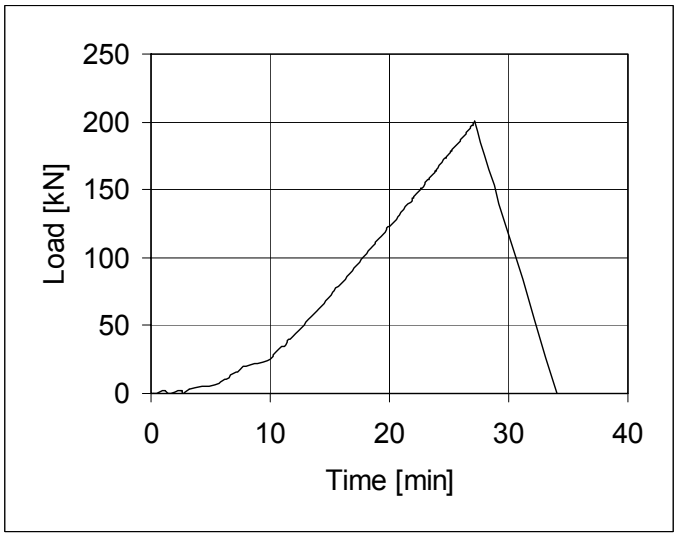

Fig. 11. PF400:2. Load-time relationship.

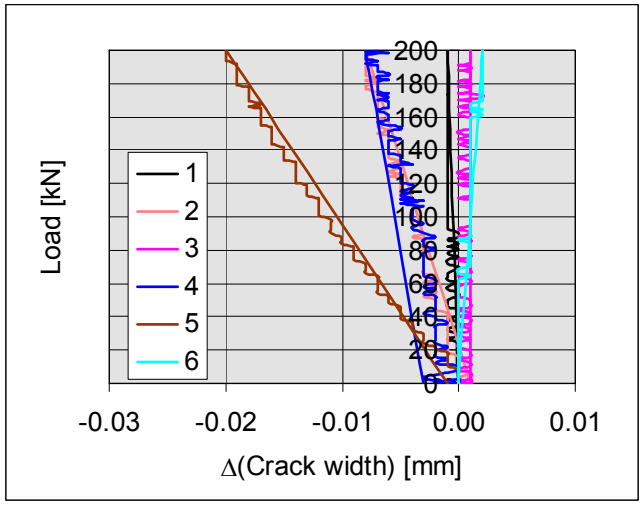

Fig. 12. PF400:2. Change of crack width measured by transducers 1–6.

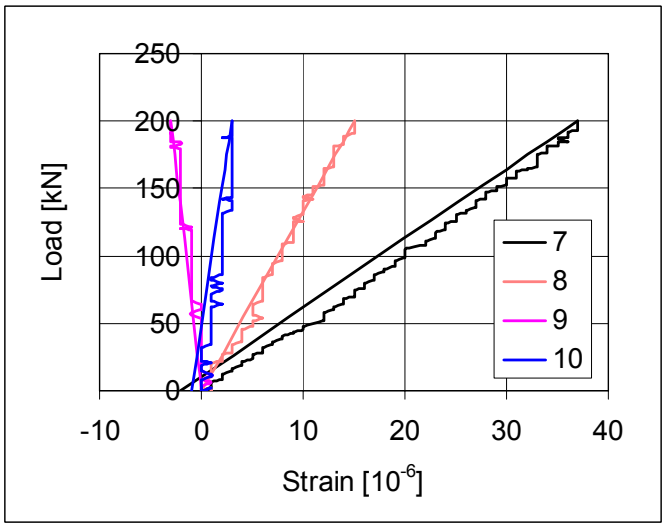

Fig. 13. PF400:2. Strain in tie reinforcement measured by transducers 7–9.

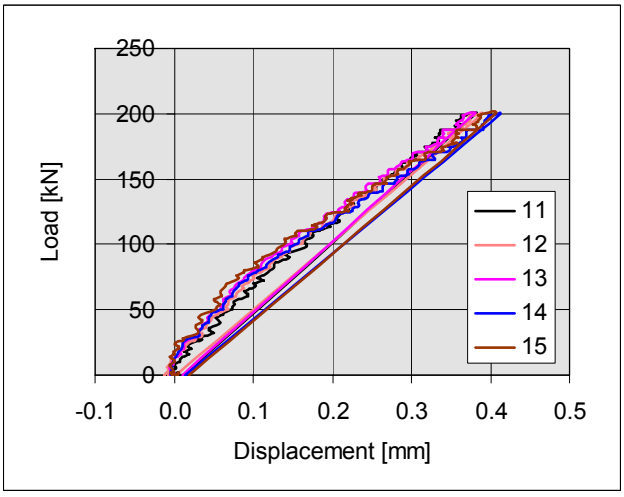

Fig. 14. PF400:2. Vertical displacement measured by transducers 11–15.

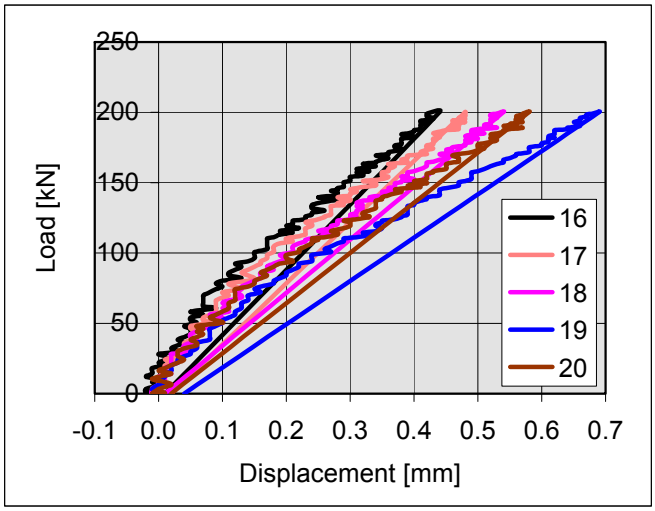

Fig. 15. PF400:2. Vertical displacement measured by transducers 16–20.

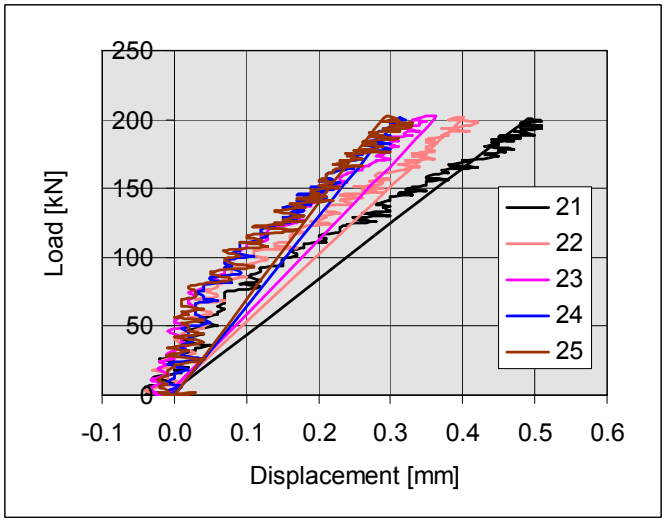

Fig. 16. PF400:2. Vertical displacement measured by transducers 21–25.

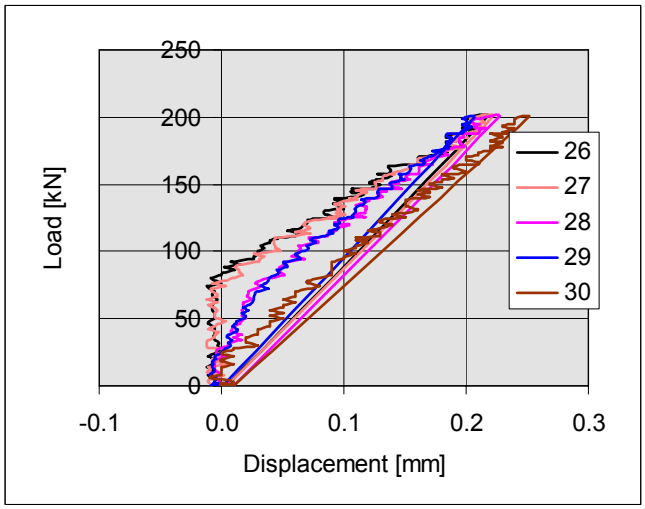

Fig. 17. PF400:2. Vertical displacement measured by transducers 26–30.

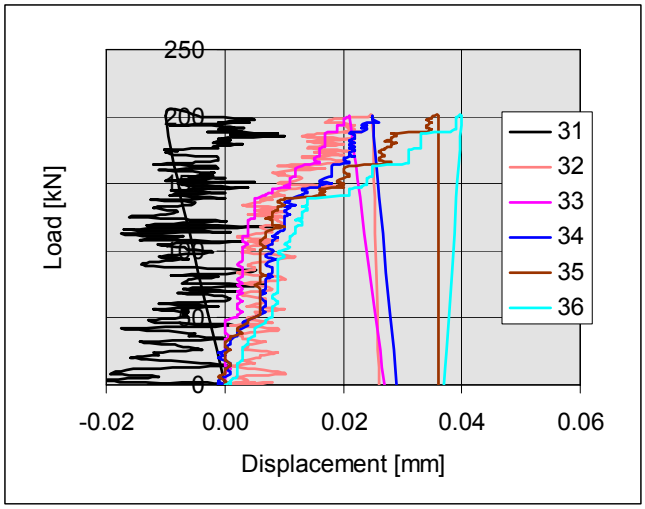

Fig. 18. PF400:2. Vertical displacement measured by transducers 31–36.

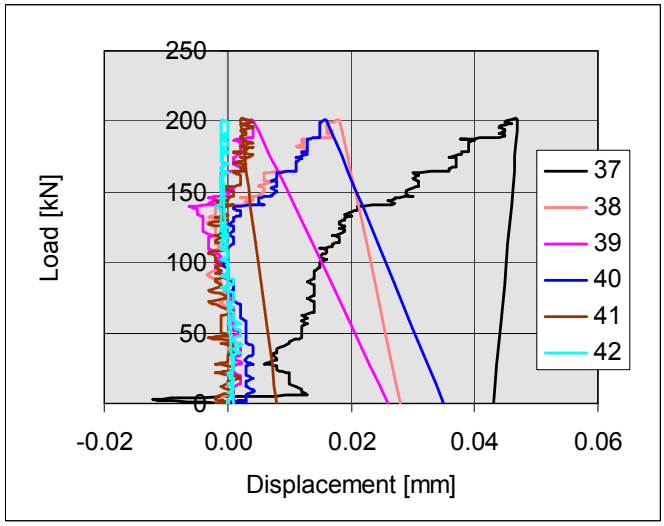

Fig. 19. PF400:2. Vertical displacement measured by transducers 37–42.

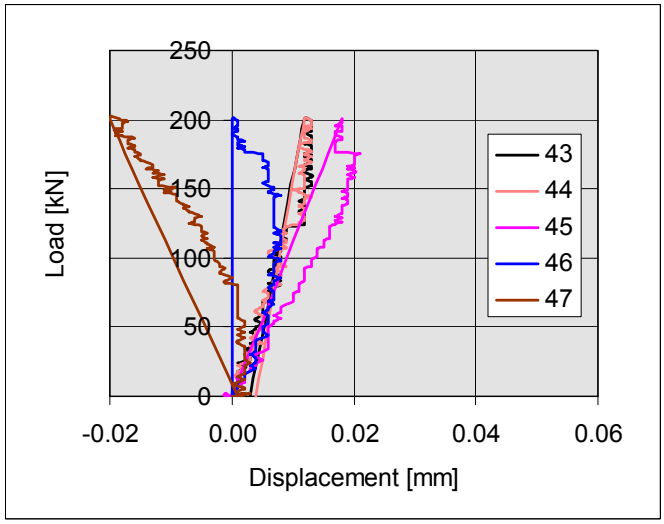

Fig. 20. PF400:2. Vertical displacement measured by transducers 43–47.

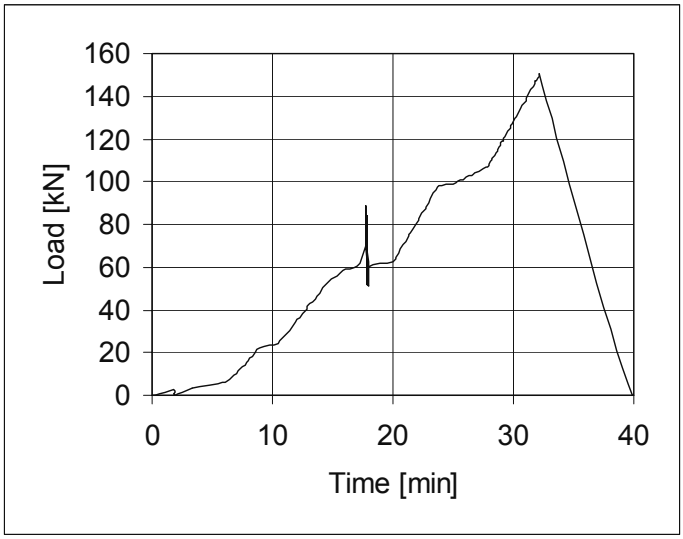

Fig. 21. PF400:3. Load-time relationship.

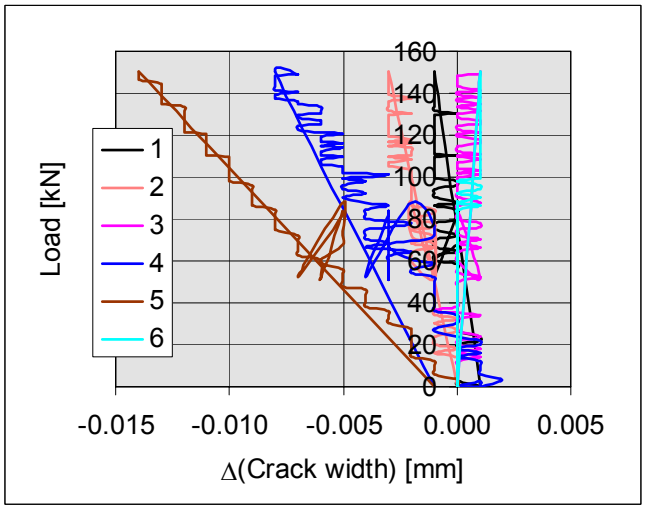

Fig. 22. PF400:3. Change of crack width measured by transducers 1–6.

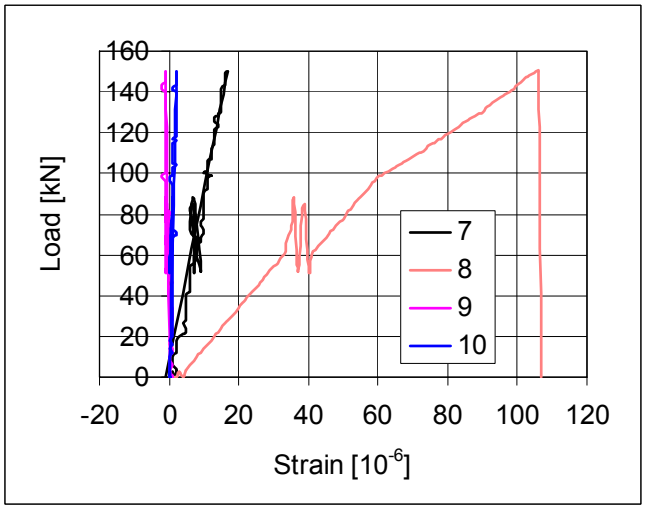

Fig. 23. PF400:3. Strain in tie reinforcement measured by transducers 7–9.

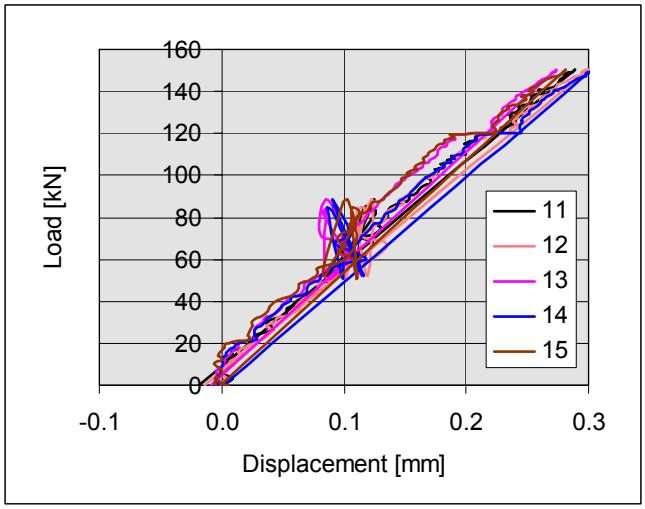

Fig. 24. PF400:3. Vertical displacement measured by transducers 11–15.

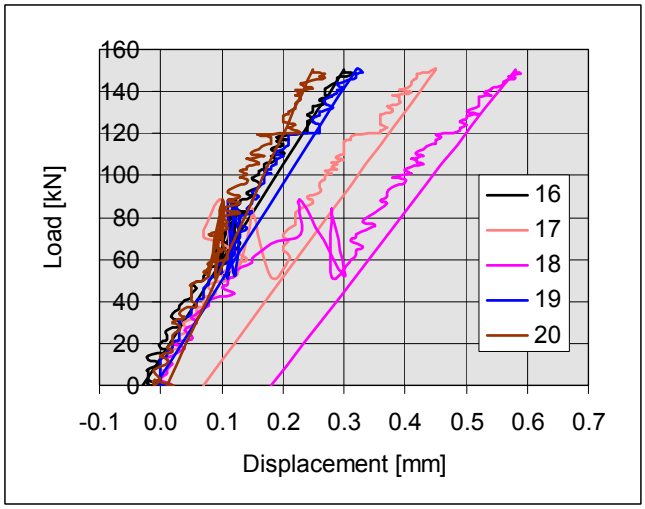

Fig. 25. PF400:3. Vertical displacement measured by transducers 16–20.

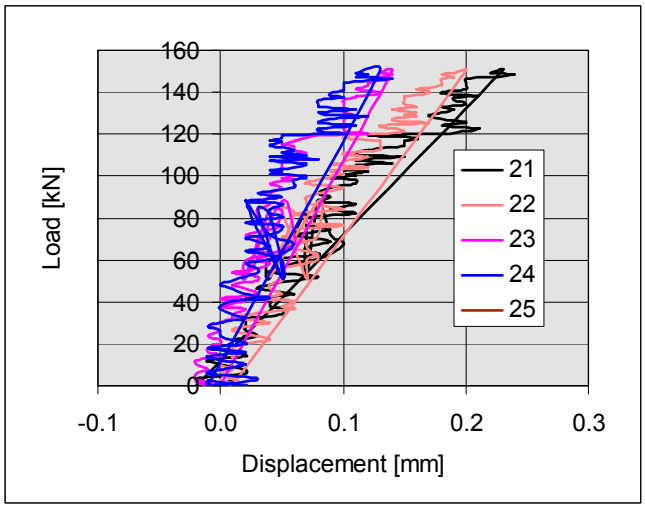

Fig. 26. PF400:3. Vertical displacement measured by transducers 21–25.

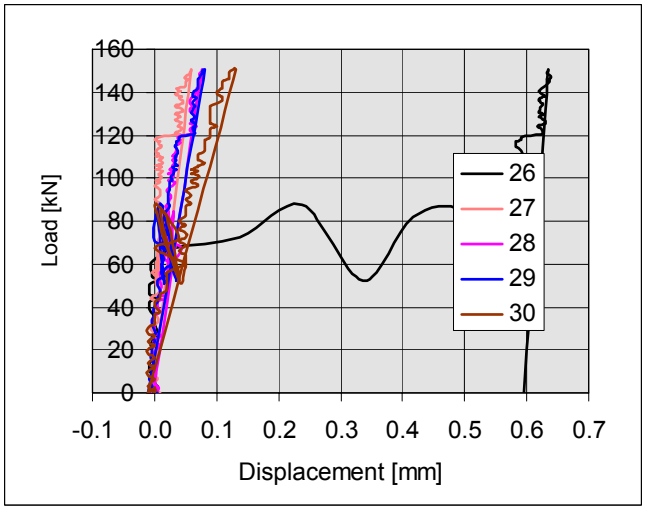

Fig. 27. PF400:3. Vertical displacement measured by transducers 26–30. Transducer 26 out of action.

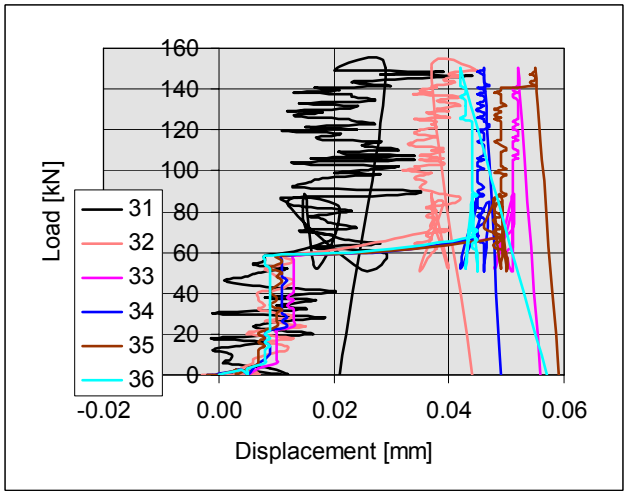

Fig. 28. PF400:3. Vertical displacement measured by transducers 31–36.

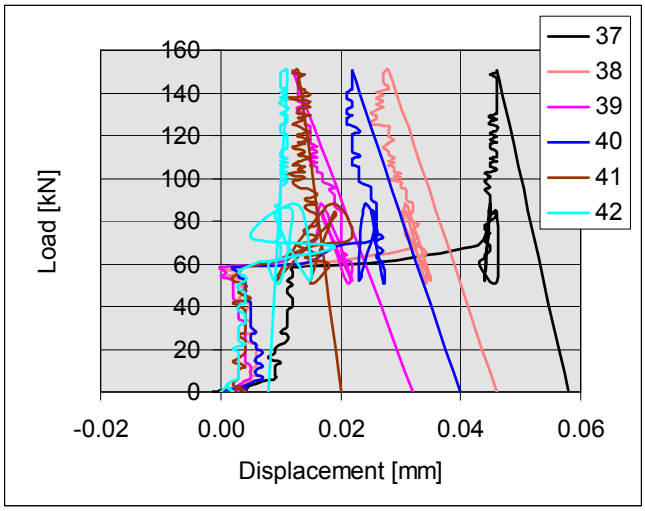

Fig. 29. PF400:3. Vertical displacement measured by transducers 37–42.

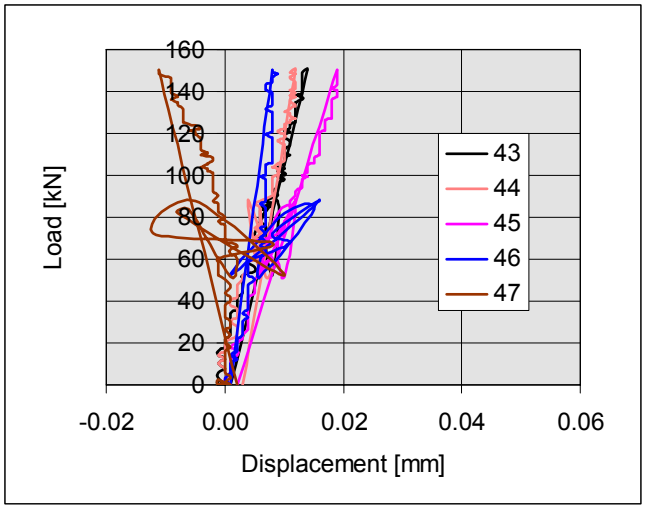

Fig. 30. PF400:3. Vertical displacement measured by transducers 43–47.

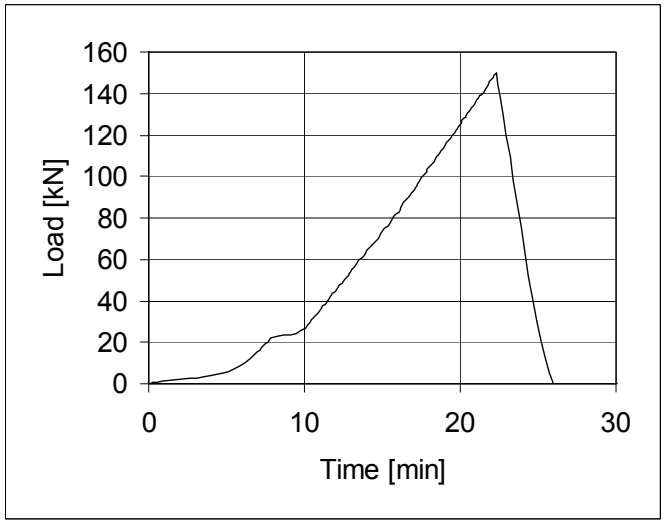

Fig. 31. PF400:4. Load-time relationship.

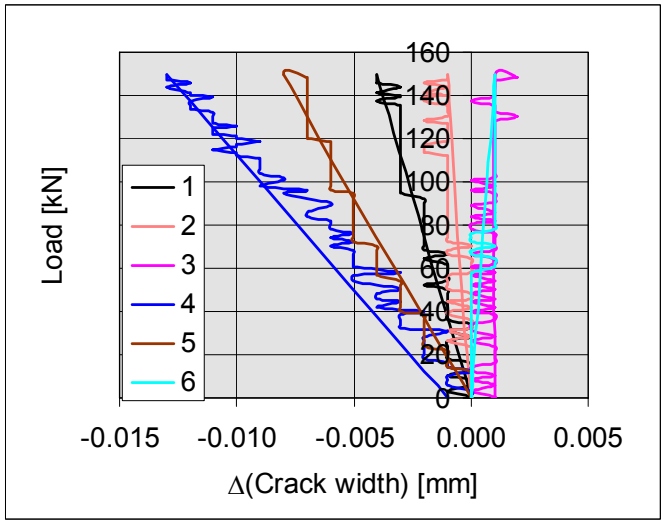

Fig. 32. PF400:4. Change of crack width measured by transducers 1–6.

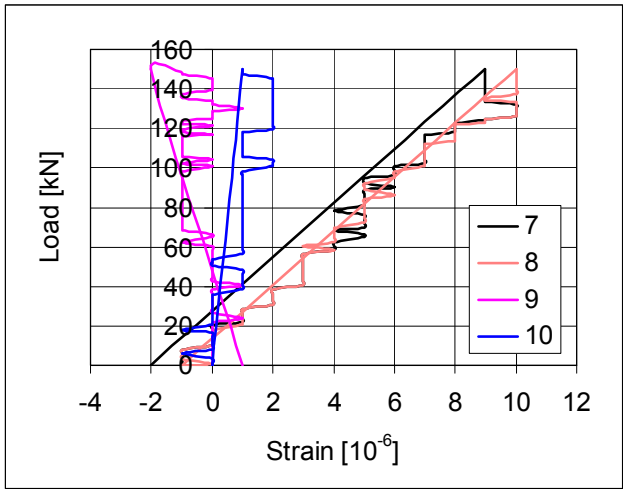

Fig. 33. PF400:4. Strain in tie reinforcement measured by transducers 7–9.

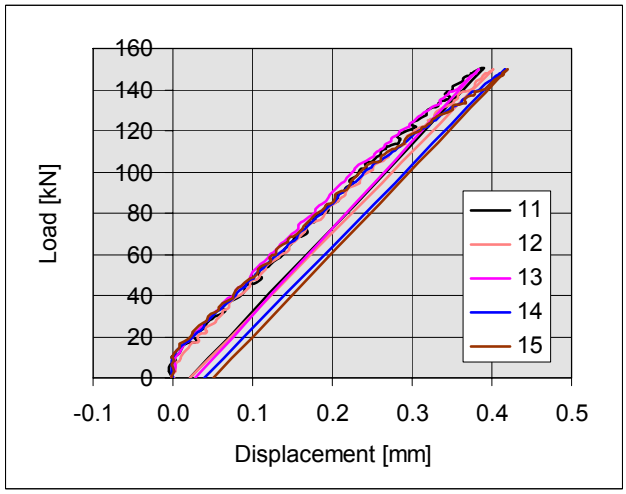

Fig. 34. PF400:4. Vertical displacement measured by transducers 11–15.

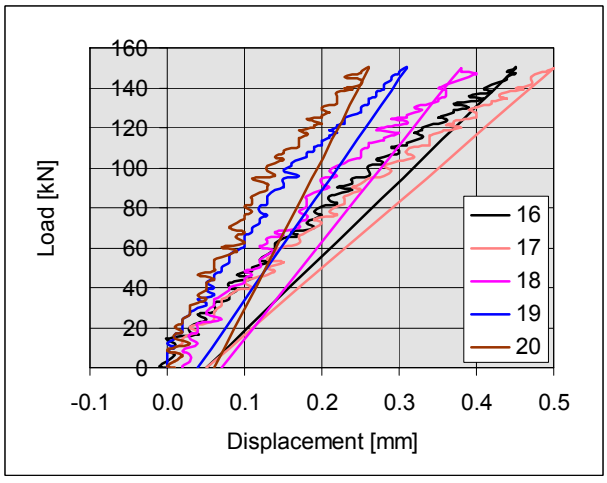

Fig. 35. PF400:4. Vertical displacement measured by transducers 16–20.

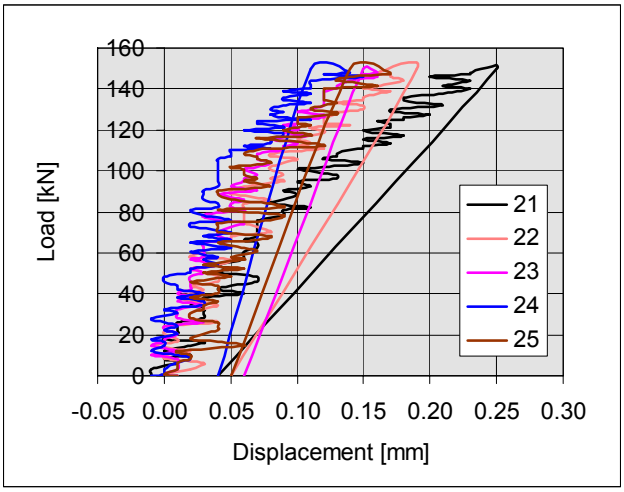

Fig. 36. PF400:4. Vertical displacement measured by transducers 21–25.

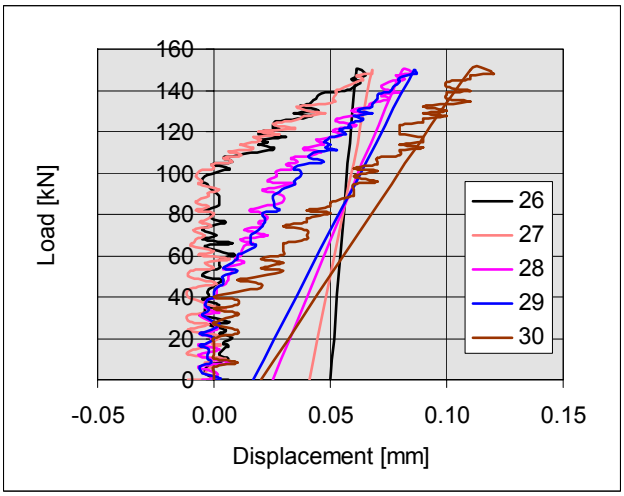

Fig. 37. PF400:4. Vertical displacement measured by transducers 26–30.

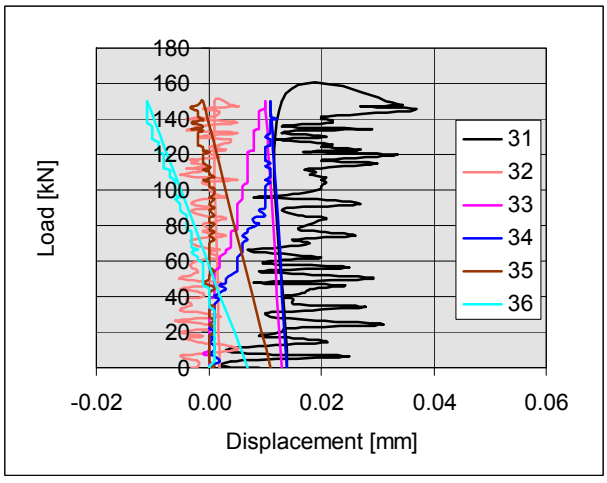

Fig. 38. PF400:4. Vertical displacement measured by transducers 31–36.

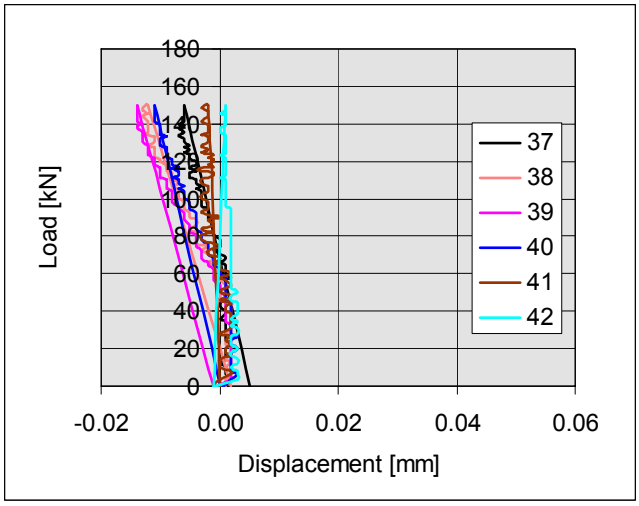

Fig. 39. PF400:4. Vertical displacement measured by transducers 37–42.

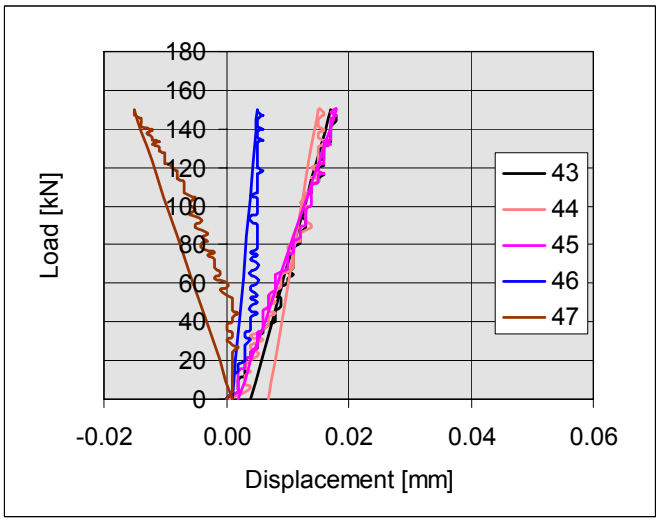

Fig. 40. PF400:4. Vertical displacement measured by transducers 43–47.

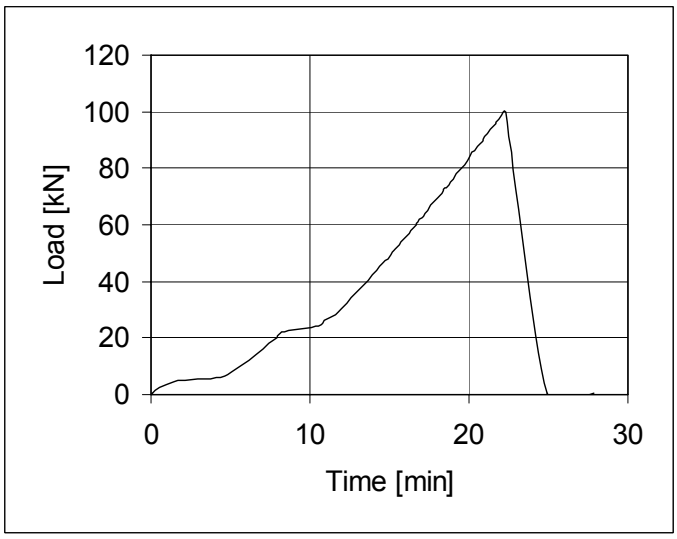

Fig. 41. PF400:5. Load-time relationship.

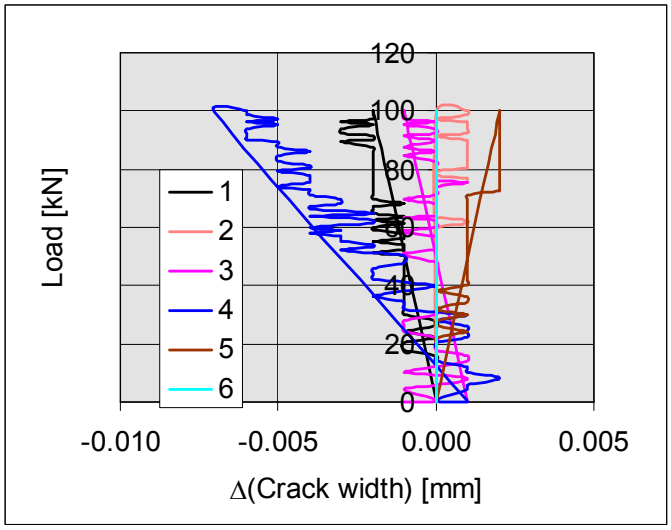

Fig. 42. PF400:5. Change of crack width measured by transducers 1–6.

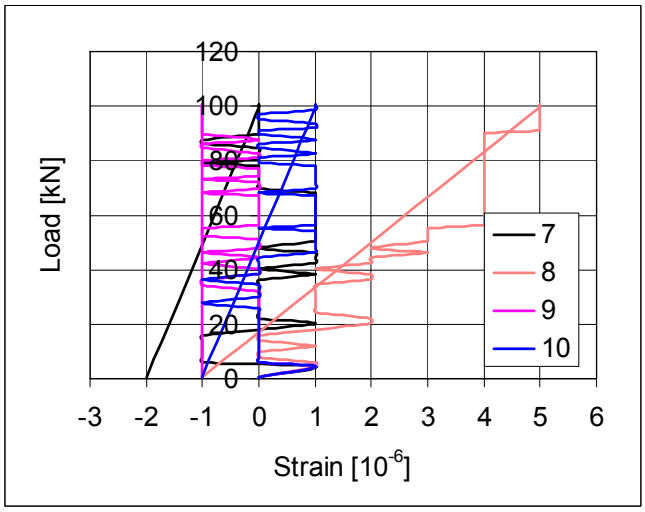

Fig. 43. PF400:5. Strain in tie reinforcement measured by transducers 7–9.

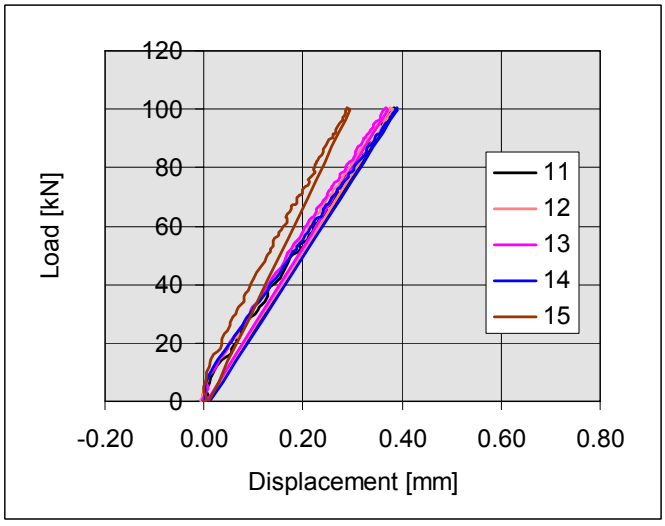

Fig. 44. PF400:5. Vertical displacement measured by transducers 11–15.

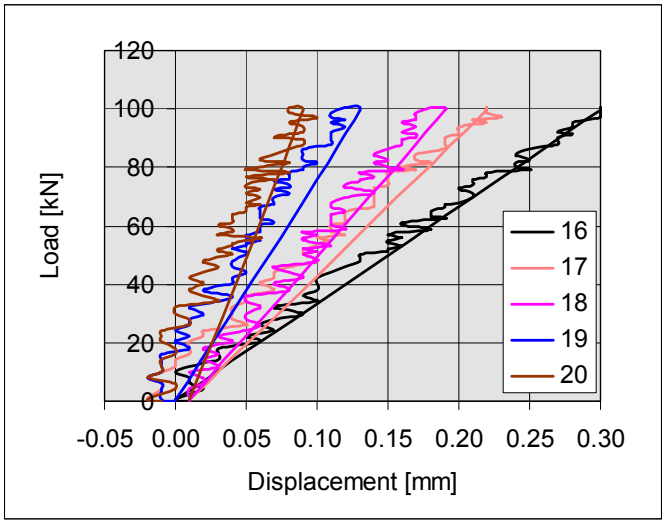

Fig. 45. PF400:5. Vertical displacement measured by transducers 16–20.

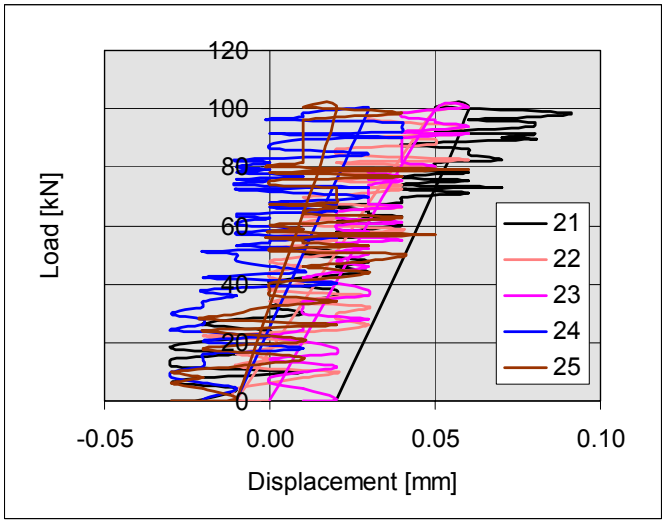

Fig. 46. PF400:5. Vertical displacement measured by transducers 21–25.

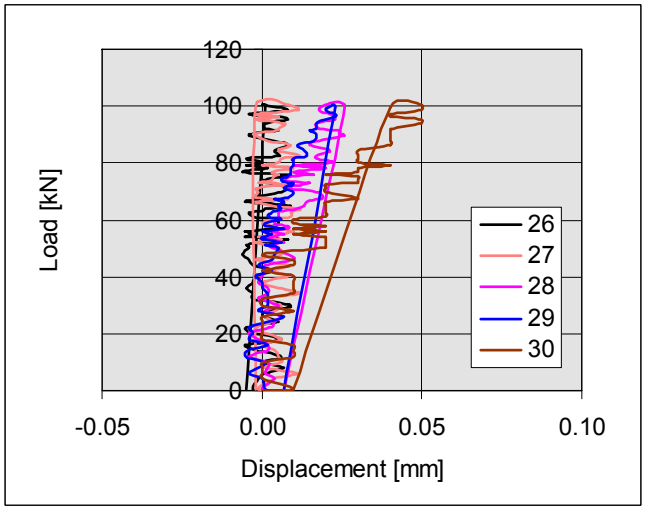

Fig. 47. PF400:5. Vertical displacement measured by transducers 26–30.

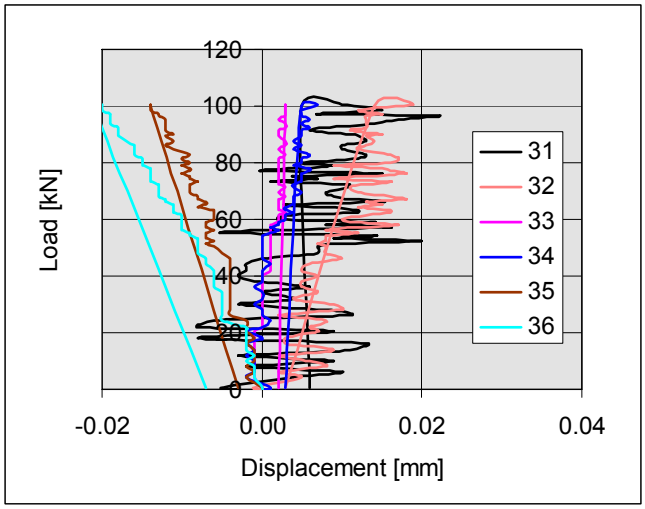

Fig. 48. PF400:5. Vertical displacement measured by transducers 31–36.

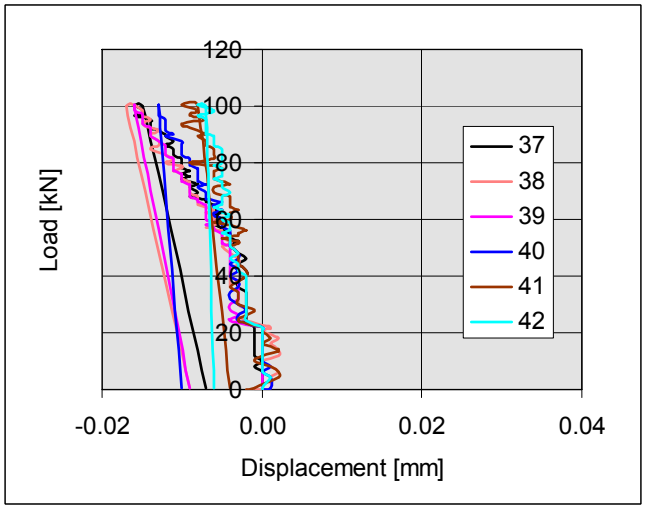

Fig. 49. PF400:5. Vertical displacement measured by transducers 37–42.

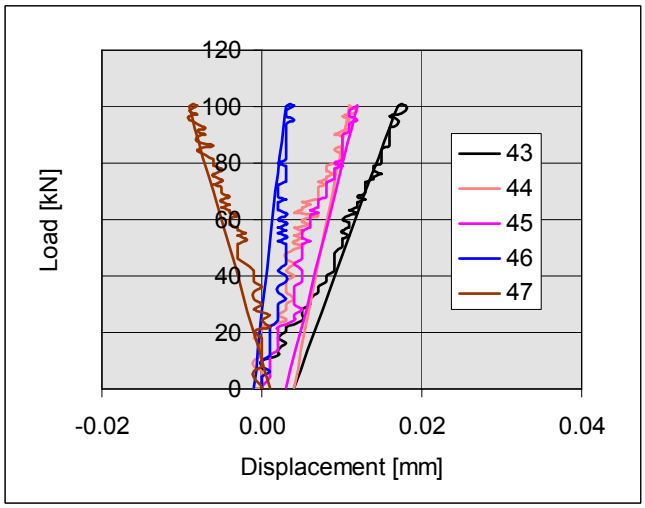

Fig. 50. PF400:5. Vertical displacement measured by transducers 43–47.

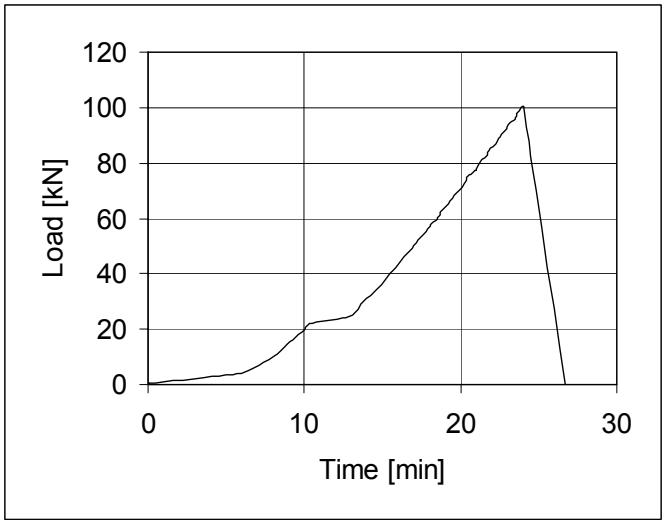

Fig. 51. PF400:6. Load-time relationship.

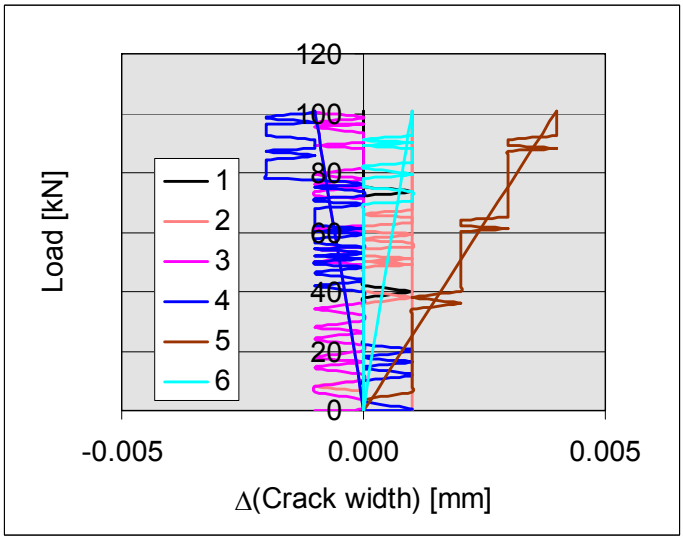

Fig. 52. PF400:6. Change of crack width measured by transducers 1–6.

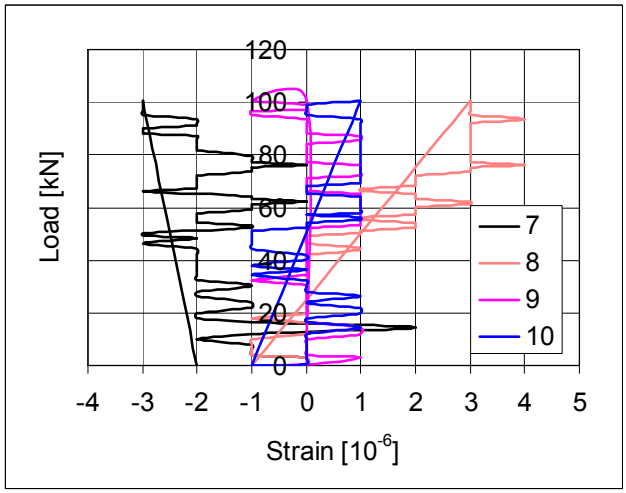

Fig. 53. PF400:6. Strain in tie reinforcement measured by transducers 7–9.

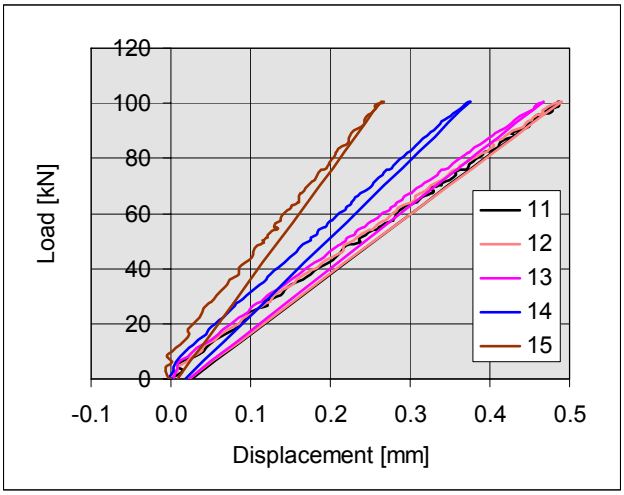

Fig. 54. PF400:6. Vertical displacement measured by transducers 11–15.

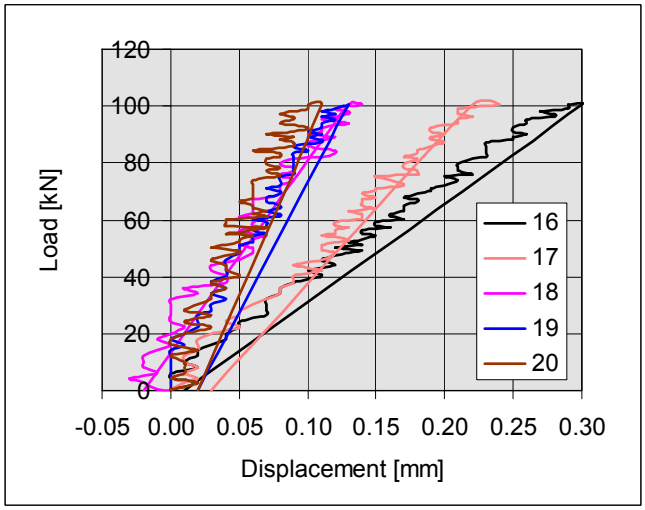

Fig. 55. PF400:6. Vertical displacement measured by transducers 16–20.

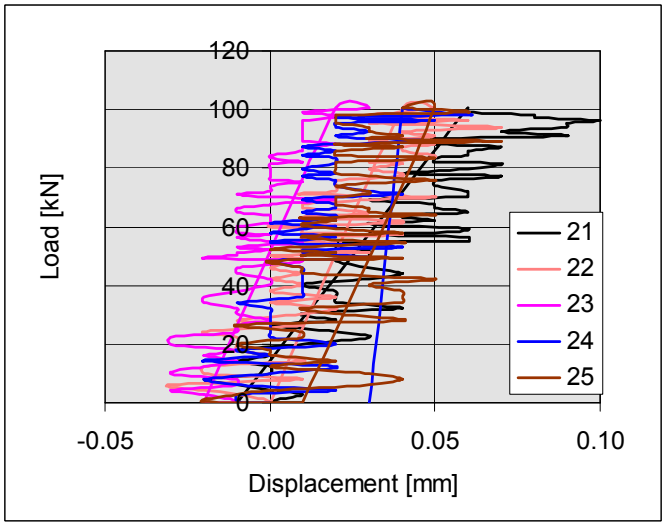

Fig. 56. PF400:6. Vertical displacement measured by transducers 21–25.

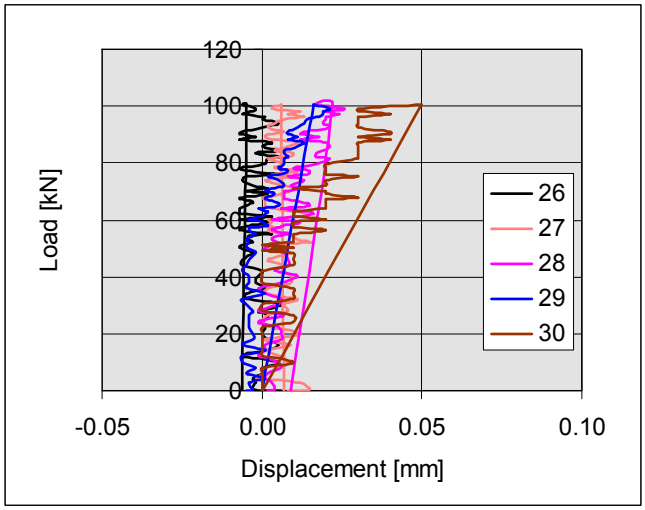

Fig. 57. PF400:6. Vertical displacement measured by transducers 26–30.

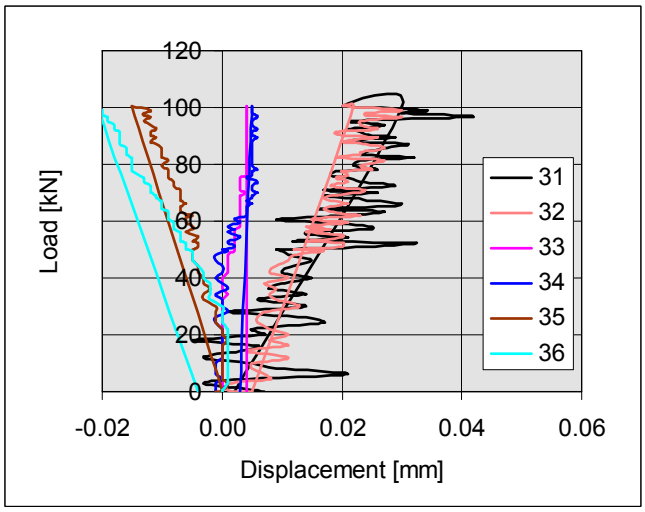

Fig. 58. PF400:6. Vertical displacement measured by transducers 31–36.

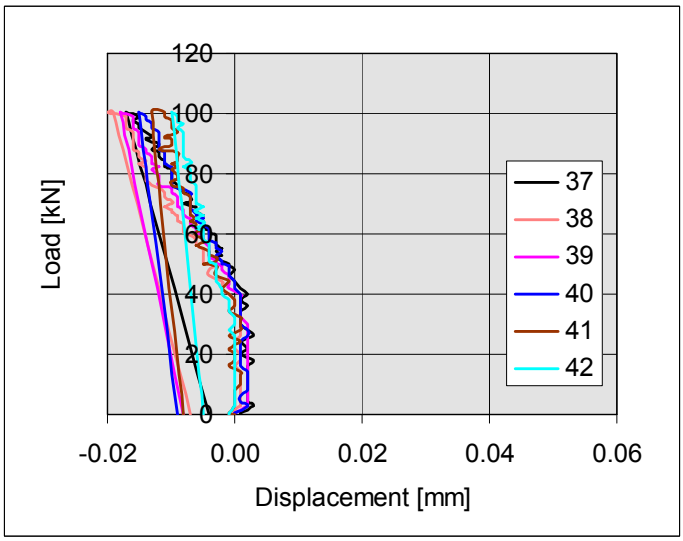

Fig. 59. PF400:6. Vertical displacement measured by transducers 37–42.

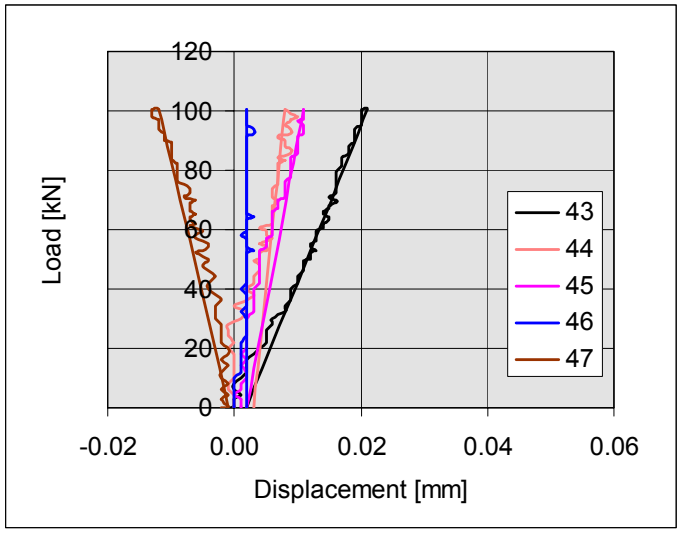

Fig. 60. PF400:6. Vertical displacement measured by transducers 43–47.

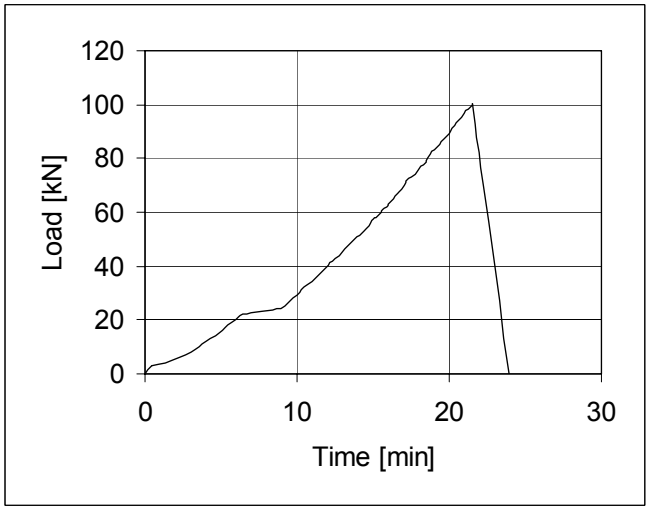

Fig. 61. PF400:7. Load-time relationship.

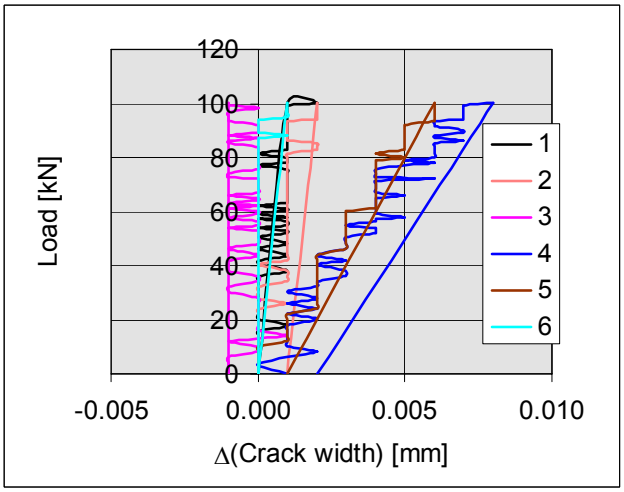

Fig. 62. PF400:7. Change of crack width measured by transducers 1–6.

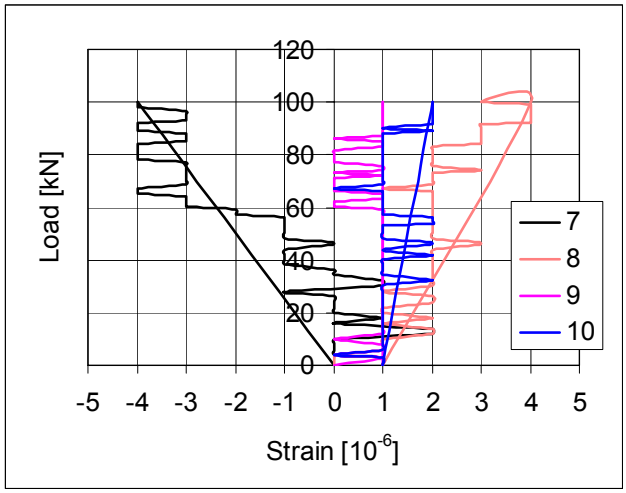

Fig. 63. PF400:7. Strain in tie reinforcement measured by transducers 7–9.

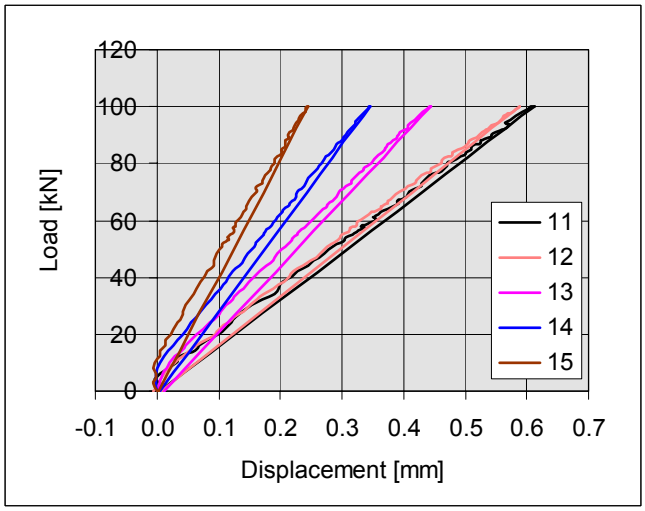

Fig. 64. PF400:7. Vertical displacement measured by transducers 11–15.

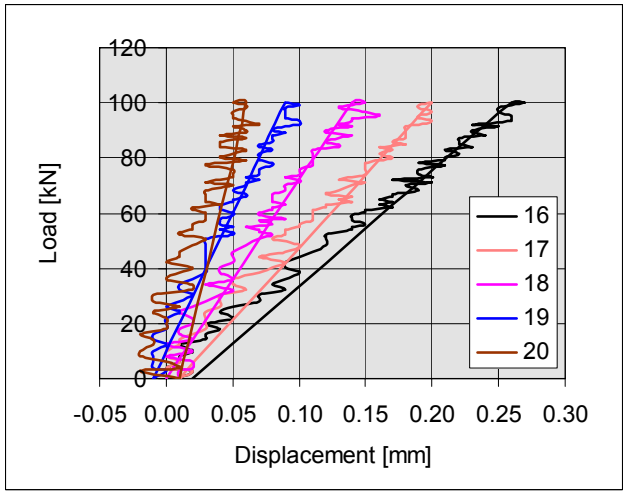

Fig. 65. PF400:7. Vertical displacement measured by transducers 16–20.

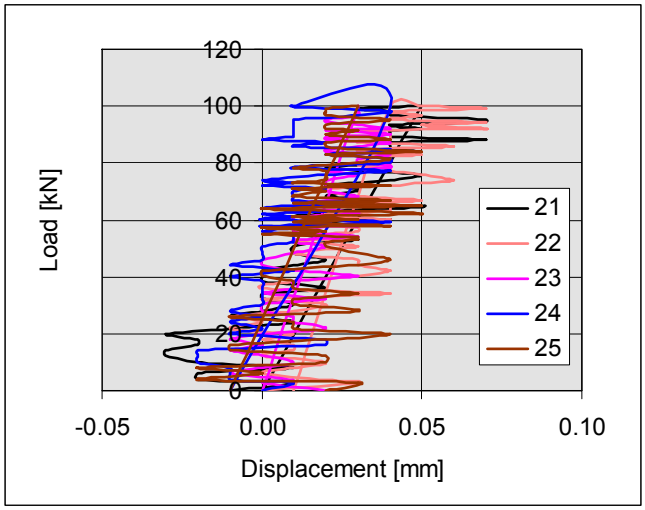

Fig. 66. PF400:7. Vertical displacement measured by transducers 21–25.

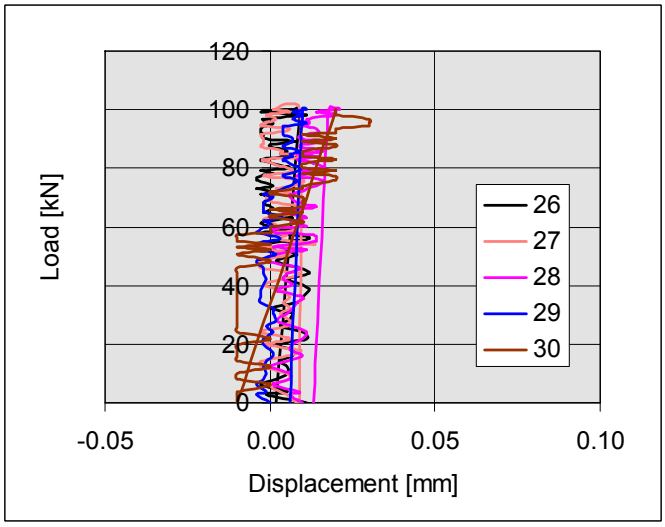

Fig. 67. PF400:7. Vertical displacement measured by transducers 26–30.

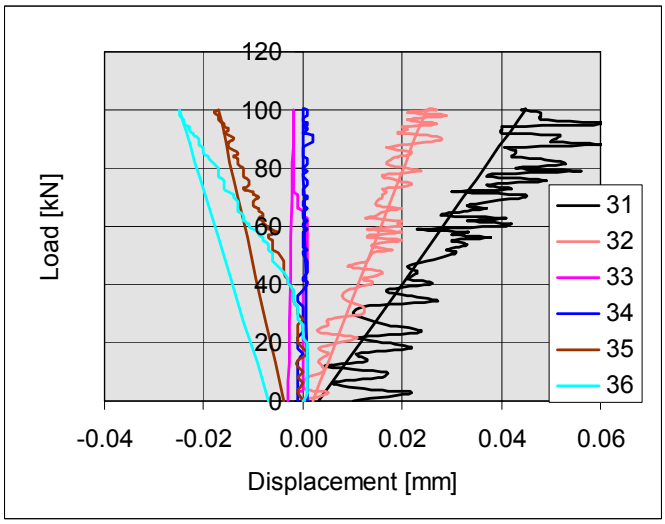

Fig. 68. PF400:7. Vertical displacement measured by transducers 31–36.

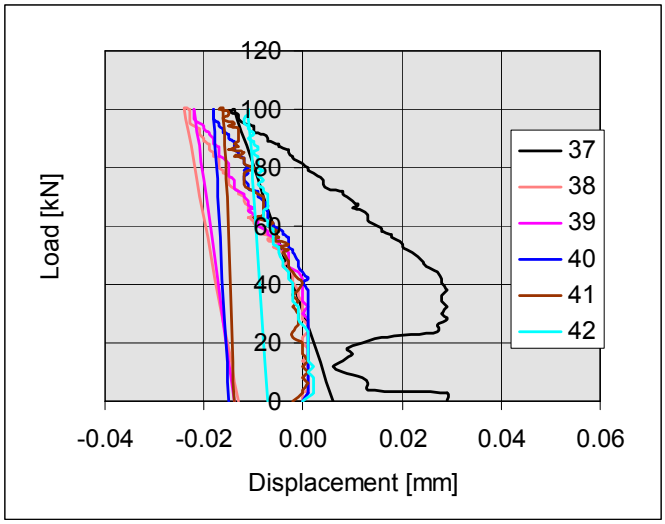

Fig. 69. PF400:7. Vertical displacement measured by transducers 37–42.

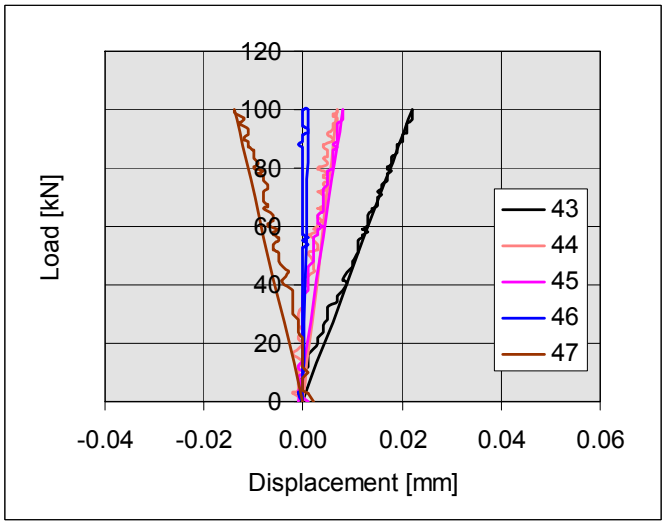

Fig. 70. PF400:7. Vertical displacement measured by transducers 43–47.

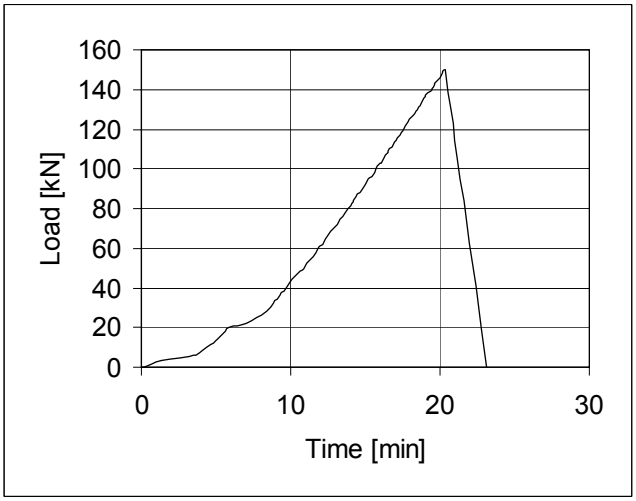

Fig. 71. PF400:8. Load-time relationship.

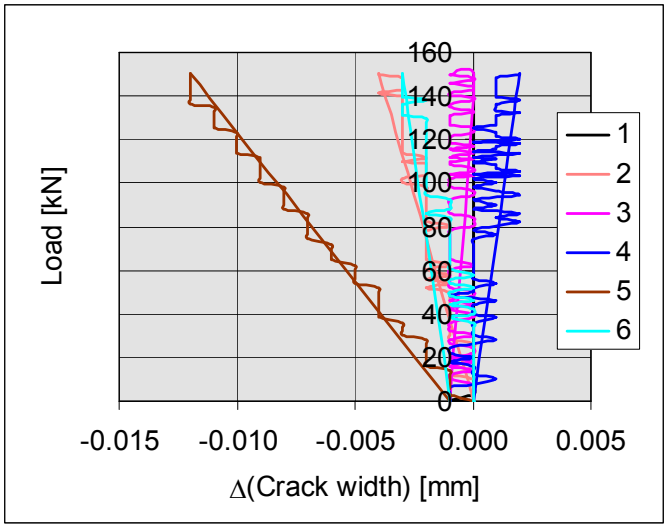

Fig. 72. PF400:8. Change of crack width measured by transducers 1–6.

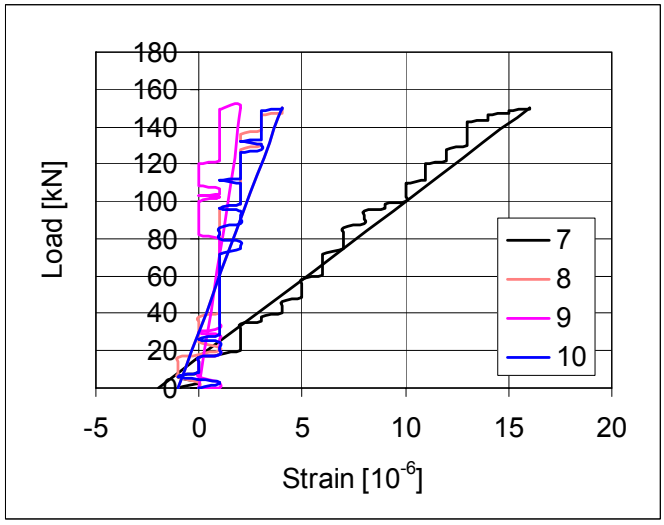

Fig. 73. PF400:8. Strain in tie reinforcement measured by transducers 7–9.

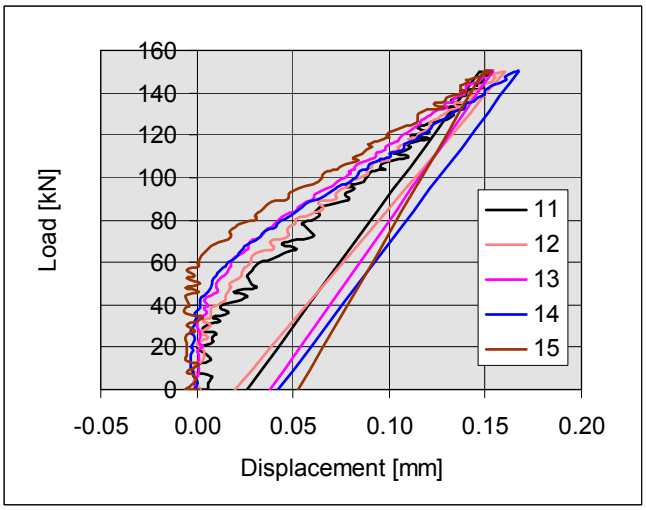

Fig. 74. PF400:8. Vertical displacement measured by transducers 11–15.

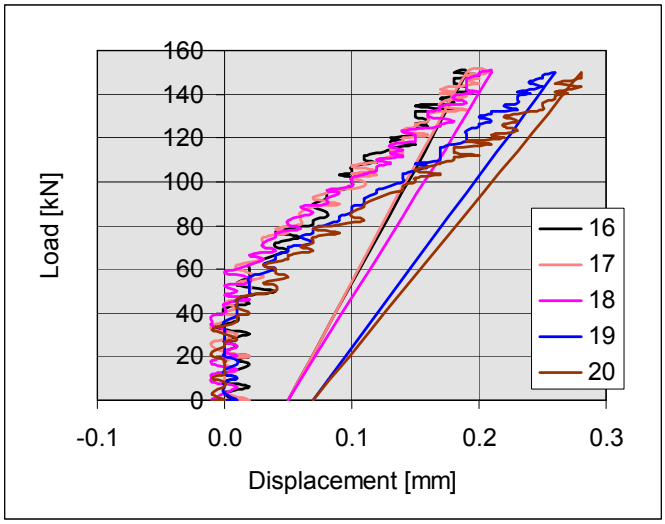

Fig. 75. PF400:8. Vertical displacement measured by transducers 16–20.

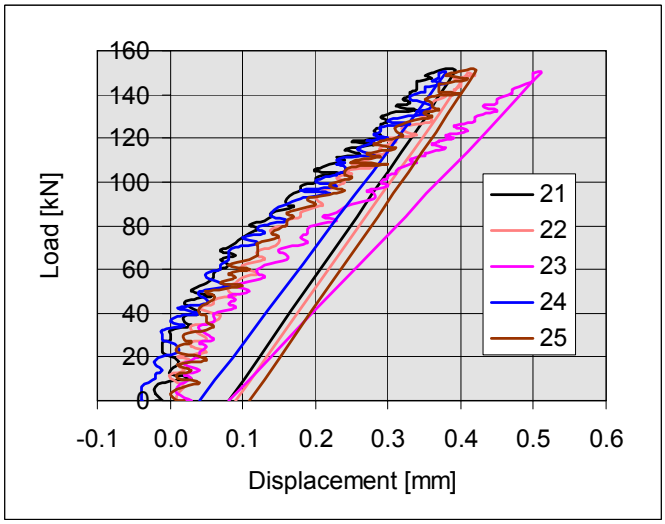

Fig. 76. PF400:8. Vertical displacement measured by transducers 21–25.

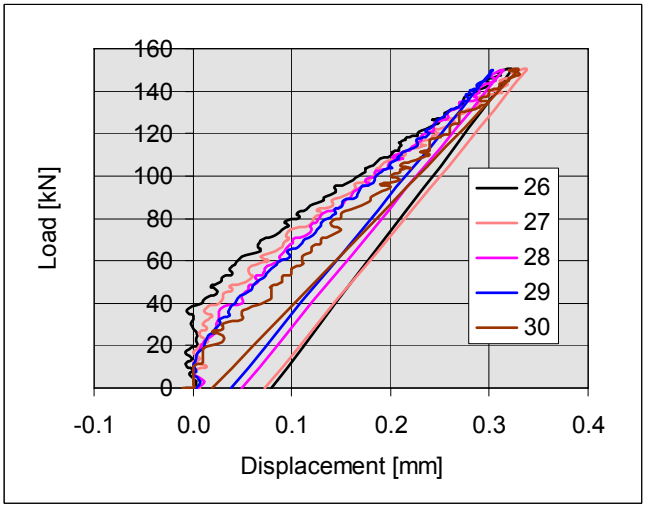

Fig. 77. PF400:8. Vertical displacement measured by transducers 26–30.

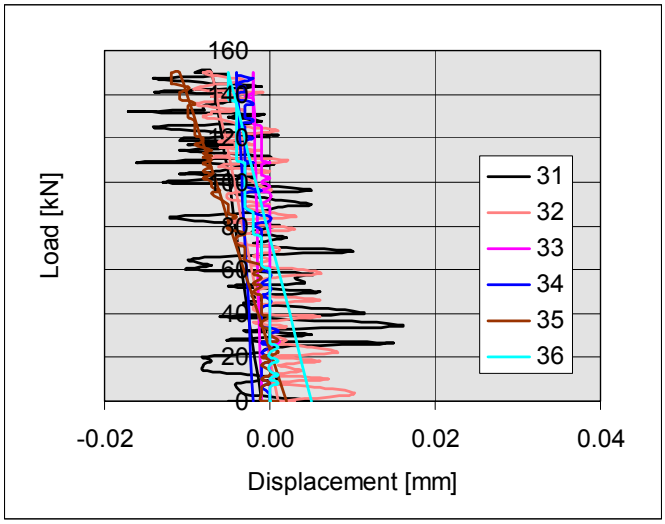

Fig. 78. PF400:8. Vertical displacement measured by transducers 31–36.

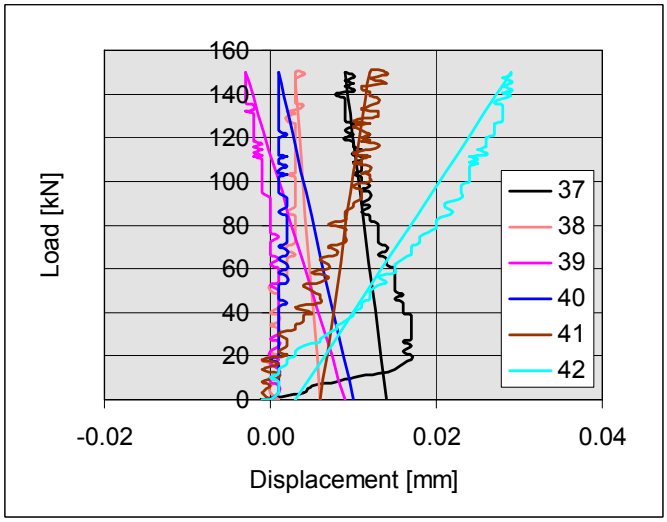

Fig. 79. PF400:8. Vertical displacement measured by transducers 37–42.

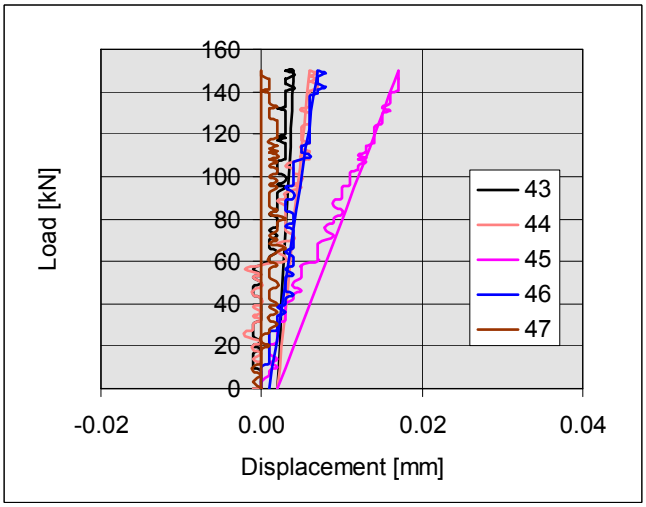

Fig. 80. PF400:8. Vertical displacement measured by transducers 43–47.

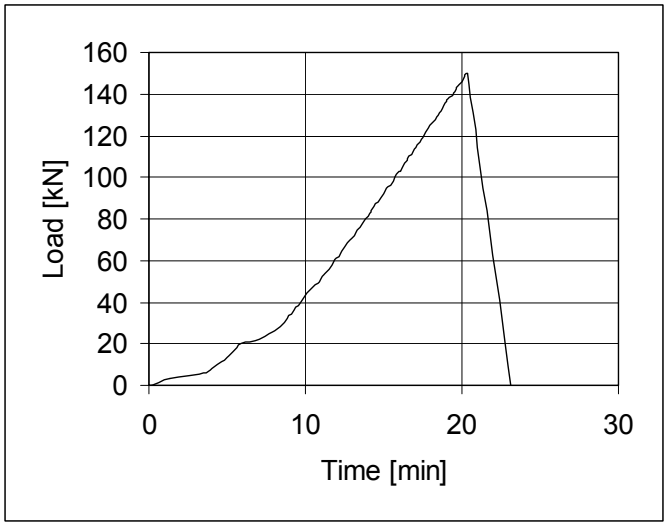

Fig. 81. PF400:9. Load-time relationship.

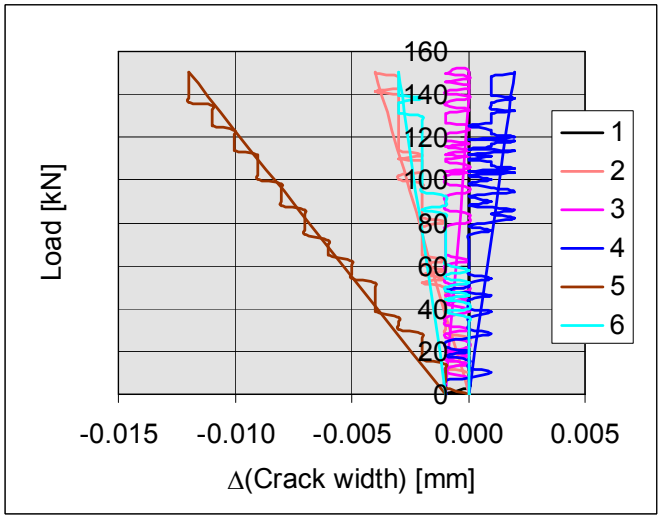

Fig. 82. PF400:9. Change of crack width measured by transducers 1–6.

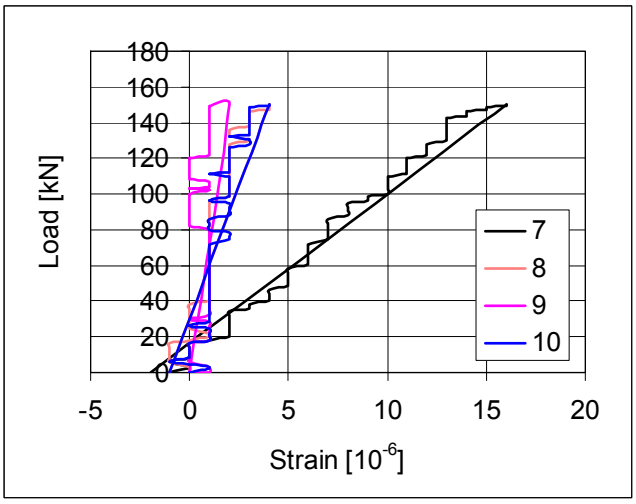

Fig. 83. PF400:9. Strain in tie reinforcement measured by transducers 7–9.

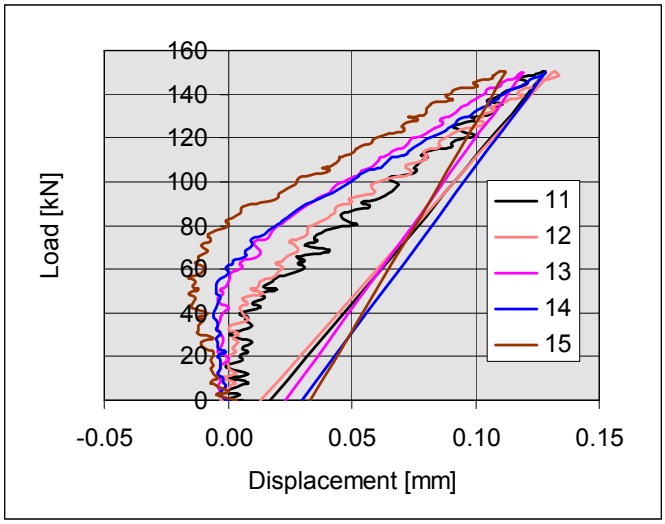

Fig. 84. PF400:9. Vertical displacement measured by transducers 11–15.

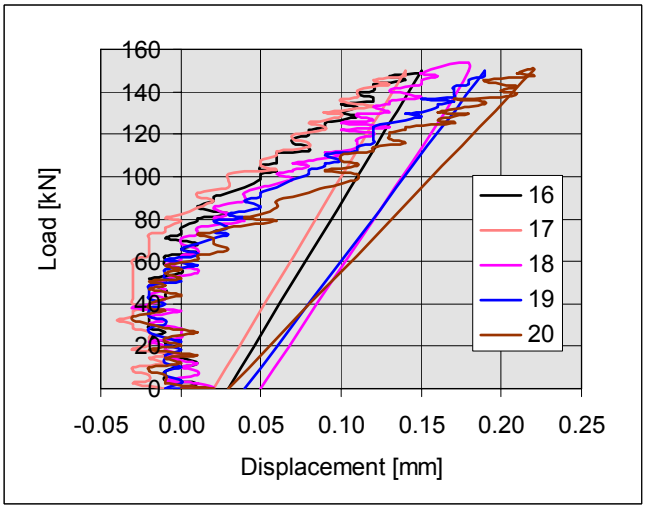

Fig. 85. PF400:9. Vertical displacement measured by transducers 16–20.

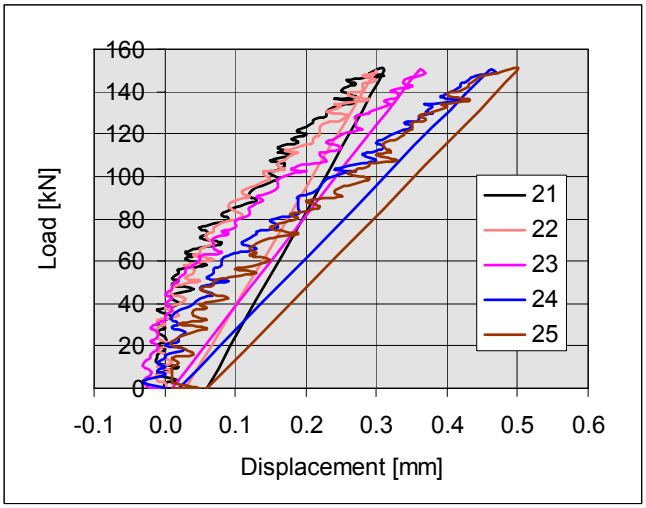

Fig. 86. PF400:9. Vertical displacement measured by transducers 21–25.

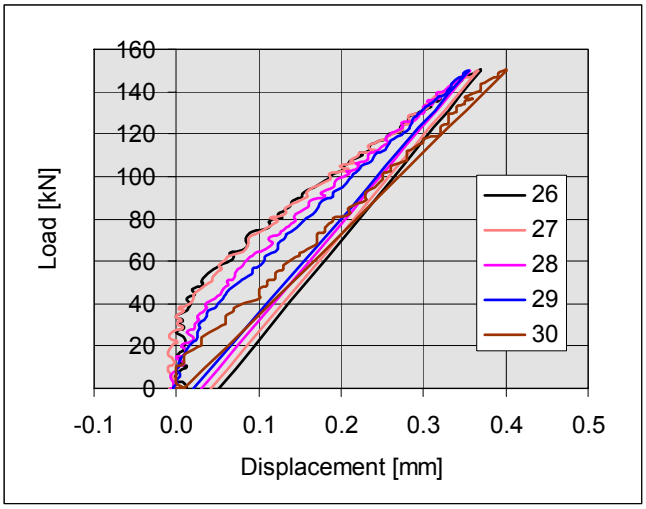

Fig. 87. PF400:9. Vertical displacement measured by transducers 26–30.

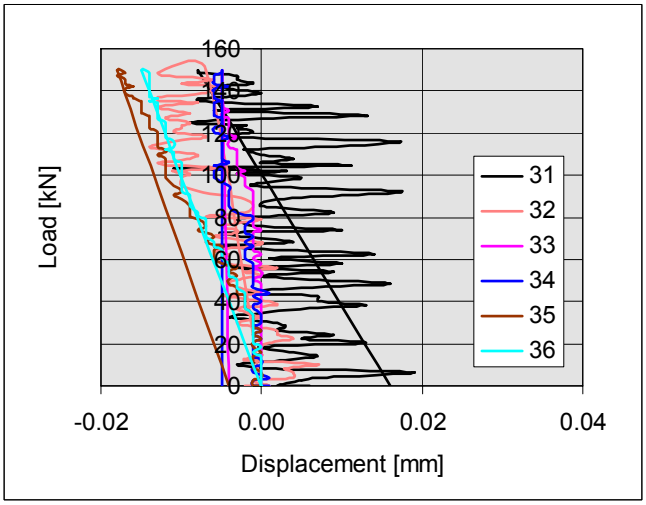

Fig. 88. PF400:9. Vertical displacement measured by transducers 31–36.

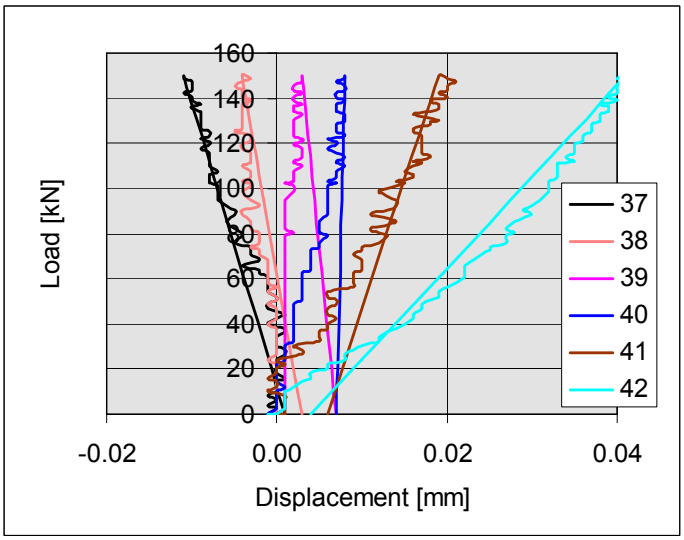

Fig. 89. PF400:9. Vertical displacement measured by transducers 37–42.

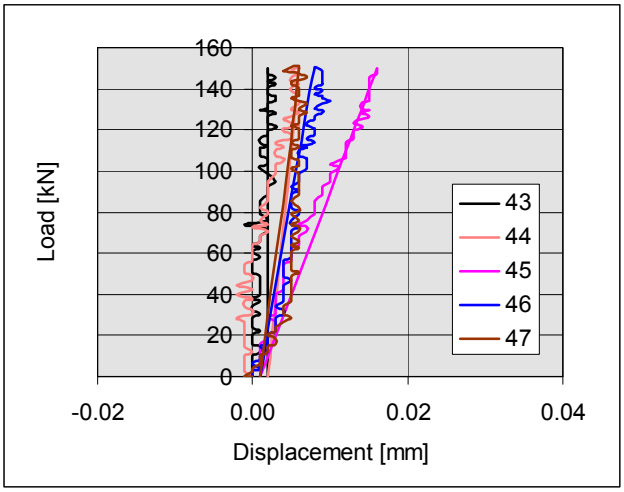

Fig. 90. PF400:9. Vertical displacement measured by transducers 43–47.

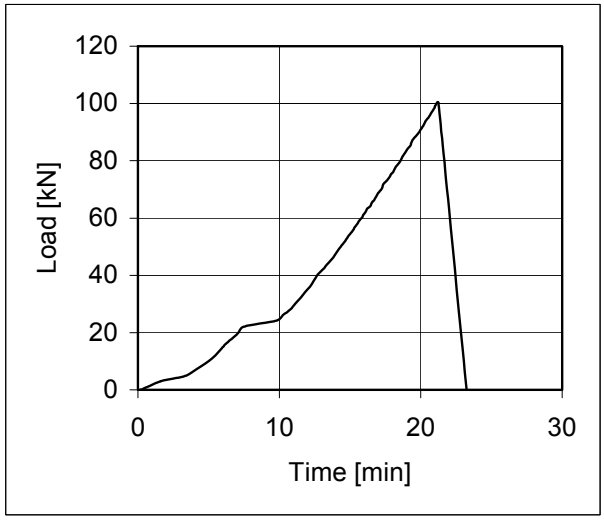

Fig. 91. PF400:10. Load-time relationship.

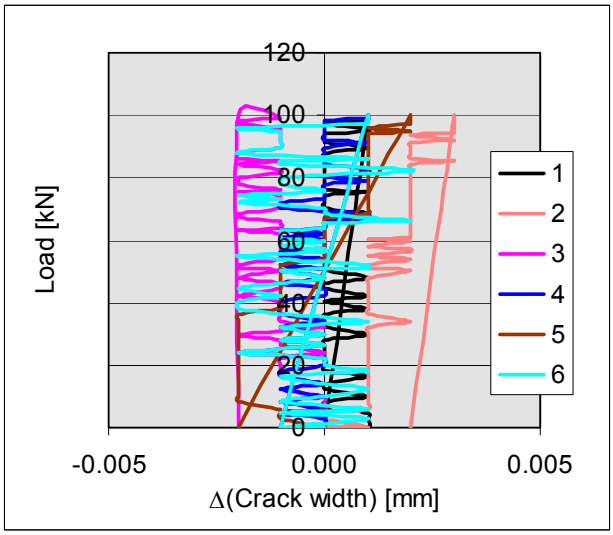

Fig. 92. PF400:10. Change of crack width measured by transducers 1–6.

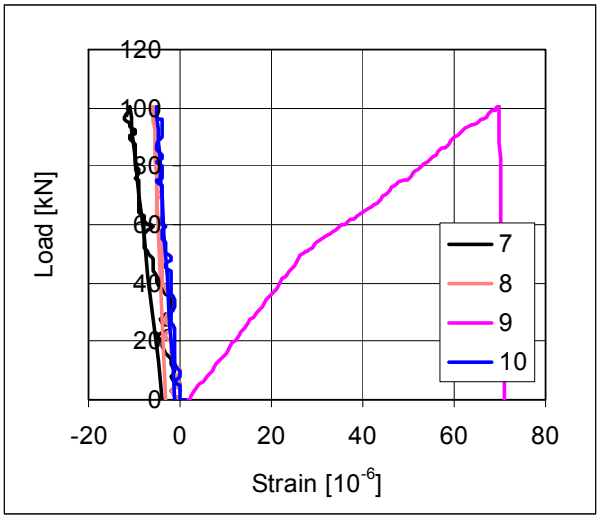

Fig. 93. PF400:10. Strain in tie reinforcement measured by transducers 7–9.

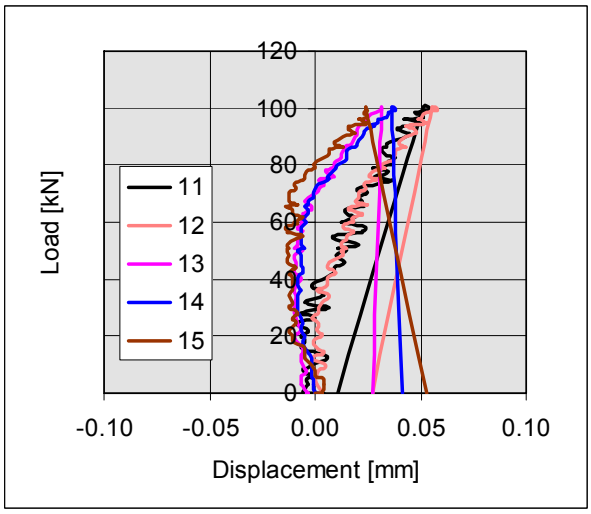

Fig. 94. PF400:10. Vertical displacement measured by transducers 11–15.

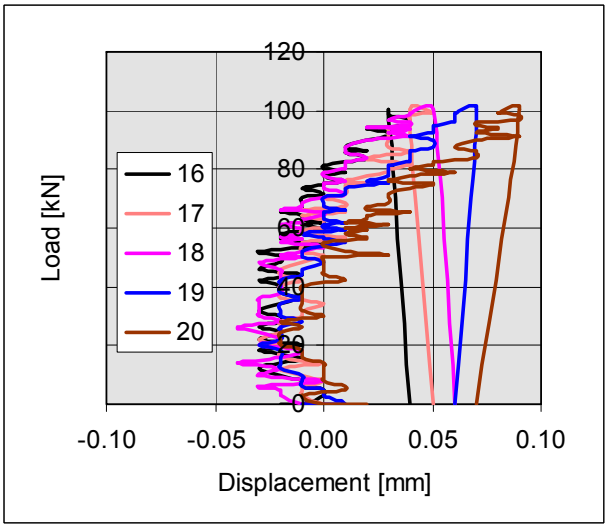

Fig. 95. PF400:10. Vertical displacement measured by transducers 16–20.

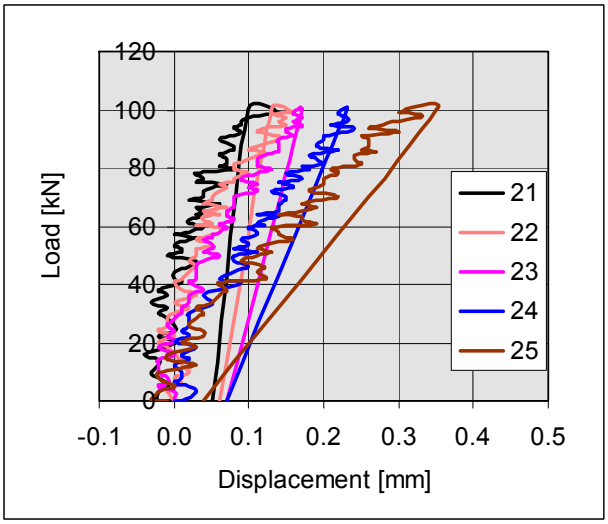

Fig. 96. PF400:10. Vertical displacement measured by transducers 21–25.

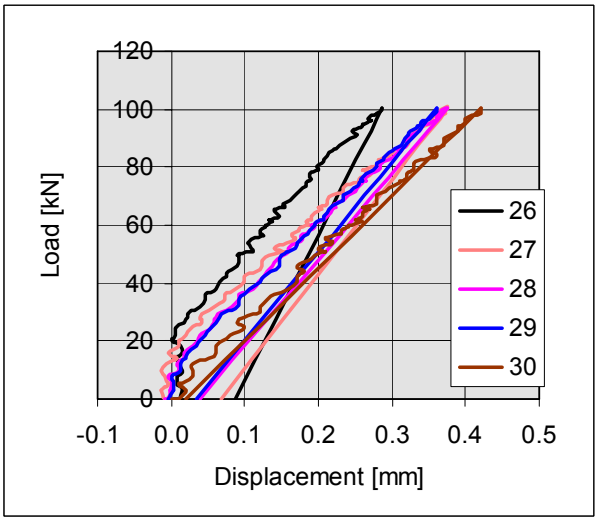

Fig. 97. PF400:10. Vertical displacement measured by transducers 26–30.

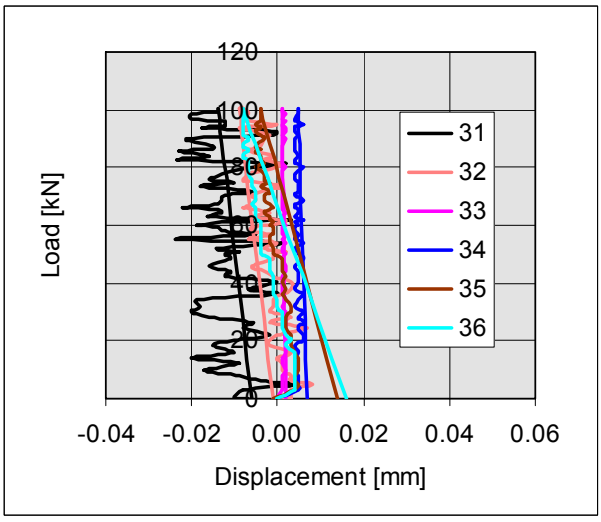

Fig. 98. PF400:10. Vertical displacement measured by transducers 31–36.

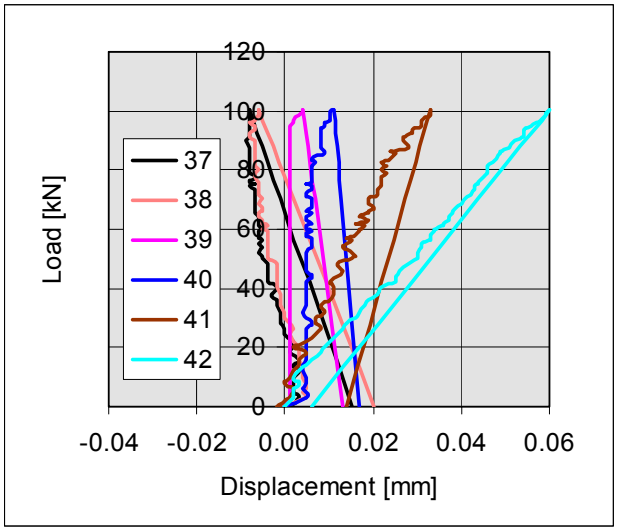

Fig. 99. PF400:10. Vertical displacement measured by transducers 37–42.

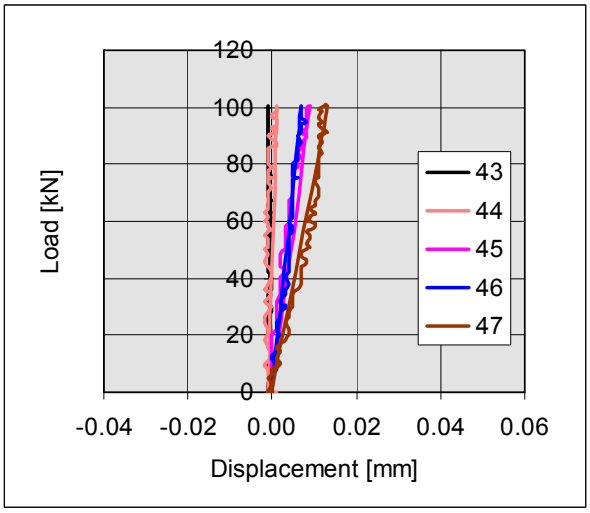

Fig. 100. PF400:10. Vertical displacement measured by transducers 43–47.

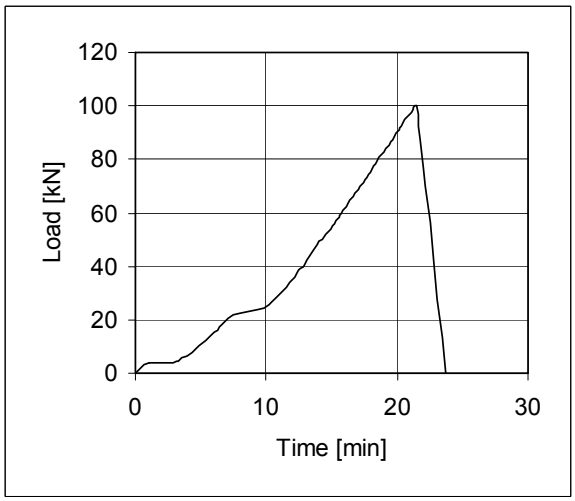

Fig. 101. PF400:11. Load-time relationship.

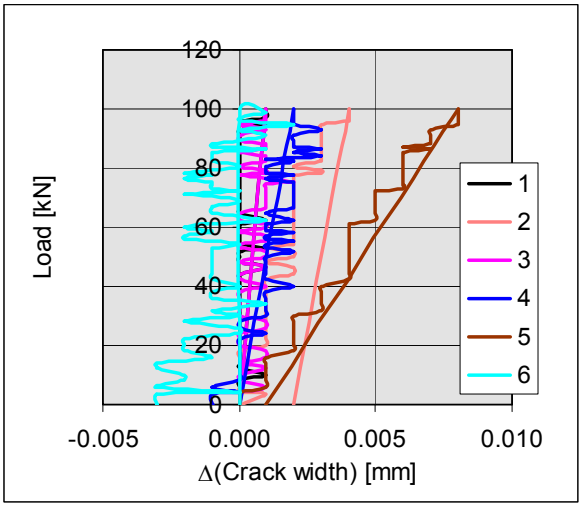

Fig. 102. PF400:11. Change of crack width measured by transducers 1–6.

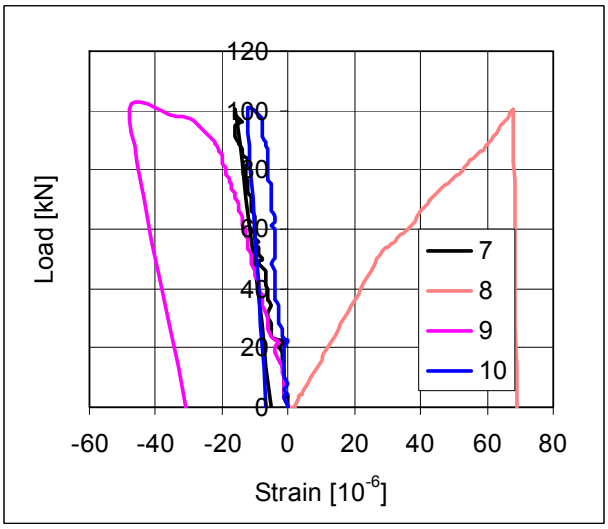

Fig. 103. PF400:11. Strain in tie reinforcement measured by transducers 7–9.

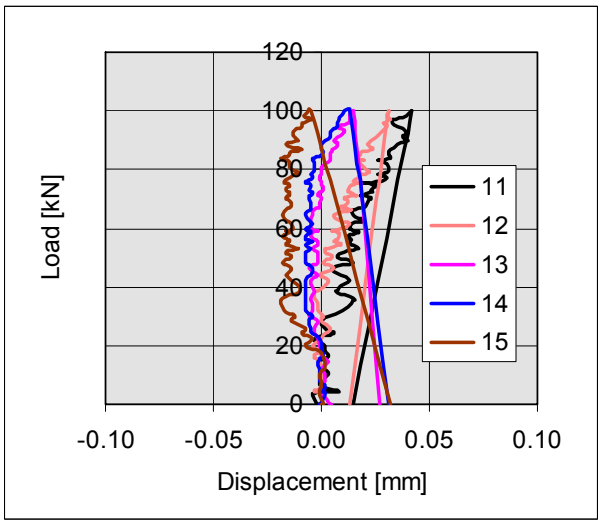

Fig. 104. PF400:11. Vertical displacement measured by transducers 11–15.

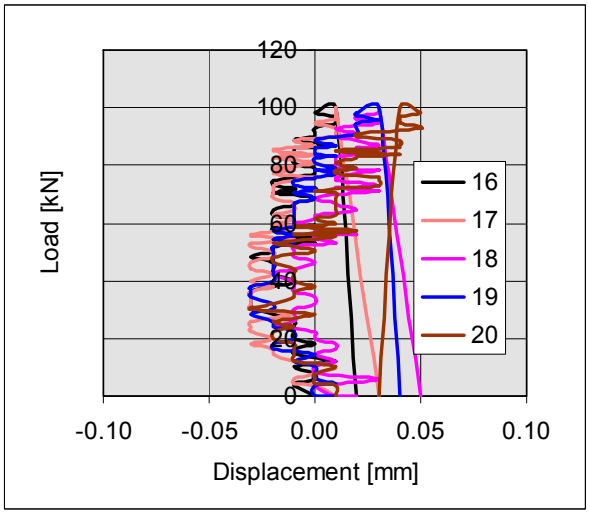

Fig. 105. PF400:11. Vertical displacement measured by transducers 16–20.

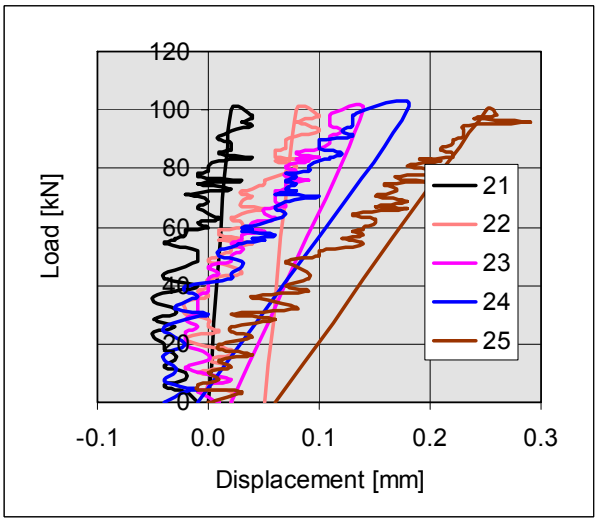

Fig. 106. PF400:11. Vertical displacement measured by transducers 21–25.

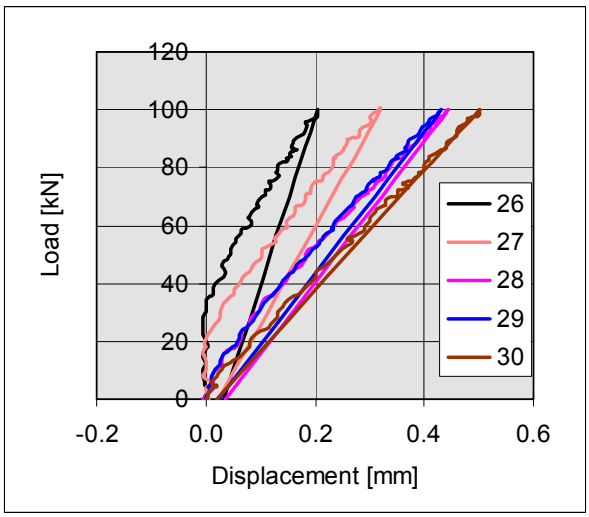

Fig. 107. PF400:11. Vertical displacement measured by transducers 26–30.

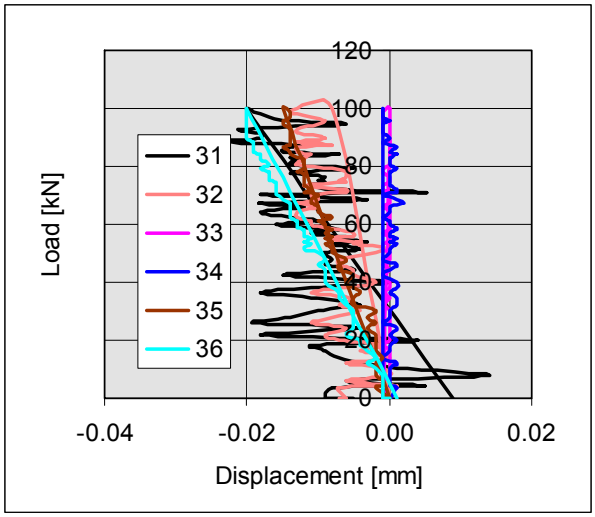

Fig. 108. PF400:11. Vertical displacement measured by transducers 31–36.

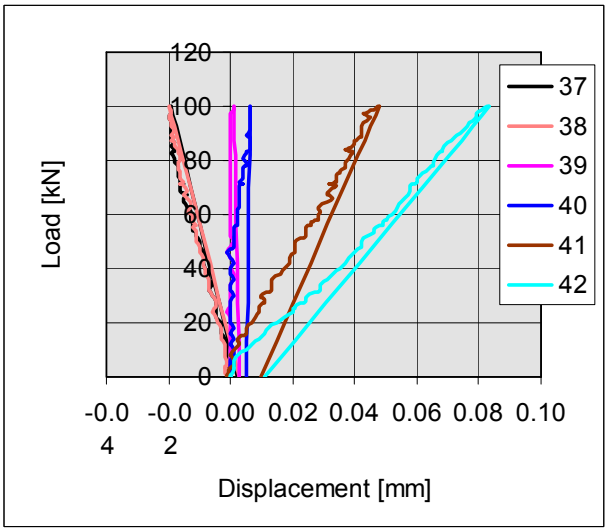

Fig. 109. PF400:11. Vertical displacement measured by transducers 37–42.

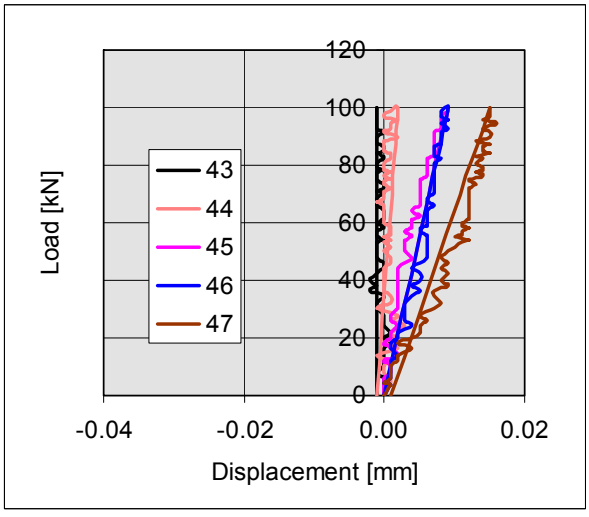

Fig. 110. PF400:11. Vertical displacement measured by transducers 43–47.

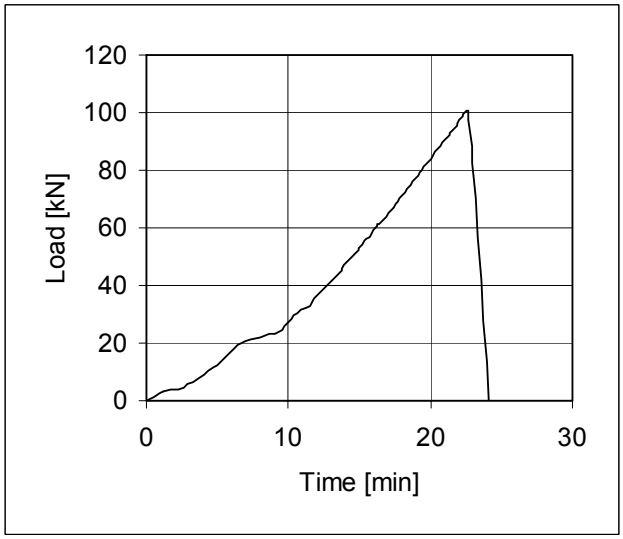

Fig. 111. PF400:12. Load-time relationship.

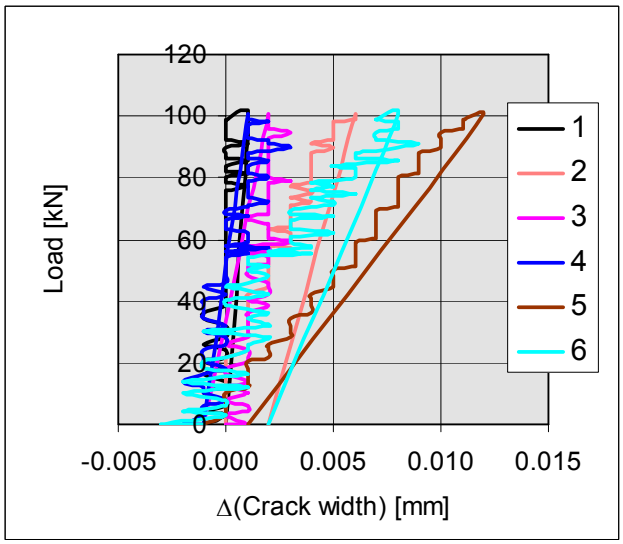

Fig. 112. PF400:12. Change of crack width measured by transducers 1–6.

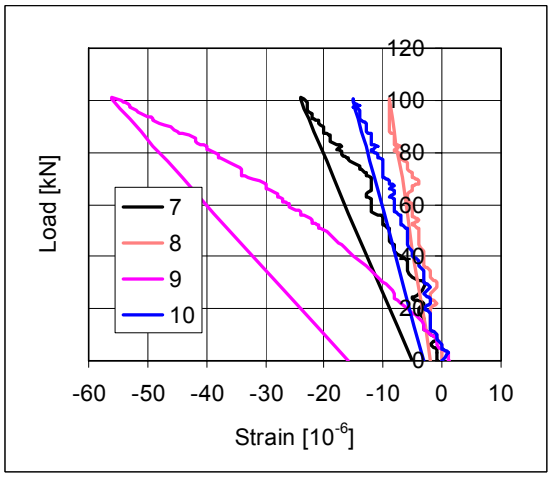

Fig. 113. PF400:12. Strain in tie reinforcement measured by transducers 7–9.

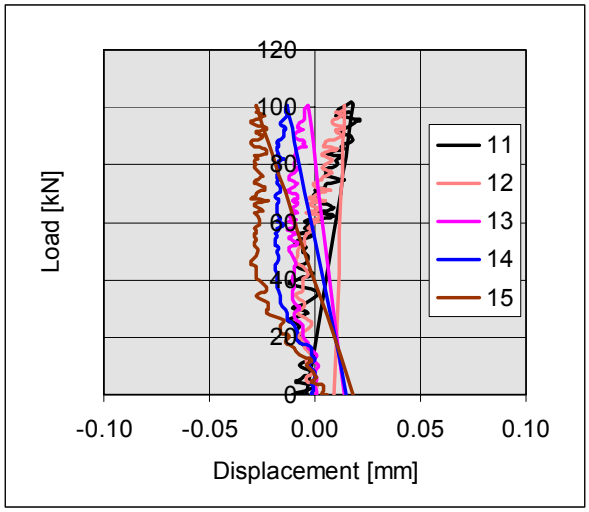

Fig. 114. PF400:12. Vertical displacement measured by transducers 11–15.

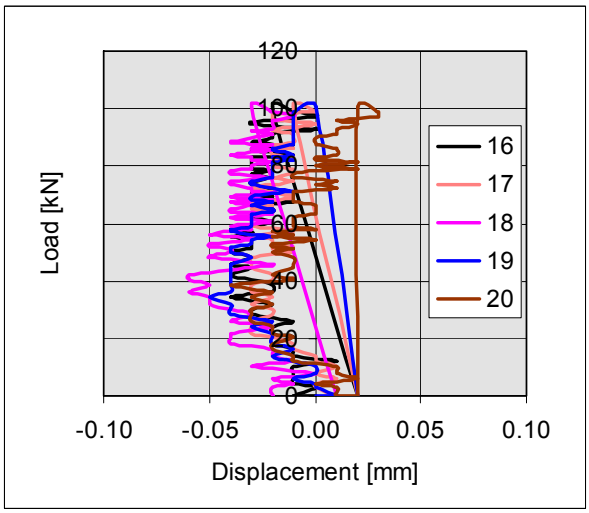

Fig. 115. PF400:12. Vertical displacement measured by transducers 16–20.

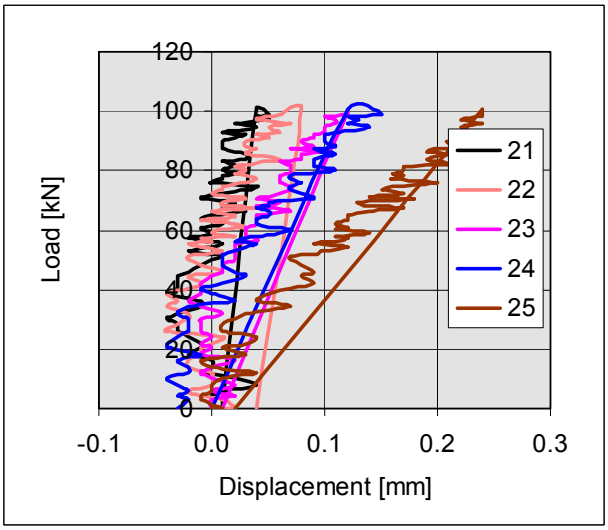

Fig. 116. PF400:12. Vertical displacement measured by transducers 21–25.

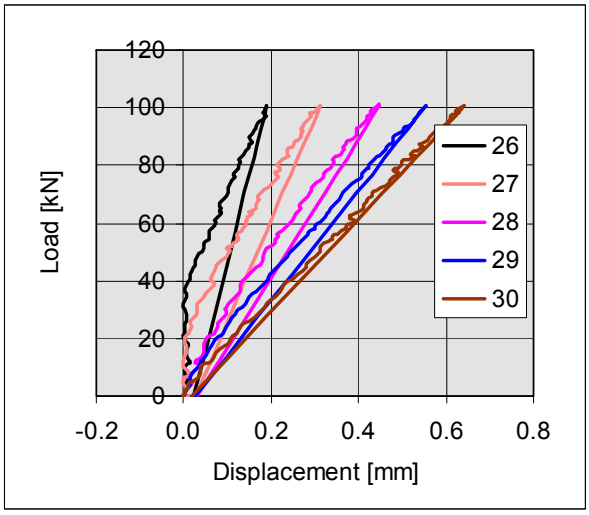

Fig. 117. PF400:12. Vertical displacement measured by transducers 26–30.

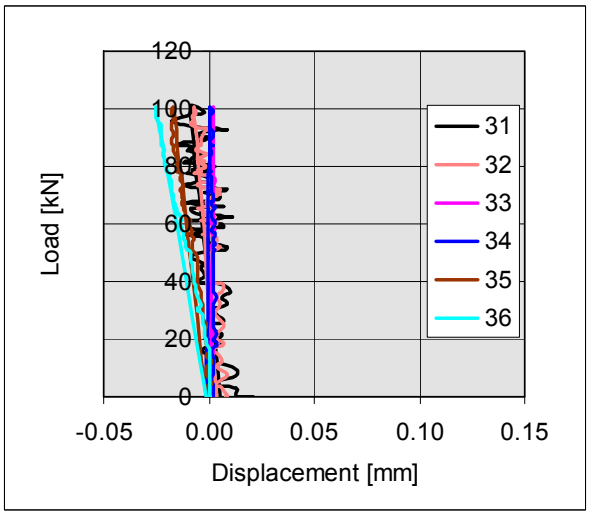

Fig. 118. PF400:12. Vertical displacement measured by transducers 31–36.

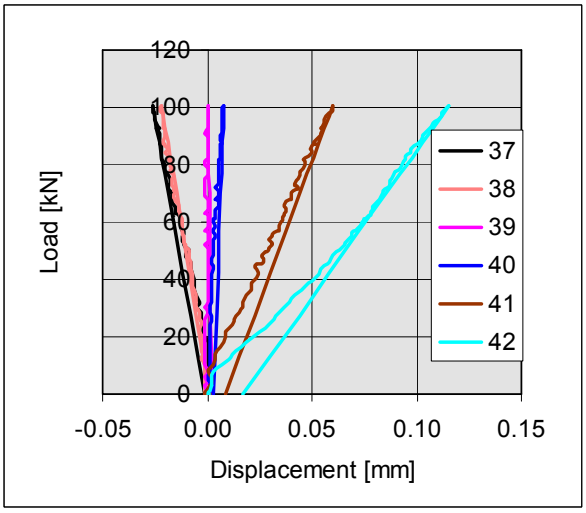

Fig. 119. PF400:12. Vertical displacement measured by transducers 37–42.

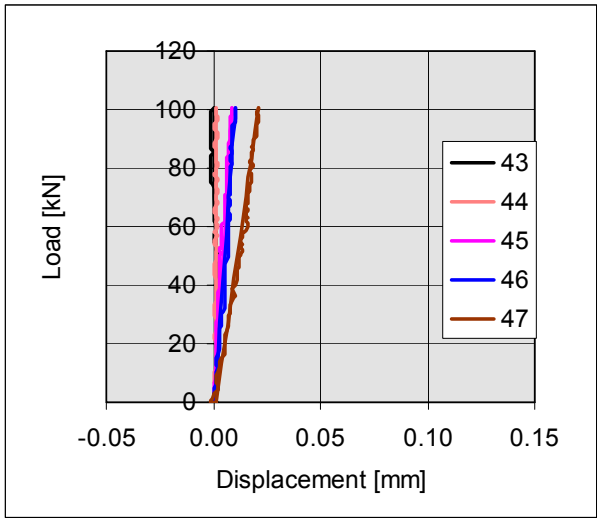

Fig. 120. PF400:12. Vertical displacement measured by transducers 43–47.

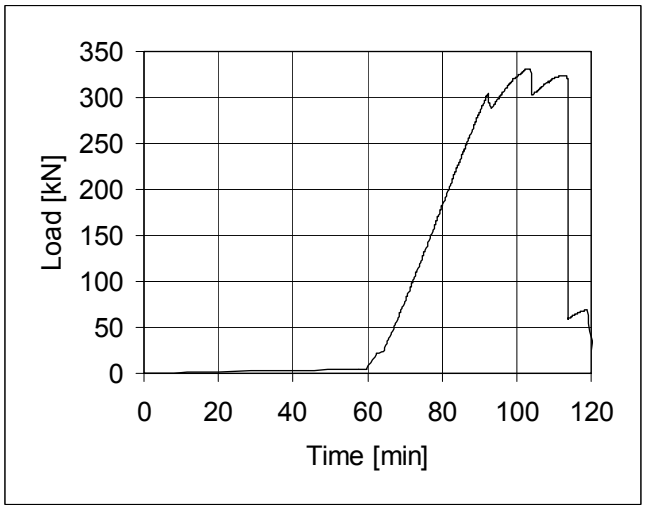

Fig. 121. PF400:13. Load-time relationship.

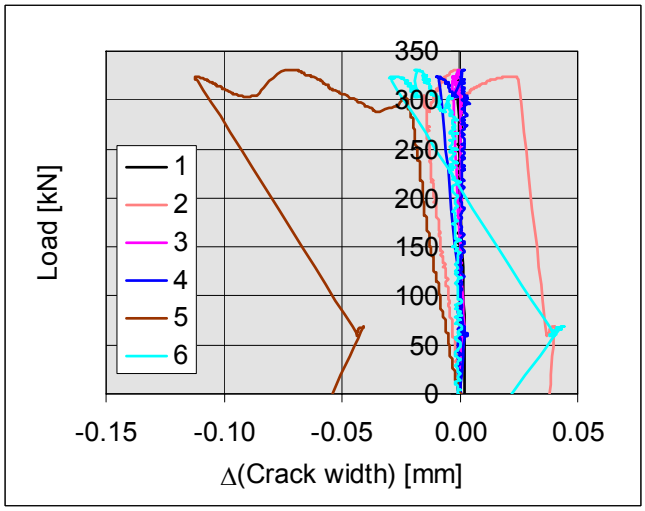

Fig. 122. PF400:13. Change of crack width measured by transducers 1–6.

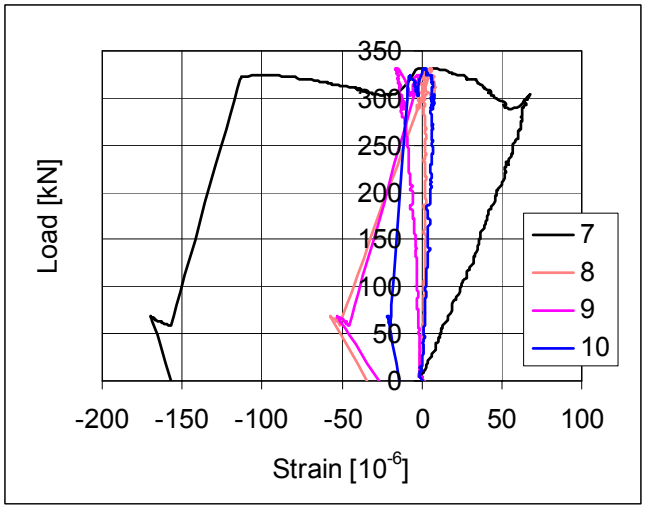

Fig. 123. PF400:13. Strain in tie reinforcement measured by transducers 7–9.

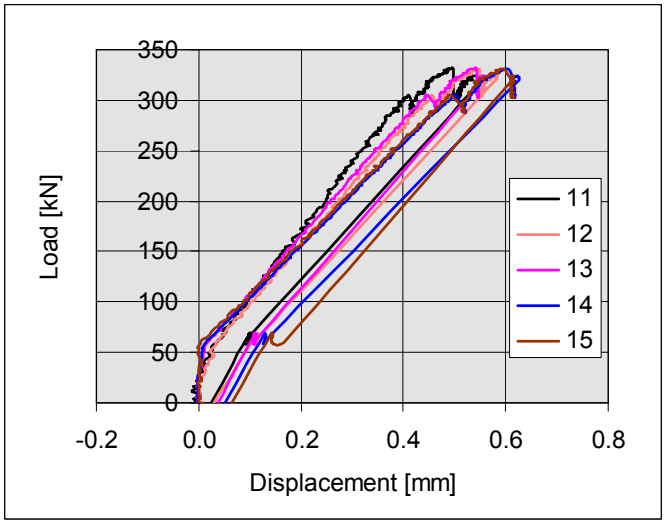

Fig. 124. PF400:13. Vertical displacement measured by transducers 11–15.

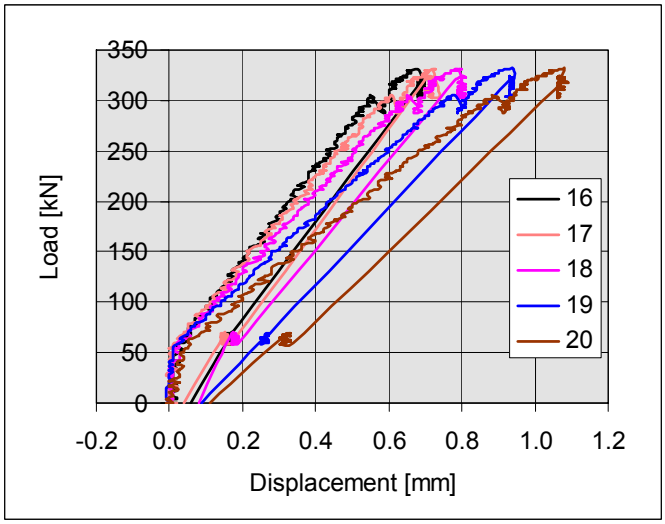

Fig. 125. PF400:13. Vertical displacement measured by transducers 16–20.

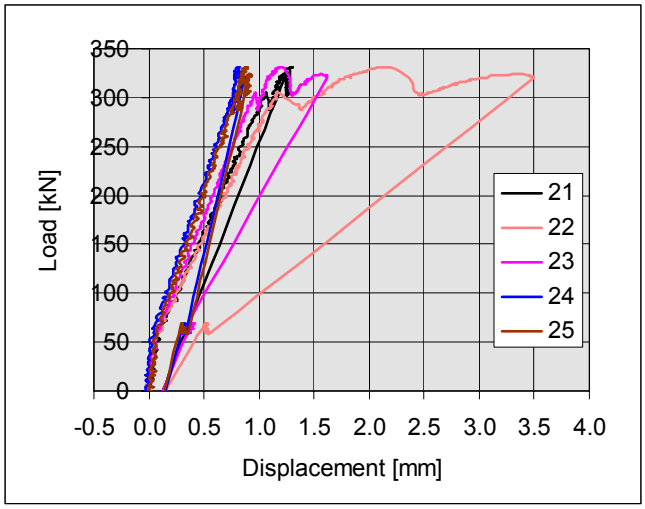

Fig. 126. PF400:13. Vertical displacement measured by transducers 21–25.

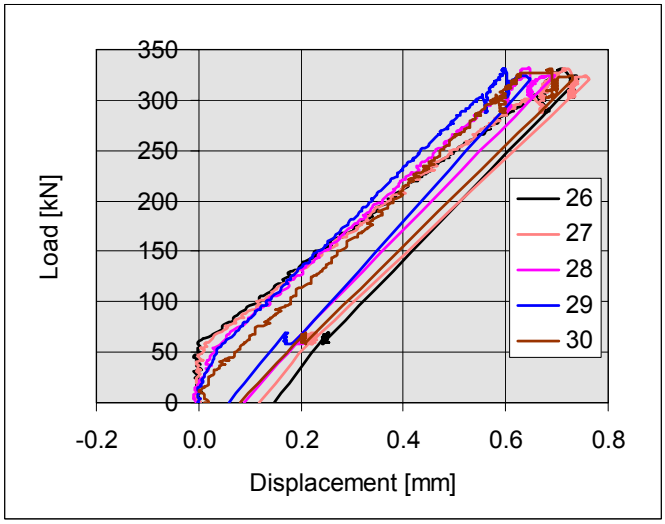

Fig. 127. PF400:13. Vertical displacement measured by transducers 26–30.

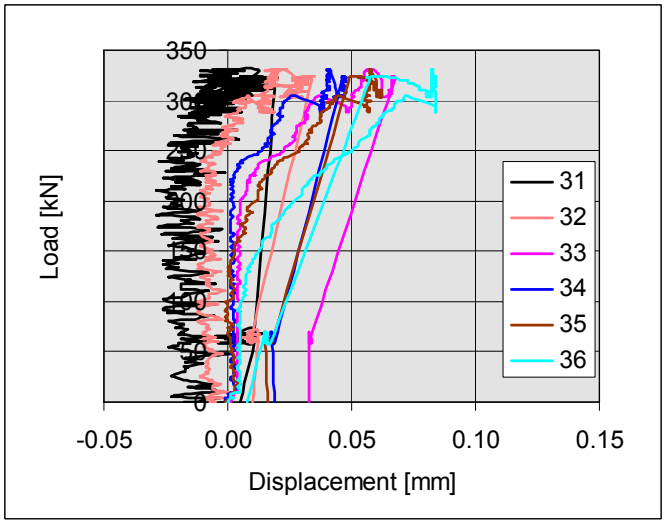

Fig. 128. PF400:13. Vertical displacement measured by transducers 31–36.

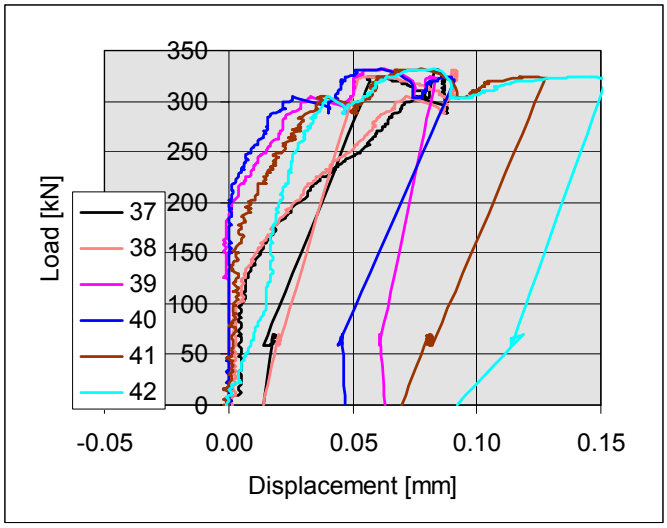

Fig. 129. PF400:13. Vertical displacement measured by transducers 37–42.

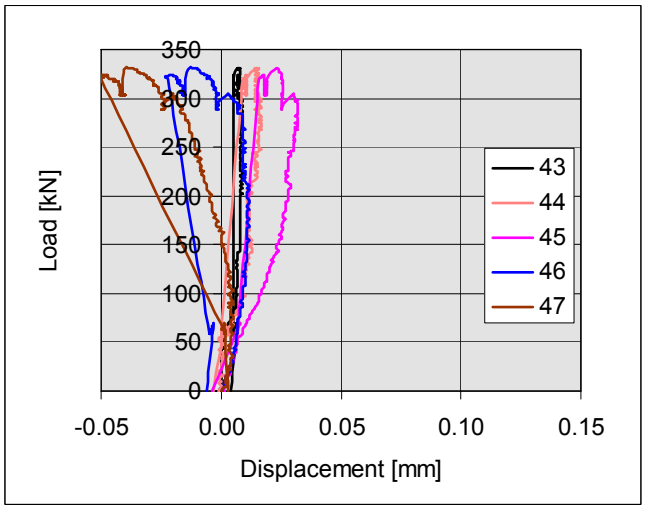

Fig. 130. PF400:13. Vertical displacement measured by transducers 43–47.

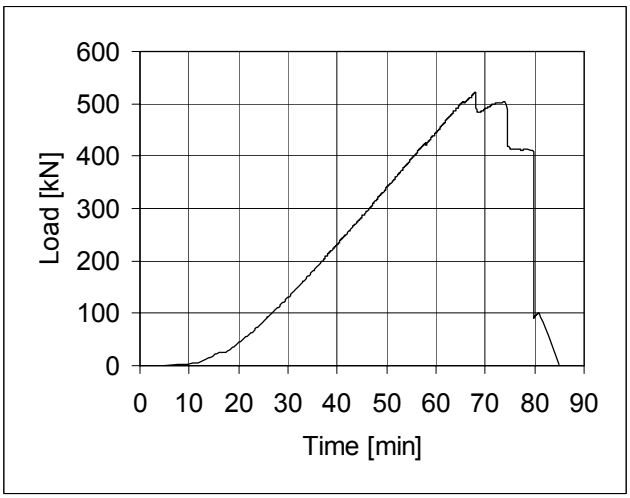

Fig. 131. PF400:14. Load-time relationship.

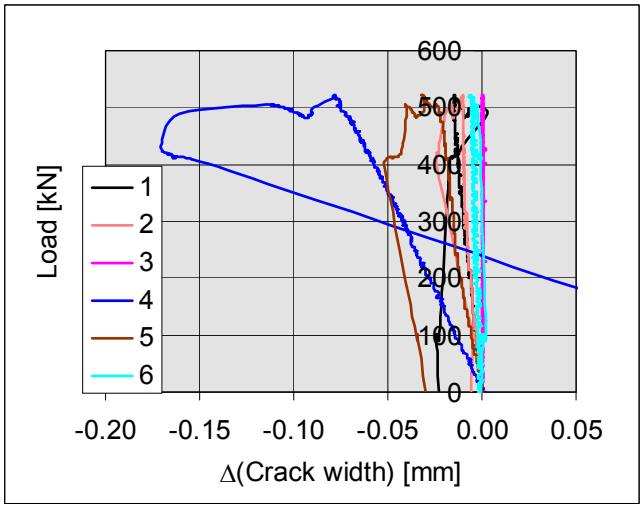

Fig. 132. PF400:14. Change of crack width measured by transducers 1–6.

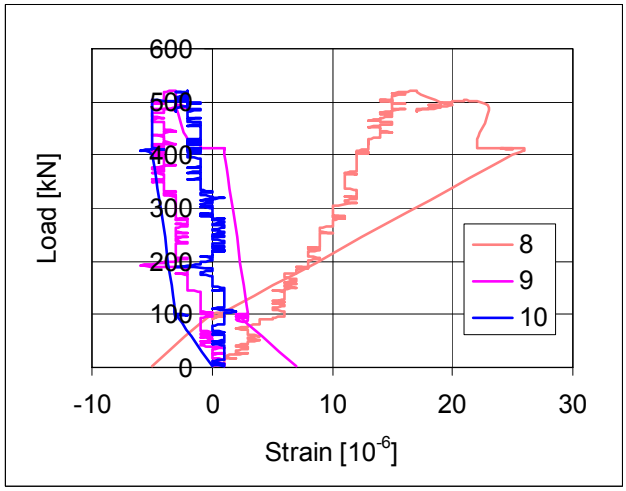

Fig. 133. PF400:14. Strain in tie reinforcement measured by transducers 8–9. (No. 7 out of action).

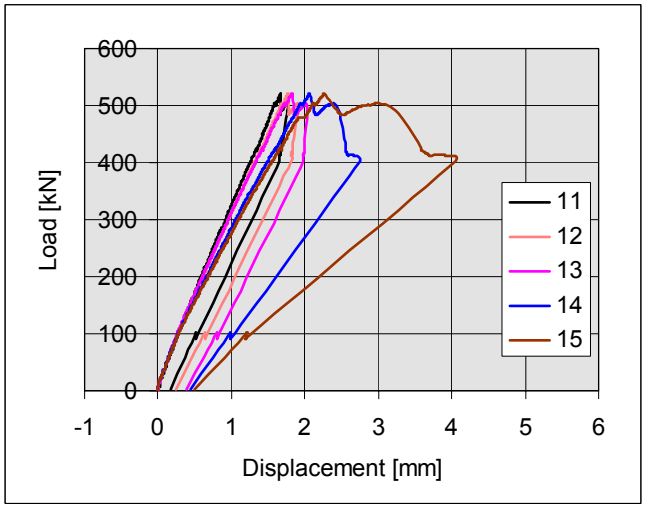

Fig. 134. PF400:14. Vertical displacement measured by transducers 11–15.

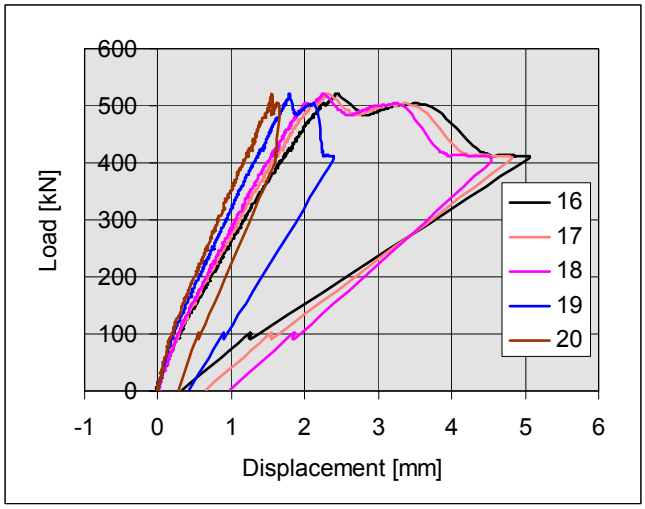

Fig. 135. PF400:14. Vertical displacement measured by transducers 16–20.

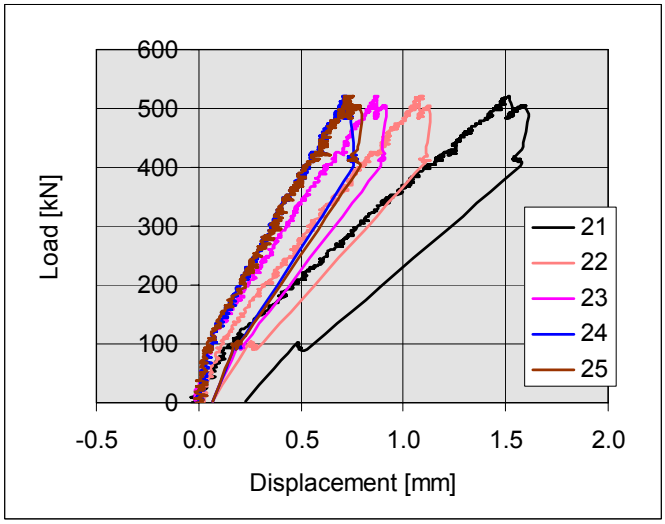

Fig. 136. PF400:14. Vertical displacement measured by transducers 21–25.

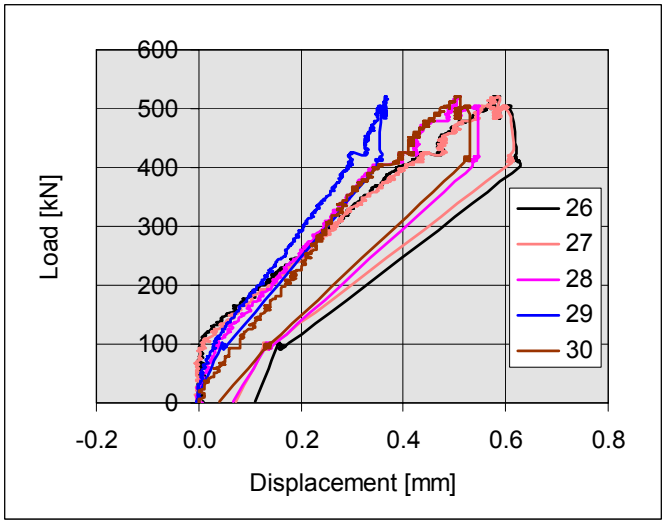

Fig. 137. PF400:14. Vertical displacement measured by transducers 26–30.

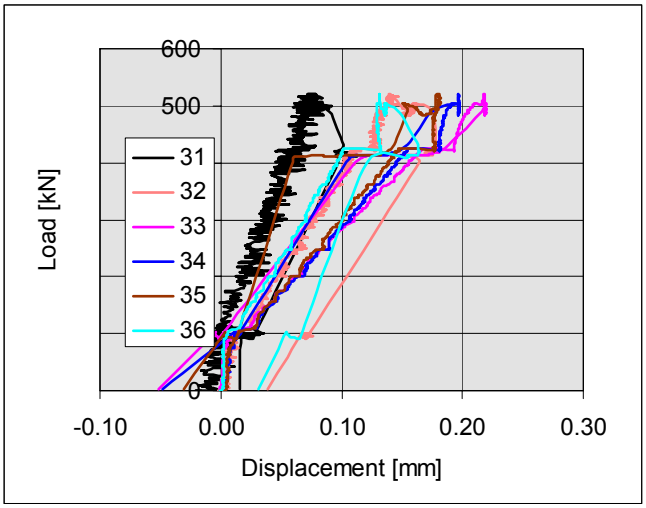

Fig. 138. PF400:14. Vertical displacement measured by transducers 31–36.

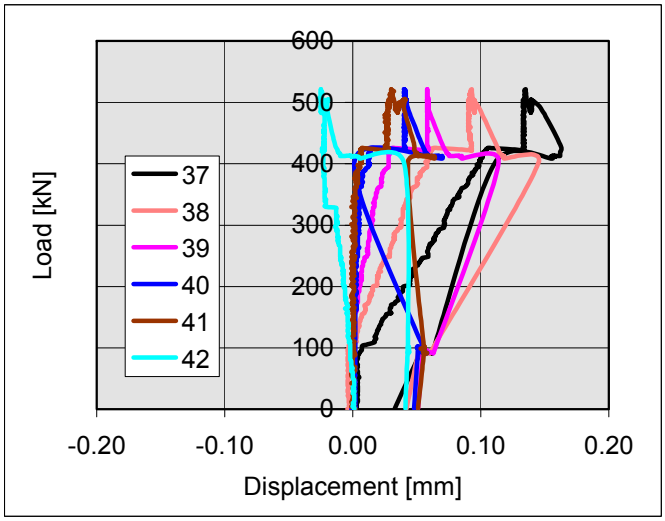

Fig. 139. PF400:14. Vertical displacement measured by transducers 37–42.

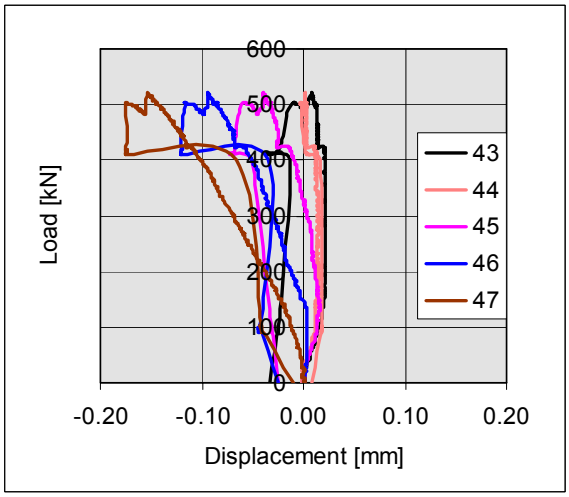

Fig. 140. PF400:14. Vertical displacement measured by transducers 43–47.

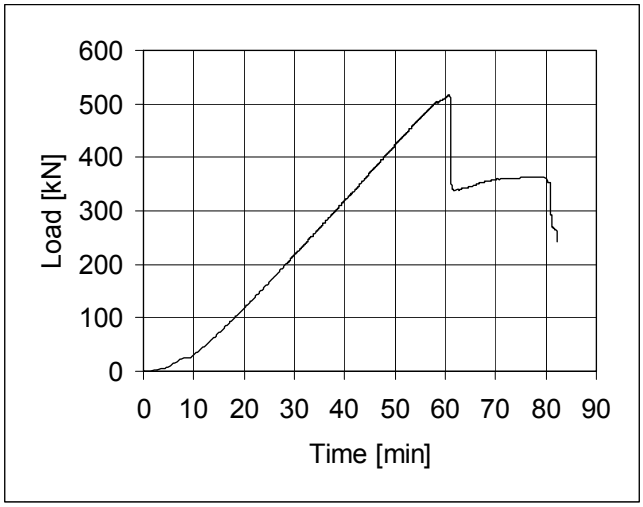

Fig. 141. PF400:15. Load-time relationship.

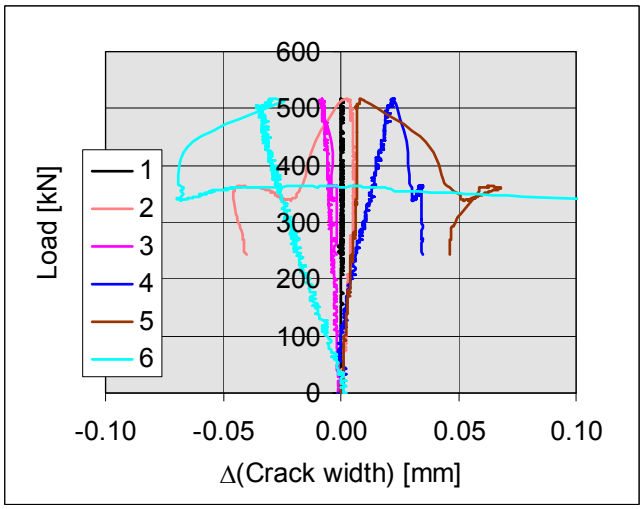

Fig. 142. PF400:15. Change of crack width measured by transducers 1–6.

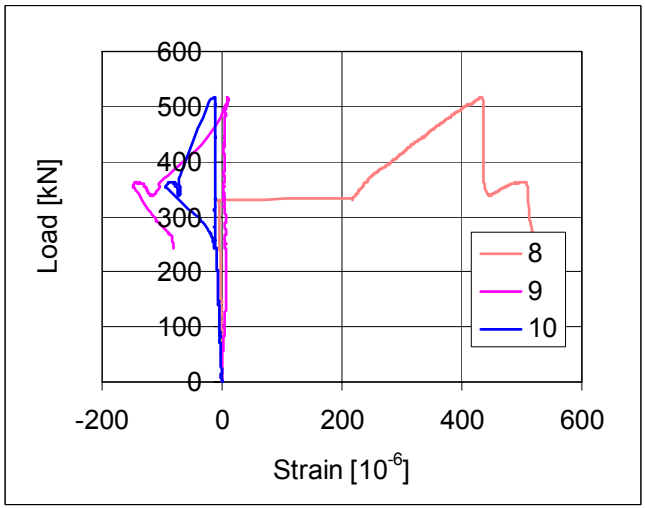

Fig. 143. PF400:15. Strain in tie reinforcement measured by transducers 8–9. (No. 7 out of action).

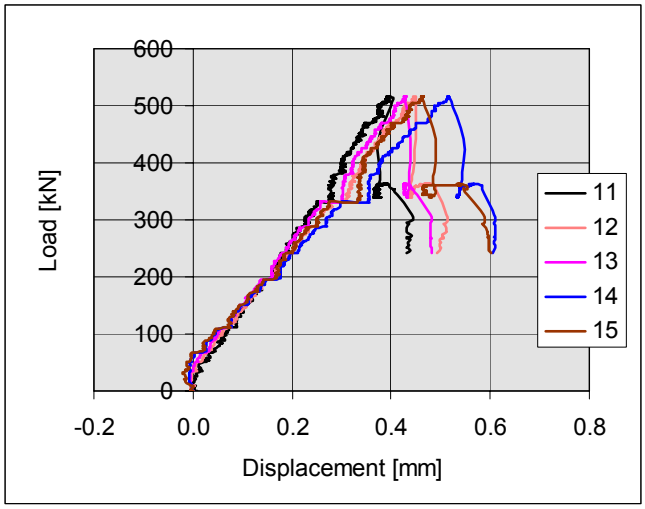

Fig. 144. PF400:15. Vertical displacement measured by transducers 11–15.

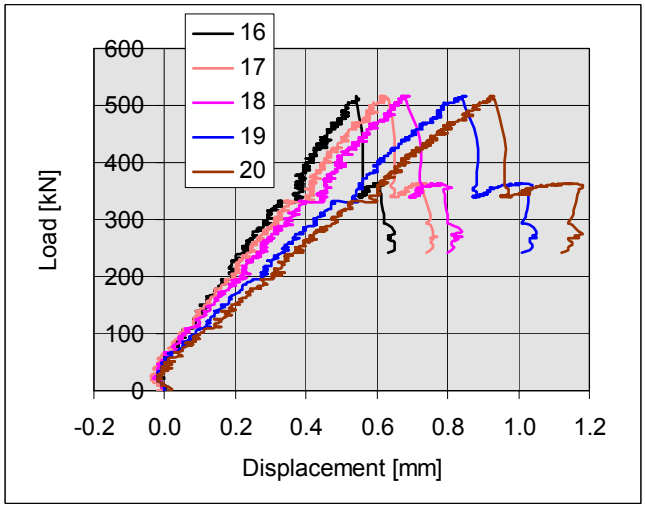

Fig. 145. PF400:15. Vertical displacement measured by transducers 16–20.

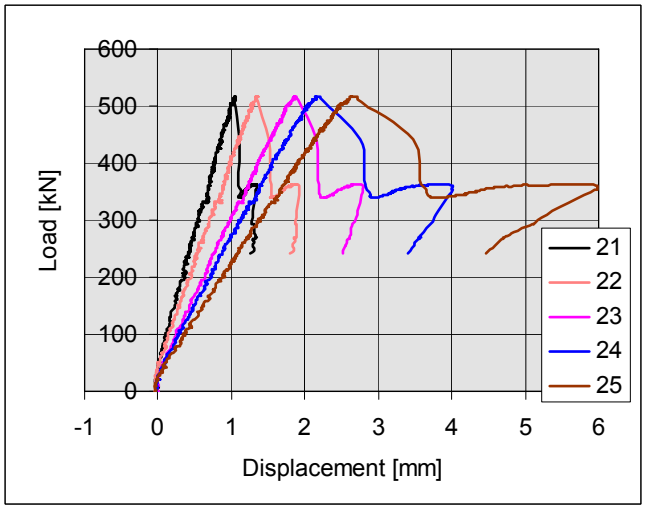

Fig. 146. PF400:15. Vertical displacement measured by transducers 21–25.

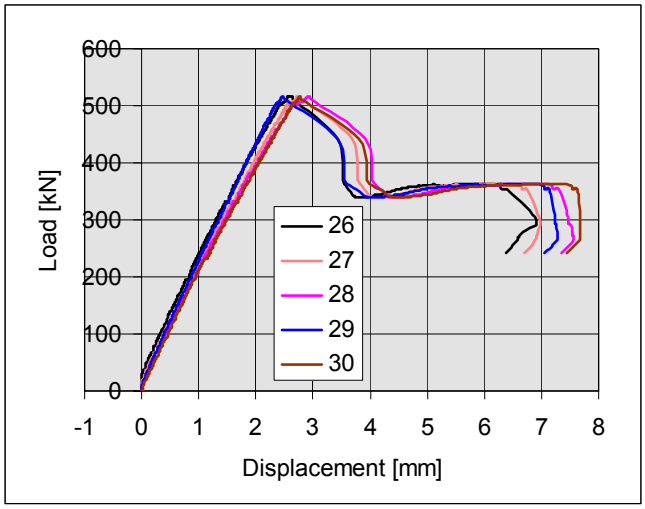

Fig. 147. PF400:15. Vertical displacement measured by transducers 26–30.

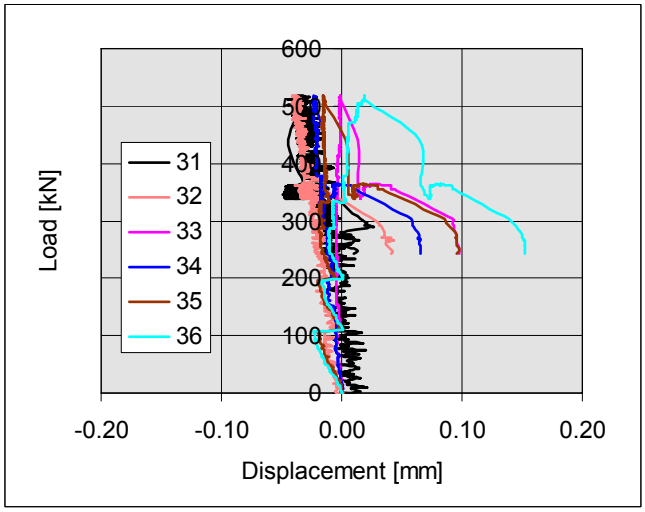

Fig. 148. PF400:15. Vertical displacement measured by transducers 31–36.

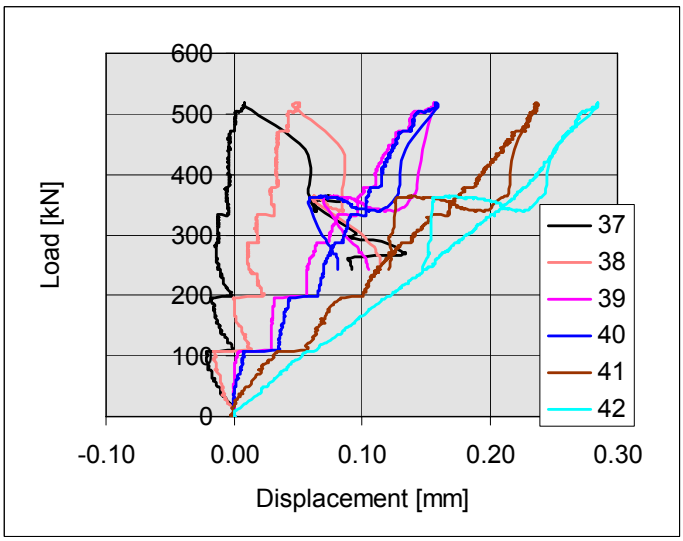

Fig. 149. PF400:15. Vertical displacement measured by transducers 37–42.

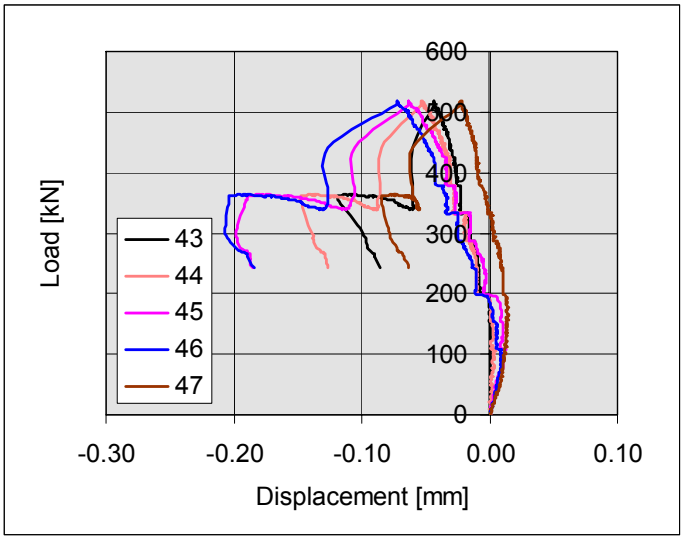

Fig. 150. PF400:15. Vertical displacement measured by transducers 43–47.

Appendix D: Initial part of load-deflection curves

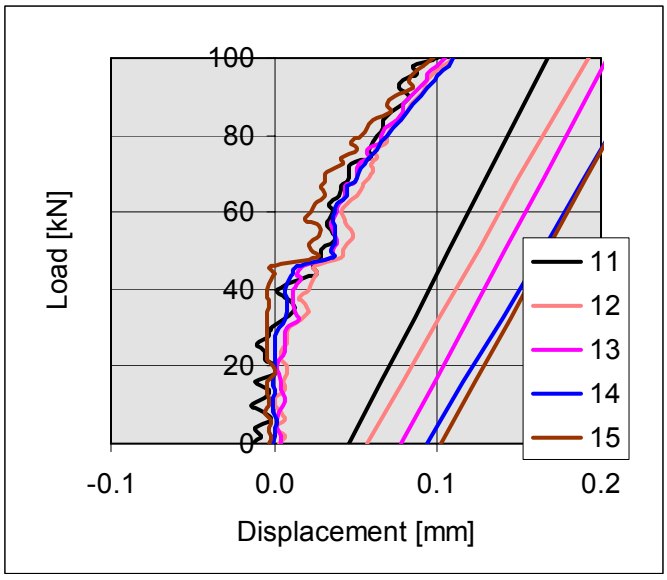

Fig. 1. PF400:1. Vertical displacement measured by transducers 11–15.

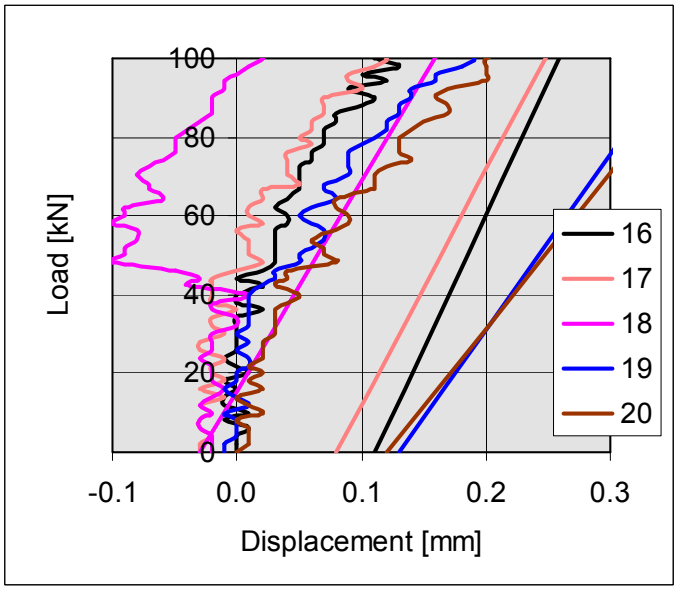

Fig. 2. PF400:1. Vertical displacement measured by transducers 16–20.

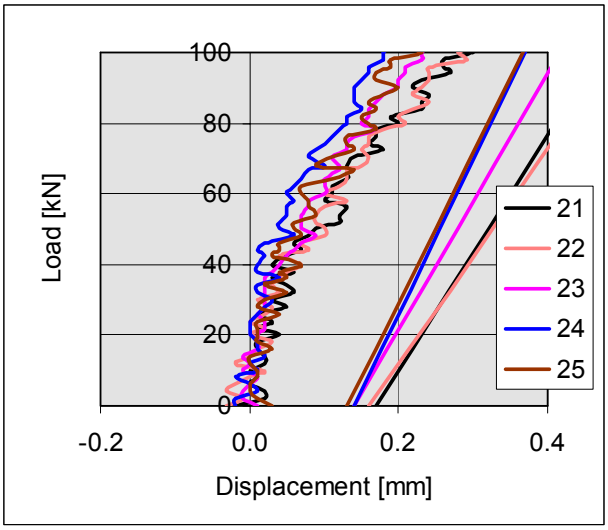

Fig. 3. PF400:1. Vertical displacement measured by transducers 21–25.

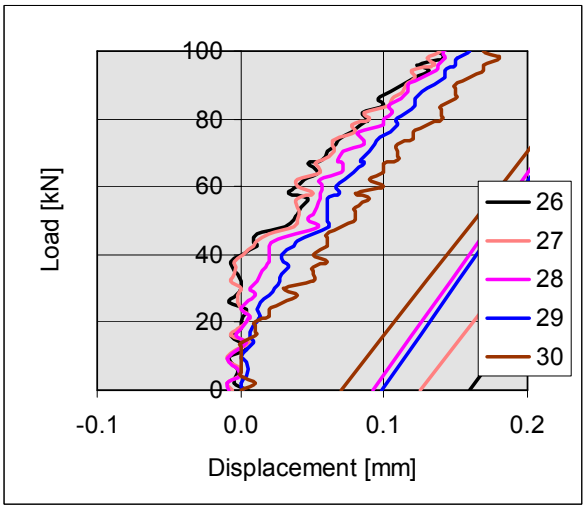

Fig. 4. PF400:1. Vertical displacement measured by transducers 26–30.

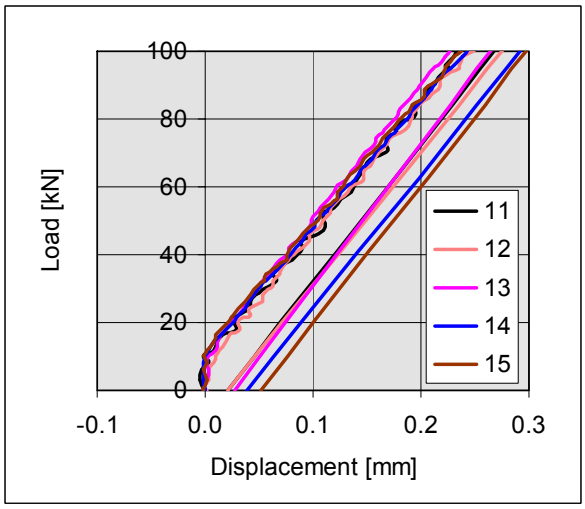

Fig. 5. PF400:4. Vertical displacement measured by transducers 11–15.

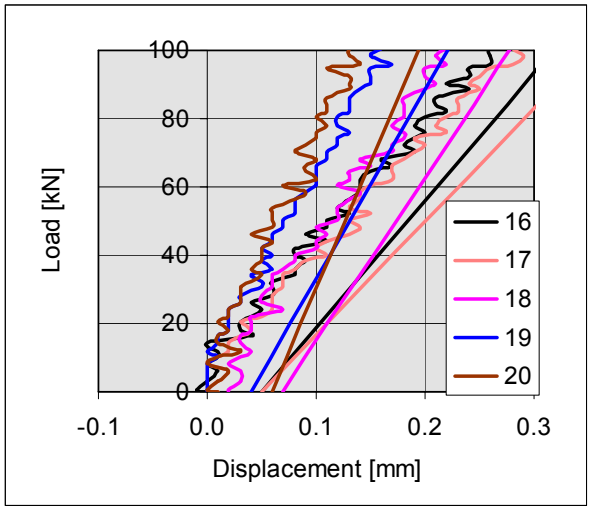

Fig. 6. PF400:4. Vertical displacement measured by transducers 16–20.

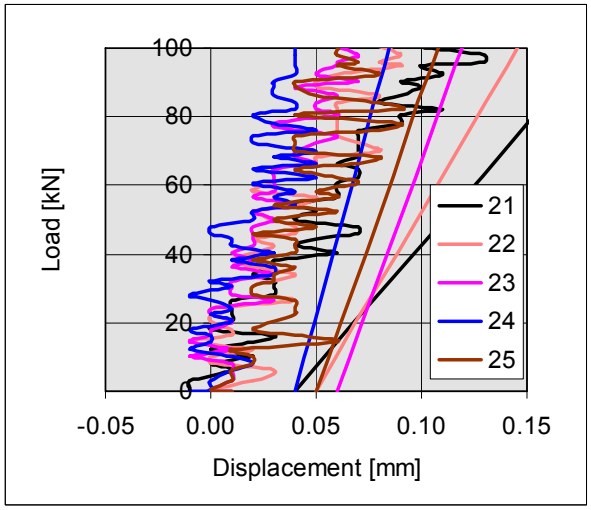

Fig. 7. PF400:4. Vertical displacement measured by transducers 21–25.

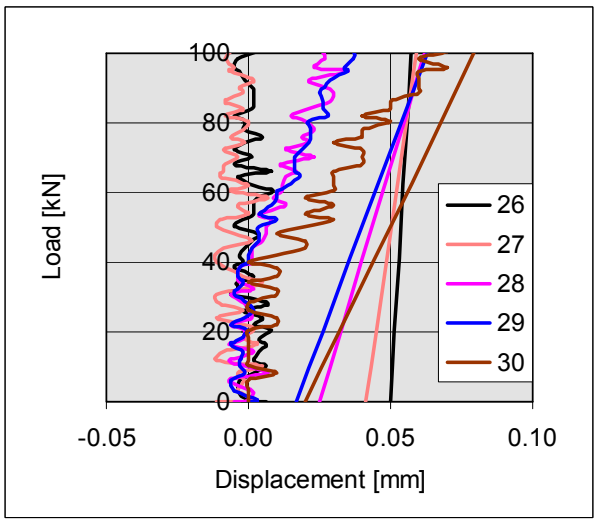

Fig. 8. PF400:4. Vertical displacement measured by transducers 26–30.

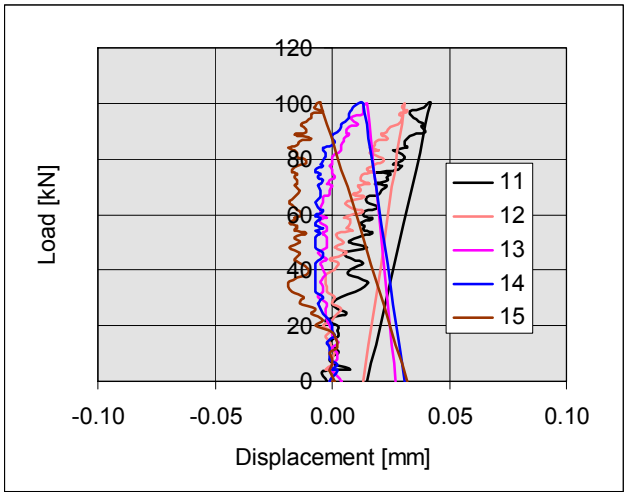

Fig. 9. PF400:10. Vertical displacement measured by transducers 11–15.

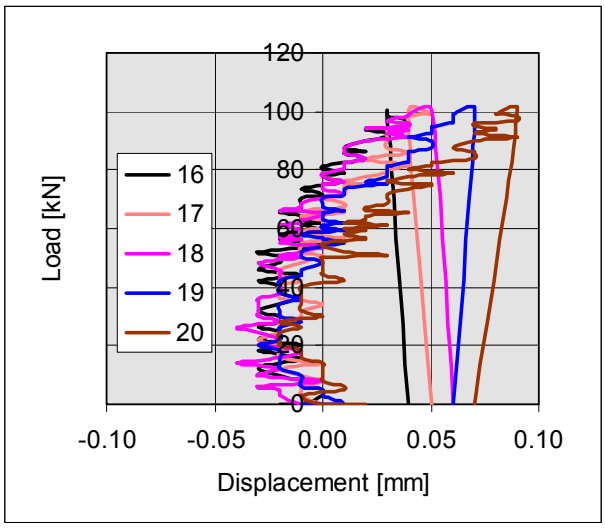

Fig. 10. PF400:10. Vertical displacement measured by transducers 16–20.

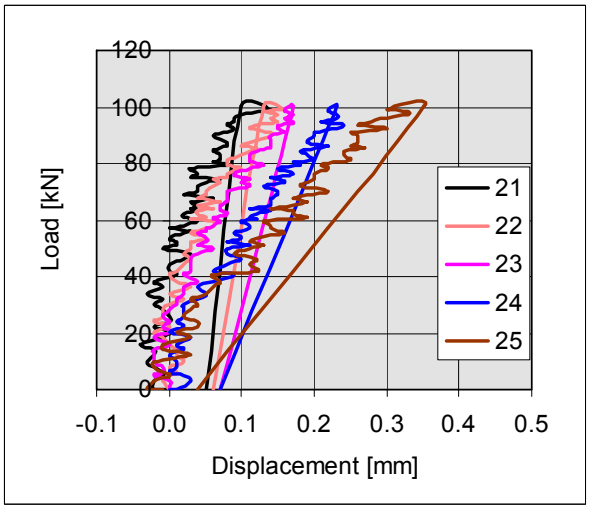

Fig. 11. PF400:10. Vertical displacement measured by transducers 21–25.

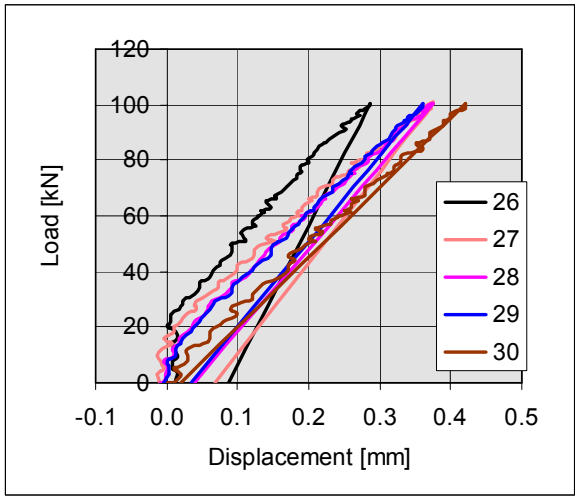

Fig. 12. PF400:10. Vertical displacement measured by transducers 26–30.

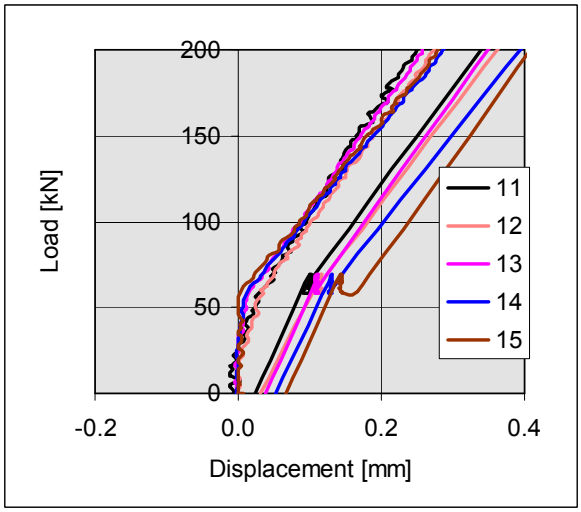

Fig. 13. PF400:13. Vertical displacement measured by transducers 11–15.

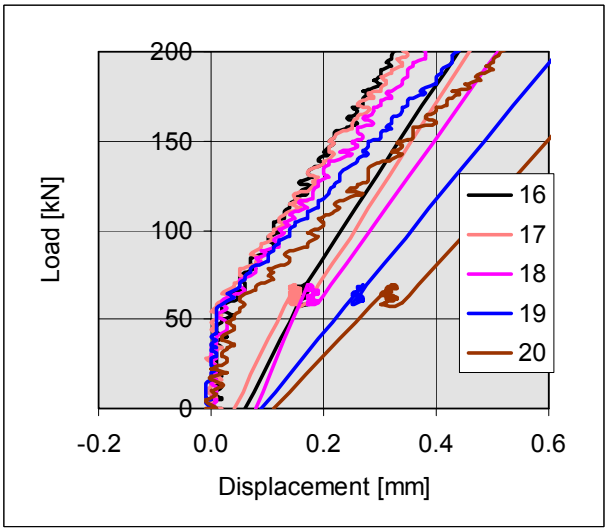

Fig. 14. PF400:13. Vertical displacement measured by transducers 16–20.

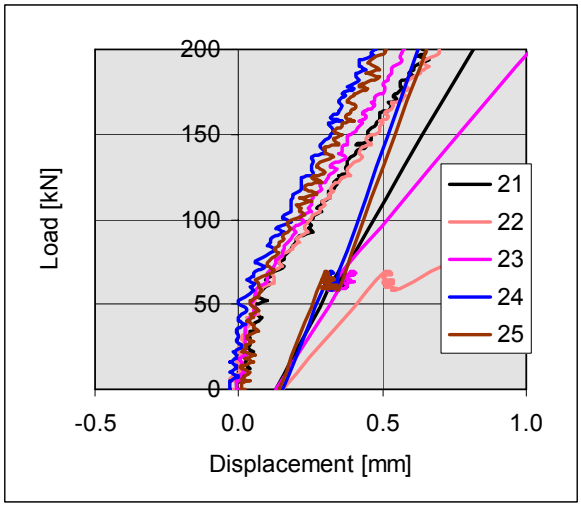

Fig. 15. PF400:13. Vertical displacement measured by transducers 21–25.

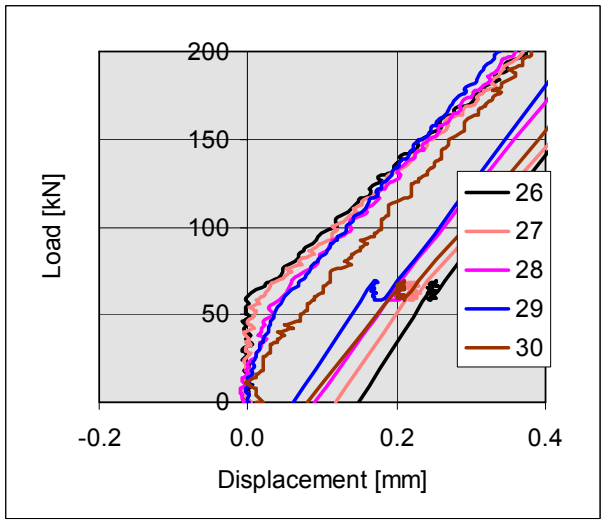

Fig. 16. PF400:13. Vertical displacement measured by transducers 26–30.

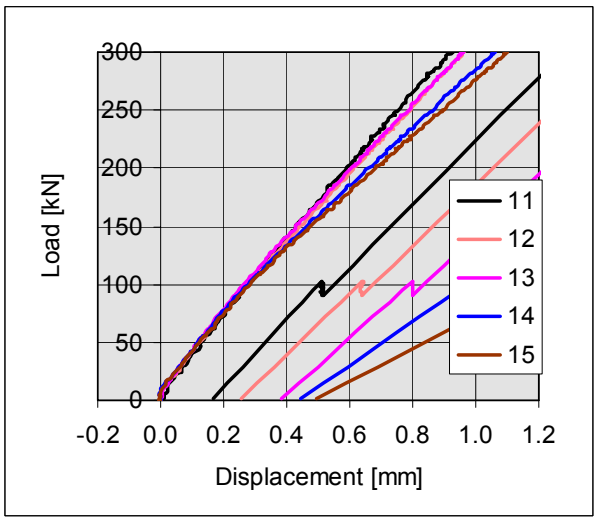

Fig. 17. PF400:14. Vertical displacement measured by transducers 11–15.

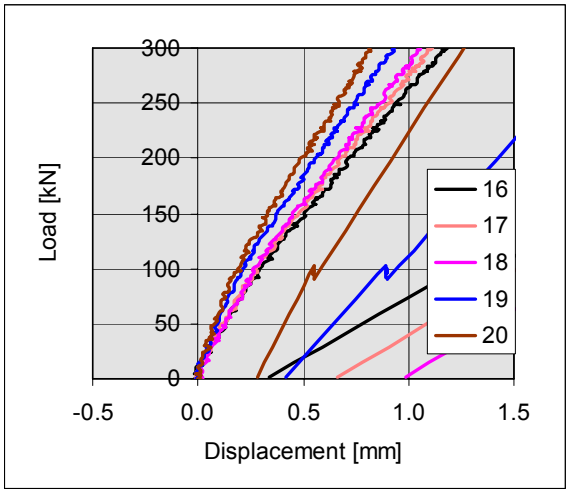

Fig. 18. PF400:14. Vertical displacement measured by transducers 16–20.

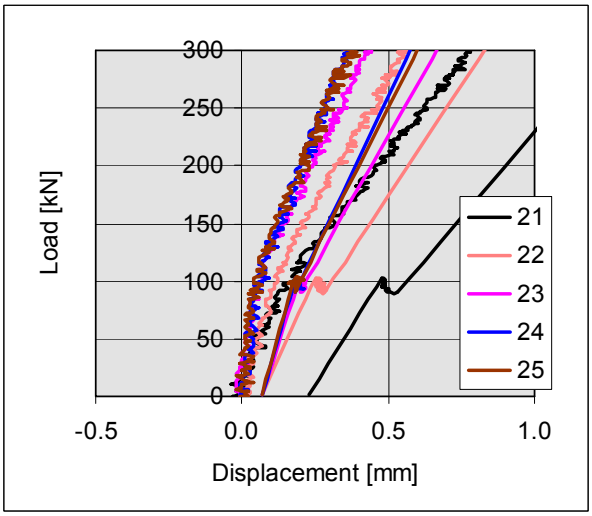

Fig. 19. PF400:14. Vertical displacement measured by transducers 21–25.

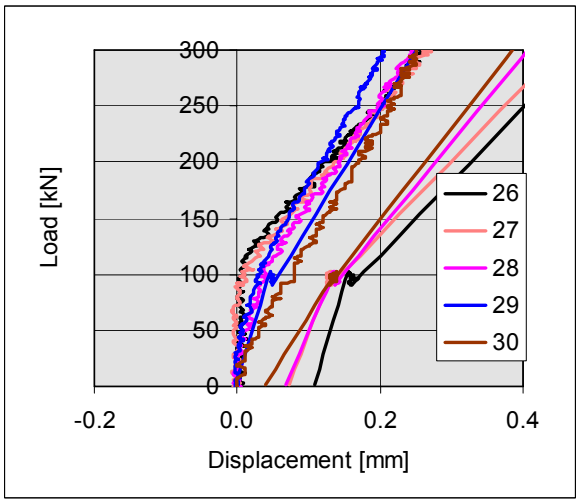

Fig. 20. PF400:14. Vertical displacement measured by transducers 26–30.

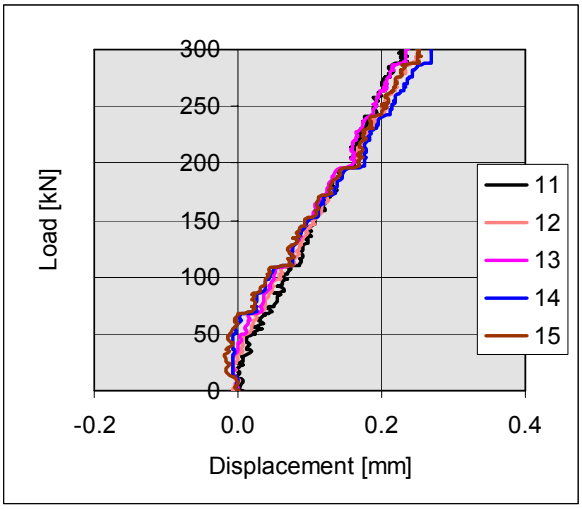

Fig. 21. PF400:15. Vertical displacement measured by transducers 11–15.

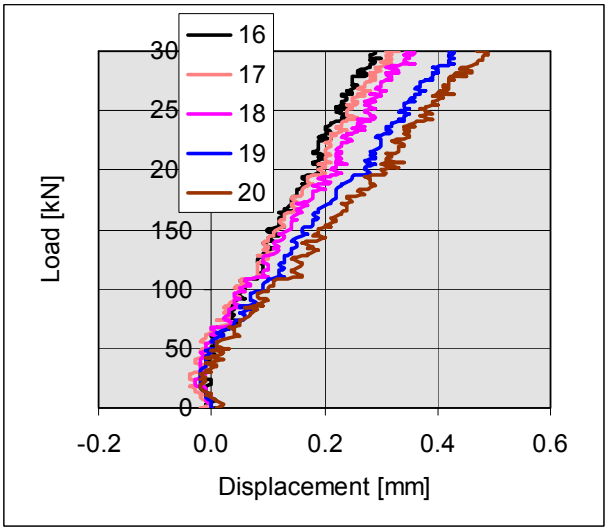

Fig. 22. PF400:15. Vertical displacement measured by transducers 16–20.

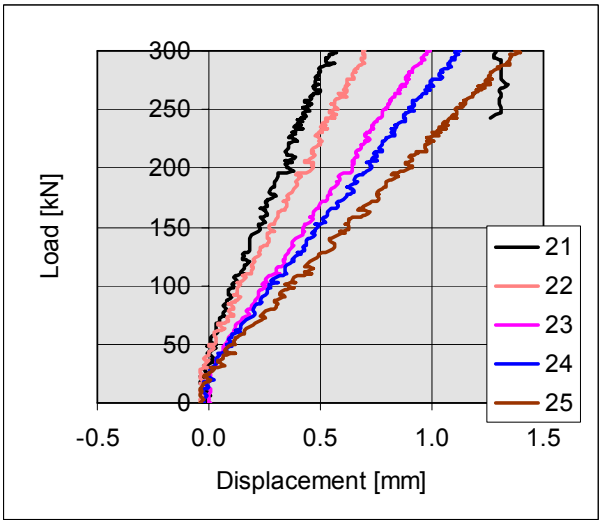

Fig. 23. PF400:15. Vertical displacement measured by transducers 21–25.

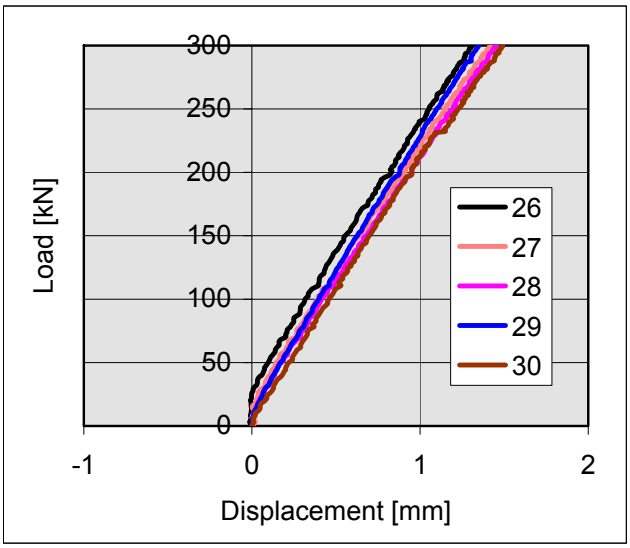

Fig. 24. PF400:15. Vertical displacement measured by transducers 26–30.

Published by

Series title, number and
report code of publication

VTT Research Notes 2274
VTT–TIED–2274

Author(s)
Pajari, Matti

Title

Shear-torsion tests on 400 mm hollow core floor

Abstract

Fifteen load tests on a floor comprising four prestressed hollow core slabs were carried out to clarify the interaction of shear and torsion. The slabs were 400 mm in depth, 1.2 m in width and 7 m in length. The ends of the slabs were simply supported on concrete beams. The loads in each test comprised one or two concentrated loads close to the support.

In twelve tests the loads were limited to a typical service load. In these tests the behaviour of the floor was relatively linear and no sign of failure could be observed. In three tests the floor failed locally. The observed failure loads were 25–97% higher than in a reference test on a single slab unit with identical support conditions. In the first failure test with one point load the failure mode was punching. In other two tests with two point loads, as well as in the reference test with one point load, the failure was a typical shear-torsion failure.

As a subtask of HOLCOTORS project, the test results have been used by Chalmers University of Technology for calibration of computerized calculation methods they have developed. This work is published elsewhere. Therefore, the present design practice has not been evaluated here in view of the obtained results.

Keywords
shear tests, torsion tests, hollow core slabs, floors, testing, test specimens, load testing, failure loads, load distribution, concrete, precast, prestressed, structure

Activity unit
VTT Building and Transport, Kemistintie 3, P.O.Box 1805, FIN–02044 VTT, Finland

ISBN			Project number
951–38–6518–5 (URL: http://www.vtt.fi/inf/pdf/)			R2SU00137
Date December 2005	Language English	Pages 30 p. + app. 82 p.	Price -
Name of project Holcotors		Commissioned by EU, Concrete industry, VTT	
Series title and ISSN VTT Tiedotteita – Research Notes 1455–0865 (URL: http://www.vtt.fi/inf/pdf/)		Published by VTT Information Service P.O.Box 2000, FIN–02044 VTT, Finland Phone internat. +358 9 456 4404 Fax +358 9 456 4374	

Fifteen load tests on a floor comprising four prestressed hollow core slabs were carried out to clarify the interaction of shear and torsion. The slabs were 400 mm in depth and 7 m in length. The ends of the slabs were simply supported on concrete beams. The loads in each test comprised one or two concentrated loads close to the support.

In twelve tests the loads were limited to a typical service load. In these tests the behaviour of the floor was relatively linear. In three tests the floor was loaded to failure. The observed failure loads were 25–97% higher than in a reference test on a single slab unit. In the first failure test with one point load, the failure mode was punching. In other two tests with two point loads, as well as in the reference test with one point load, the failure was a typical shear – torsion failure.

VTT TIETOPALVELU
PL 2000
02044 VTT
Puh. 020 722 4404
Faksi 020 722 4374

VTT INFORMATIONSTJÄNST
PB 2000
02044 VTT
Tel. 020 722 4404
Fax 020 722 4374

VTT INFORMATION SERVICE
P.O.Box 2000
FIN–02044 VTT, Finland
Phone internat. + 358 20 722 4404
Fax + 358 20 722 4374

ISBN 951–38–6518–5 (URL: http://www.vtt.fi/inf/pdf/)
ISSN 1455–0865 (URL: http://www.vtt.fi/inf/pdf/)